HELMHOLTZ
CENTRE FOR
ENVIRONMENTAL
RESEARCH – UFZ

Structural control on groundwater chemistry, recharge and flow – Integrated approach using remote sensing, GIS and modelling: The case study of Wadi Zerka Ma'in catchment area (Jordan)

Taleb S.A. Odeh

Structural control on groundwater chemistry, recharge and flow – Integrated approach using remote sensing, GIS and modelling: The case study of Wadi Zerka Ma'in catchment area (Jordan)

By the Faculty of Geosciences, Geo-Engineering and Mining
of the Technische Universität Bergakademie Freiberg

approved

THESIS

to attain the academic degree of

Doctor rerum naturalium

(Dr.rer.nat.)

Submitted by **MSc Taleb S. A Odeh,** born on the 20 October 1979 in Al Mafraq, Jordan.

Assessors:

Prof. Dr. Broder Merkel, TU Bergakademie, Freiberg, Germany.

Prof. Dr. Mario Schirmer, Eawag: Swiss Federal Institute of Aquatic Science and Technology, Dübendorf, Siwizerland.

Prof. Dr. Elias Salameh, University of Jordan, Amman, Jordan.

Prof. Dr. Lothar Ratschbacher, TU Bergakademie, Freiberg, Germany.

Dr. Stefan Geyer, Helmholtz Centre for Environmental Research – UFZ, Halle/Saale, Germany.

Dr. Richard Gloaguen, TU Bergakademie, Freiberg, Germany.

Date of the award: 19 April 2011

The fascinating impressiveness of rigorous mathematics, with its atmosphere and precision and

elegance, should not blind us to the defects of the premises that condition the whole process........

Thomas Chamberlin (1843 –1928).

Dedication

To my family

To the memory of my grandfather:

Al hajj Ahmad Mahmoud Odeh Abu Hammam

To my second home town:

Dresden

To her warm white heart, celestial eyes and angelic spirit

Yours
Taleb

Abstract

Wadi Zerka Ma'in catchment area is the smallest catchment area at the eastern side of the Dead Sea and encompasses the largest city at that side. It is characterized by two types of aquifers: 1) an upper unconfined aquifer and 2) a lower confined aquifer. The two aquifers are separated by a marl aquiclude. A major strike slip fault passes perpendicularly through the two aquifers and the aquiclude layer with embedded normal faults. Theses faults form conduits that allow groundwater to flow from the lower aquifer to the upper aquifer, resulting in a mixed groundwater. The ratio of mixing was estimated to be 94% groundwater from the upper aquifer and 6% from the lower aquifer. Since groundwater in the lower aquifer is around three times more saline than the upper aquifer, water mixing into the upper water aquifer generates a salinity hazard potential. The topographic profile of the Zerka Ma'in River exhibits two knickpoints. The first one located where the river crosses a major embedded normal fault. The second knickpoint developed as a result of the dramatic lowering of the Lisan lake water level, a lake that pre-dated the Dead Sea. The decreased water level triggered river incision into the clastic sandstone units of Wadi Zerka Ma'in. According to the transverse topographic symmetry factor (T), the catchment area is highly asymmetric. The major basin asymmetry trend is SE-oriented, parallel to the oldest set of faults. Climatically and gemorphologically, Wadi Zerka Ma'in catchment area is considered heterogeneous as a result of the major strike slip fault. The catchment area receives a direct groundwater recharge from a hydrogeological boundaries area of 611.25 km² and has a spatial distribution of groundwater recharge as a result of that heterogeneity that caused by the major strike slip fault. However, the major strike slip fault affects also groundwater flow by generating a high permeability zones.

Acknowledgments

This thesis is the ultimate outcome of my continuous work over the last five years. It would not exist without the real support of many persons and organizations. First of all, I owe my deepest gratitude to my supervisors:

Prof. Mario Schirmer for his untiring assistance, guidance and for having an open ear for my problems and scientific ideas. I am very greatful for his corrections and explanations about the scientific papers.

Dr. Stefan Geyer for his daily supervision and discussion on my research progress. It was unique chance to work with the German team and learn how to explain, discuss and do field work with them.

Dr. Tino Rödiger for his full support and concerning for both personal and scientific problems. The groundwater recharge and flow modelling would not have been possible to achieve without his help.

Dr. Richard Gloaguen for his effort and advices. I really learned different technical and methodological remote sensing approaches, as well as new academic knowledge about tectonics during my stay in the remote sensing group at TU Bergakademie Freiberg.

It is an honor for me to thank Prof. Elias Salameh for his precious discussions, guidance, recommendations and assistance. I am really greatful for his precious ideas and advises.

I am very greatfull for Prof. Broder Merkel for his corrections, and recommendations.

and being a student in Higrade school to attend different advance courses. My deepest thanks to Ms. Brigitte Grosser and Dr. Vera Bissinger.

I will never forget the continuous personal support from my family and my friends: Dr. Wissam S Ibrahim, Dr. Hassan Hamasha, Riyad Bisharat and Dr. Lara Jaber.

TABLE OF CONTENTS

VI

List of figures

VIII

List of tables

Chapter 1

Introduction

1.1 Scope and objectives of this study

Groundwater constitutes the most important reservoir of available drinkable water in the arid and semi arid climatic regions (Seiler and Gat 2007). Jordan has an arid and semi arid climate and is considered as one of the nine water poorest countries in the world. The capita water supply is only about 170 cubic meters per year and most of its water demands are supplied by direct groundwater mining (Salameh & Bannayan 1993, Margane et al 2002).

Several factors lead to critical serious water problem in Jordan such as the shortage and irregular spatial distribution of water resources, the high concentration of people in urban areas, a high population growth rate, reach up to 2.4% per year for the last 5 years, and waves of refugees that arrived during 1948, 1967 and 1991 wars (Chebaane et al. 2004, Department of Statistics 2009). Furthermore, the quality of the water resources in Jordan is degrading rapidly. This is a result of the liquid and solid waste contamination in addition to the passive degradation due to salinization as a result of overpumping and depletion of the groundwater table (Salameh 1996).

The Wadi Zerka Ma'in catchment area is located at the north-eastern side of the Dead Sea, in Jordan, and spans an area of 272 km² (Fig. 1.1). It is the smallest catchment area and contains the largest city, Madaba, at the eastern side of the Dead Sea. Madaba has about 149500 inhabitants and its water demands are supplied by local groundwater (Department of Statistics

1
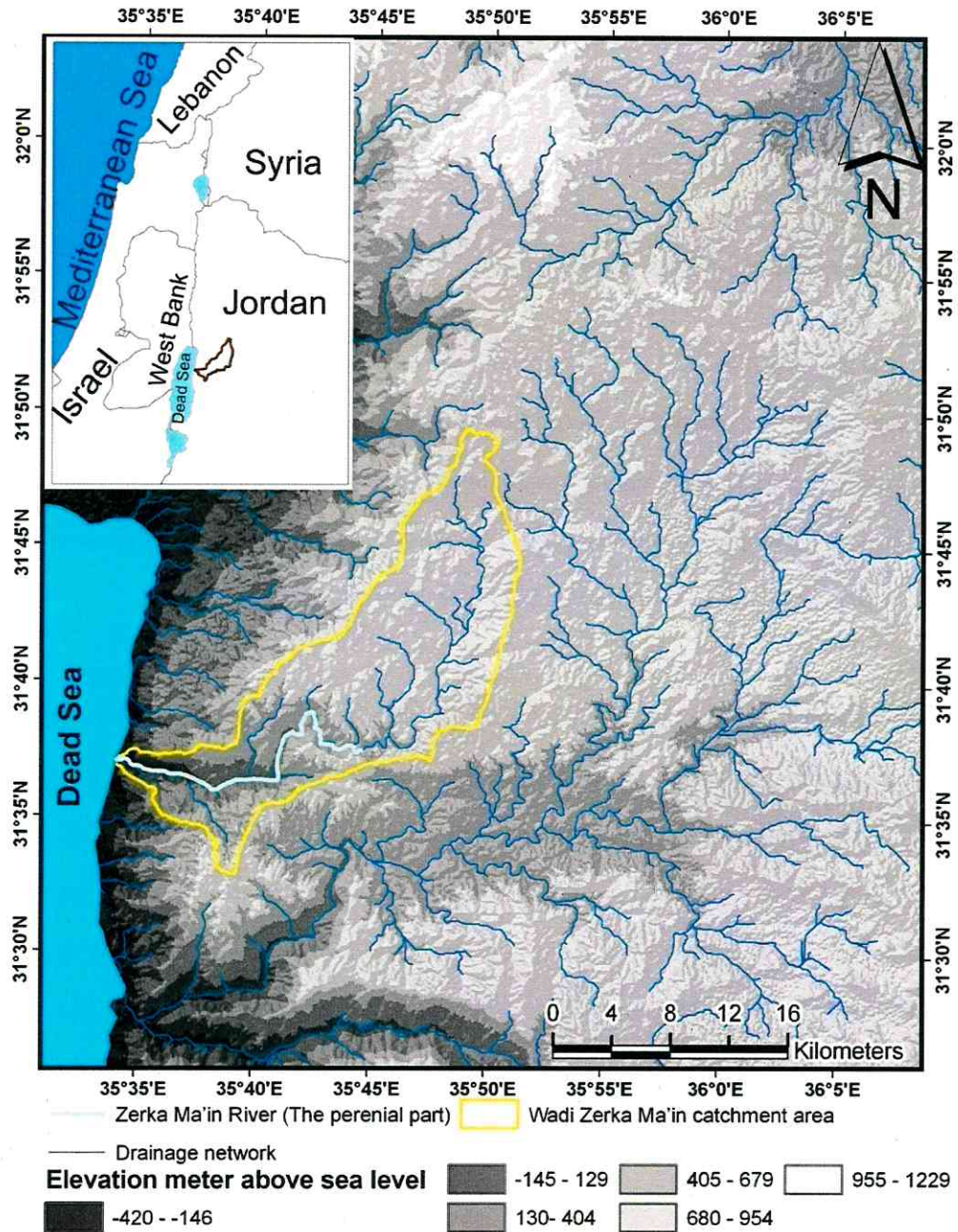
Fig. 1.1: Location of the study area, characterized by strong high relief topography where the elevation varies from -420 to 1020 m above sea level.

2009). Therefore, understanding the groundwater system of Wadi Zerka Ma'in is of a high importance. However, data scarcity and system complexity of the Dead Sea basin are major challenges for doing groundwater modelling, that could be used for sustainable groundwater management, in that region (Al Sawarieh 2005, Margane et al 2002).

Wadi Zerka Ma'in catchment area has two aquifers: an upper unconfined aquifer and a lower confined aquifer. The lower aquifer is represented by Early Cretaceous and Permo-Triassic sandstones. It is covered by aquiclude marl rocks of the Late Cretaceous. The upper aquifer is represented by late Cretaceous and Cenozoic limestone (Shawabekeh 1998, Margane et al 2002).

Groundwater systems of Wadis have interactions between their structural geology and groundwater flow, recharge and chemistry (Domenico & Schwartz 1999, Şen 2008). The structural geology controls: 1) aquifers geometry and physical isotropy and hence the groundwater flow regime, 2) groundwater mixing and hence groundwater chemistry and 3) surface runoff and water percolation and hence groundwater recharge (Fitts 2002, Şen 2008, Domenico & Schwartz 1997). Therefore interdisciplinary research, that involves structural geology and groundwater processes, is requested to understand the complicated groundwater systems of the Wadis (Hatheway & Kanaori 2002, Şen 2008). Therefore, a modelling approach is required to analyze these systems (Domenico & Schwartz 1997, Fitts 2002, Clark & Fritz 1997). Groundwater modelling requests different data (aquifer properties, digital elevation model, groundwater pressure head, recharge, groundwater utiisation). These data can be collected, analyzed and managed through an integrated approach of remote sensing and a geographic information system(GIS) (Saraf et al.2004). Therefore, the objectives of this research, using integrated approaches of remote sensing, GIS and modelling, are as follows:

1) Structural evaluation of the wadi according to surface deformation analysis as follow:

3

- Comprehensive description and characterization of the drainage network;
- Evaluation of the catchment area asymmetry and similarity (Hypsometry plot);
- Stream profile analysis of the Zerka Ma'in River.

2) Groundwater assessment of the Wadi aquifers by modeling the followings:
- Groundwater chemistry;
- Groundwater recharge;
- Groundwater flow.

3) Understanding the relationships between the structural setting and the groundwater system in form of interdisciplinary research.

However, it is advocated to have an integrative understanding for groundwater and geological processes that are occurring and related to each other (Ingebritse 2006). The interdisciplinary research is a part of the integrative scientific understanding. It finds and realizes the relationships between different academic disciplines and creates new scientific knowledge (Audi 2003).

Faults are common structural feature in active tectonic areas such as the Dead Sea rift area. Faulting may control the groundwater chemistry through groundwater mixing (Eugster & Jones 1979). In addition, groundwater chemistry anomalies may have been generated through changes in the regional stress/strain field that created simultaneously with faulting (Guangcai et al 2005). Furthermore, faults may also be a zone of faster contamination from cesspools or other surface contaminated liquids because they may generate more permeable flow paths for the pollutants (Odeh et al. 2009).

Faults may control groundwater flow by being either channelling or obstructing groundwater flow (Smith et al 1990). There are two major mechanisms how faults govern the groundwater flow: 1) changing the petrophysical properties of the hydrogeological units attributable to fault slip and 2) changing the hydrogeological unit positions, geometry or continuity. The petrophysical properties of the native rock control the permeability of the hydrogeological units in two different ways: (1) deformation along the fault displacement and (2) subsequent digenetic changes. During the deformation along the fault slip of crystalline rock, a zone of more permeable media is generated as a result of the rocks brecciation. However, in the less well consolidated rocks and during the deformation, along the fault slip, a low permeability zone will be generated as a result of comminution, gouge formation (grains smashing and splitting), reorientation and repacking of clasts, subsequent digenetic changes, (Aydin & Johnson1978, Aydin & Reches 1982, Pittman 1981). Therefore, a profound knowledge of the stress field in the area of interest is a prerequisite for evaluation fractured groundwater systems.

Quantifying the groundwater recharge, in the arid and semi arid regions, is necessary for a sustainable groundwater resource management. In arid regions, water resources shortage often retards the economic development and therefore groundwater recharge modelling is necessary. According to the water balance equation, surface water runoff is one of the hydrological processes that controls the groundwater recharge (Bier 2007).

Catchment area geomorphology is one of the factors having a direct influence in the runoff generation through the direct control of some runoff factors. These factors include: drainage pattern directions, water divide, slope and aspect of the surface, soil, vegetation and topographical elevation. On the other hand, catchment area geomorphology reflects the interaction between the surface deformation and underlying structural geology. Hence

5

structural geology has indirect effects on the runoff that is a component of the groundwater recharge process (Van der Beek et al. 2002, Beven 2001, Srinivasan & Engel 1991).

To evaluate the complicated groundwater system of the study area three models were applied:

(1) The geochemical code PHREEQC to calculate saturation indices and groundwater mixing.

(2) The groundwater recharge model JAMS (Jena Adaptable Modelling System) to investigate spatial distribution of the groundwater recharge and comparing the results with the spatial distribution of the geomorphological units that is controlled by the underline structure.

(3) The groundwater flow model FeFlow for investigating the spatial distribution of the permeability, groundwater flow and comparing it to spatial distributions of faults.

An integrated approach of remote sensing (RS) and geographic information systems (GIS) was used to supply the models with the land surface spatial data. The structural origin of the Wadi was investigated by geomorphologic indices to understand the types and the distributions of the faults in the study area. The geomorphologic indices were extracted by analyzing high resolution DEMs that were extracted and analyzed by a remote sensing and GIS approach too. Accordingly, the groundwater system was interpreted through the correlation between the groundwater related processes and the structural setting of the catchment area.

1.2 Background information

1.2.1 Geology and hydrogeology

The Arabian-Nubian Shield is composed of Pre-Cambrian crystalline basement rocks and crops out in south-western Jordan (Johnson, 1998) (Fig. 1.2). This shield underwent several epirogenic activities since Pre-Cambrian time that resulted in transgressions and regressions of the Tethys Sea (Bender 1974). The geological layers were deposited during the northwest transgressions and the erosion of the uplifted Arabian-Nubian Shield from the south during regression (Andrews 1991). Jurassic and Cretaceous sediments of considerable thickness were laid down and reach up to 4000 m in the southeast of Jordan (Flexer 1968, Andrews 1991). In the Upper Eocene, the Tethys regressed with deposition of fluviatile and lacustrine deposits mainly in the Jordan Rift Valley and Wadi Araba in western Jordan (Horowitz 2001). From the Oligocene to Quaternary basalt flows erupted during the volcanic activity in the Harrat Ash Shaam volcanic system, a massive alkaline volcanic field extending from the south of Syria to northwest Saudia Arabia (Bender 1974, BGR 1992).

The out cropping rocks of the study area are mostly sedimentary rocks and belong to Paleozoic, Mesozoic and Cenozoic ages (Shawabekeh 1998) (Fig. 1.3). Palaeozoic and Mesozoic rocks were deposited during the phases of Paleotethys and Tethys transgressions and regressions, respectively. Ordovician, Silurian and Jurassic formations are found elsewhere in Jordan but not in the study area. It is not known whether these rocks were never actually present or were removed by erosion (Bender 1974, Andrews 1991). The Cenozoic rocks consist of clastic and nonclastic sedimentary rocks and extrusive igneous rocks. They can be summarized as follows:

A) Pleistocene gravel: fluviatile and lacustrine gravels clasts are of chert, limeston
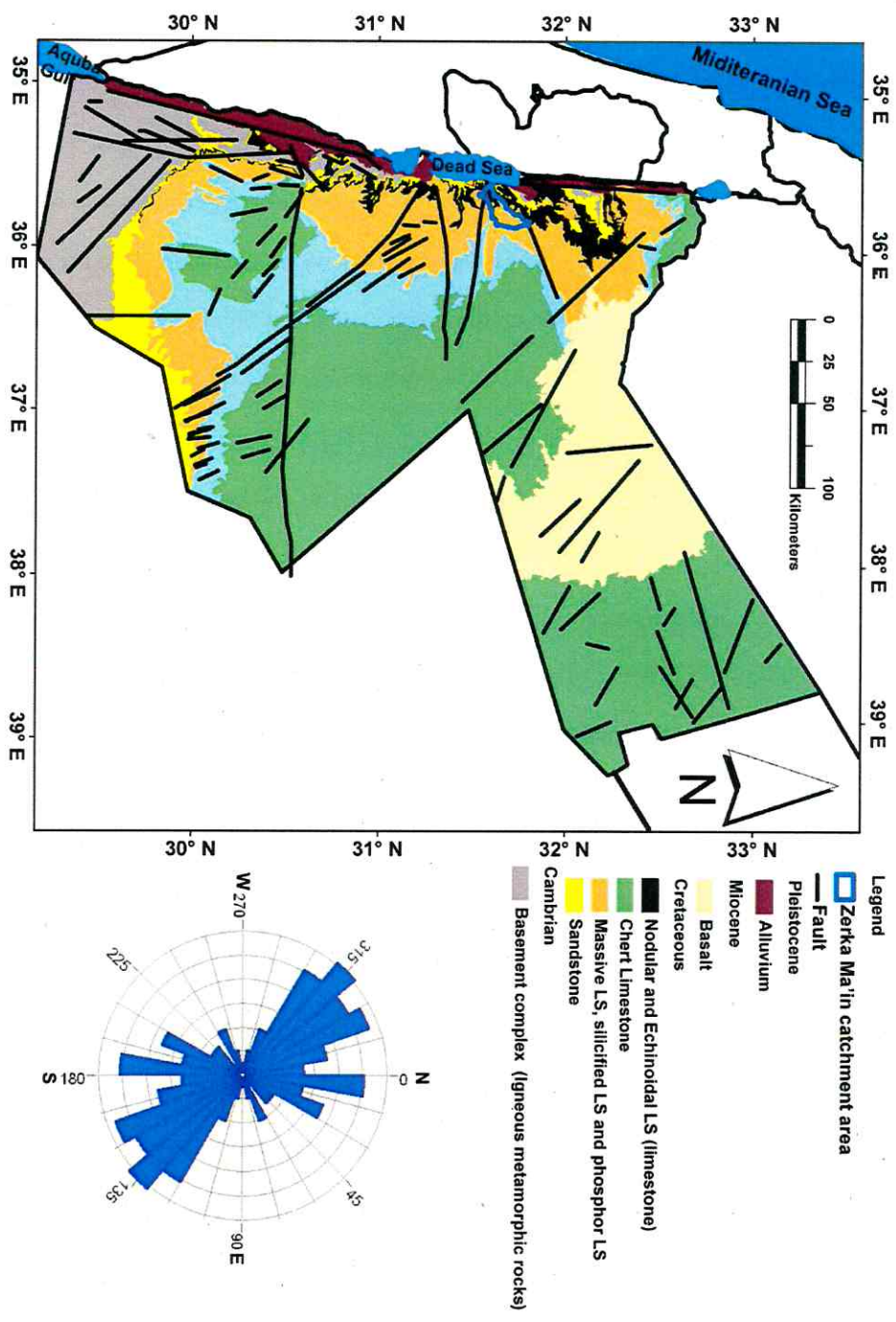
Fig. 1.2: Geological map of Jordan (after Bender 1974). The major fault system direction is in N – S parallel to the Red Sea.

8
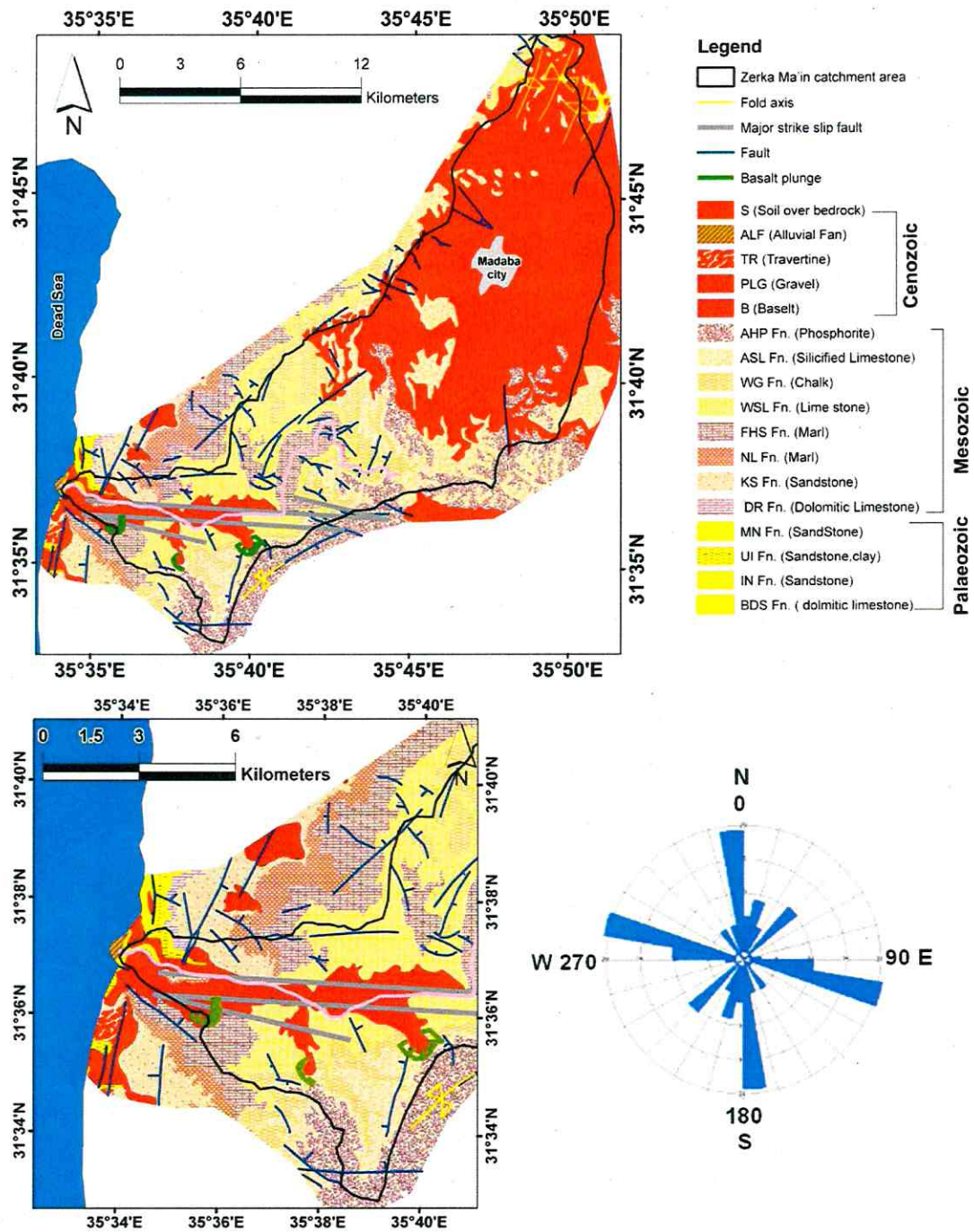
Fig. 1.3: Geological map of the study area (after Shawabekeh 1989). There is limited exposure of Palaeozoic layers in the lower part of the catchment area while Mesozoic layers cover most of the lower and middle parts.

9

dolomite, dolomitic limestone, sandstone and basalt (Shawabekeh 1998).

B) Travertine: two types of travertine are found in the study area. Recent soft white travertines with the main component of aragonite and older hard black travertine mainly composed of calcite in locations near the Dead Sea (Khouri et al. 1984).

C) Basaltic rocks: The south west region of the study area is partly covered by Basaltic rocks from three cones. Three stages of eruptions are suggested by Stienitz and Barttov (1992) which are specified by geomorphologic evidences and K-Ar dating: (1) The first stage (6 Ma BP (Before Present time)) is characterized by breccia fragments of basalt mixed with older sediments. This is at the bottom of the Zerka Ma'in wadi. (2) The second stage (3.4 Ma BP) is characterized by fresher Basaltic cones cutting through the breccia of the first stage. (3) The last stage of eruption (0.6 Ma BP) is characterized by lava flows covering recent alluvium.

The lithological units were classified into three hydrogeological units (Tab. 1.1). The upper aquifer is built by mainly limestone and has an average thickness of about 235 m. The average permeability and storage coefficient is about 1.5×10^{-5} m/s and 1×10^{-5} m/s respectively. The groundwater level in this aquifer is between 158 m to 850 m above sea level (absl.) (Fig. 1.4). The groundwater flows from north to south and turns westwards in the lower part of the catchment. The confined lower aquifer consists mainly of sandstone and has an average thickness of about 500 m. The average permeability and storage is 1.9×10^{-6} m/s and 1×10^{-5} m/s, respectively (Margane et al. 2002). The groundwater level of this aquifer is between 300m to - 420 m absl. (Fig. 1.6). The lower aquifer has a fossil groundwater moves from east to west. The aquiclude consists of marly rocks with a thickness of about 164 m (Margane et al. 2002).

Tab. 1.1: Geological formations in the study area (after Shawabekeh 1989). Three unconformities are found in the study area. The lithological units were classified as three hydrogeological units (the symbol # means not defined).

Formation (Formation symbol)	Group	Period	Epoch	Major rocks component	Thickness average (m)	Hydrogeo-logical unit
#	#	Quaternary	Holocene	Travertine (TR)	20	Upper aquifer (unconfined unsaturated aquifer) Average thickness 275 m
#	#	Quaternary	Pleistocene	Fluviatile Gravels (PLG)	10	
#	#	Tertiary (Neogene)	Miocene	Basalt (B)	#	
Disconformity Surface						
Al Hisa (AHP)	Belqa	Cretaceous	Late	Phosphate	61	
Amman (ASL)	Belqa	Cretaceous	Late	Silicified Limestone	65	
Wadi UmmGhudran (WG)	Belqa	Cretaceous	Late	Chalk	47	
Wadi as Sir (WSL)	Ajlun	Cretaceous	Late	Limestone	102	Upper aquiclud Average thickness 369 m
Fuhays, Hummar and Shu'ayb (FHS)	Ajlun	Cretaceous	Late	Marl	169	
Na'ur (NL)	Ajlun	Cretaceous	Late	Marly Limestone	149	
Kurnub (KS)	Kurnub	Cretaceous	Early	SandStone	220	Lower aquifer (confined aquifer) Average thickness 525 m
Disconformity Surface						
Dardur (DR)	Zerka Main	Permo-Triassic	#	Sandstone	57	
Ma'in (MN)	Zerka Main	Permo-Triassic	#	Sandstone,	47	
Umm Irna (UI)	Zerka Main	Permo-Triassic	#	Sandstone,	67	
Disconformity Surface						
Umm Ishrin (IN)	Rum	Cambrian	Middle, Upper	Sandstone	280	
Burj (BDS)	Rum	Cambrian	Early	Dolmitic Limestone	74	
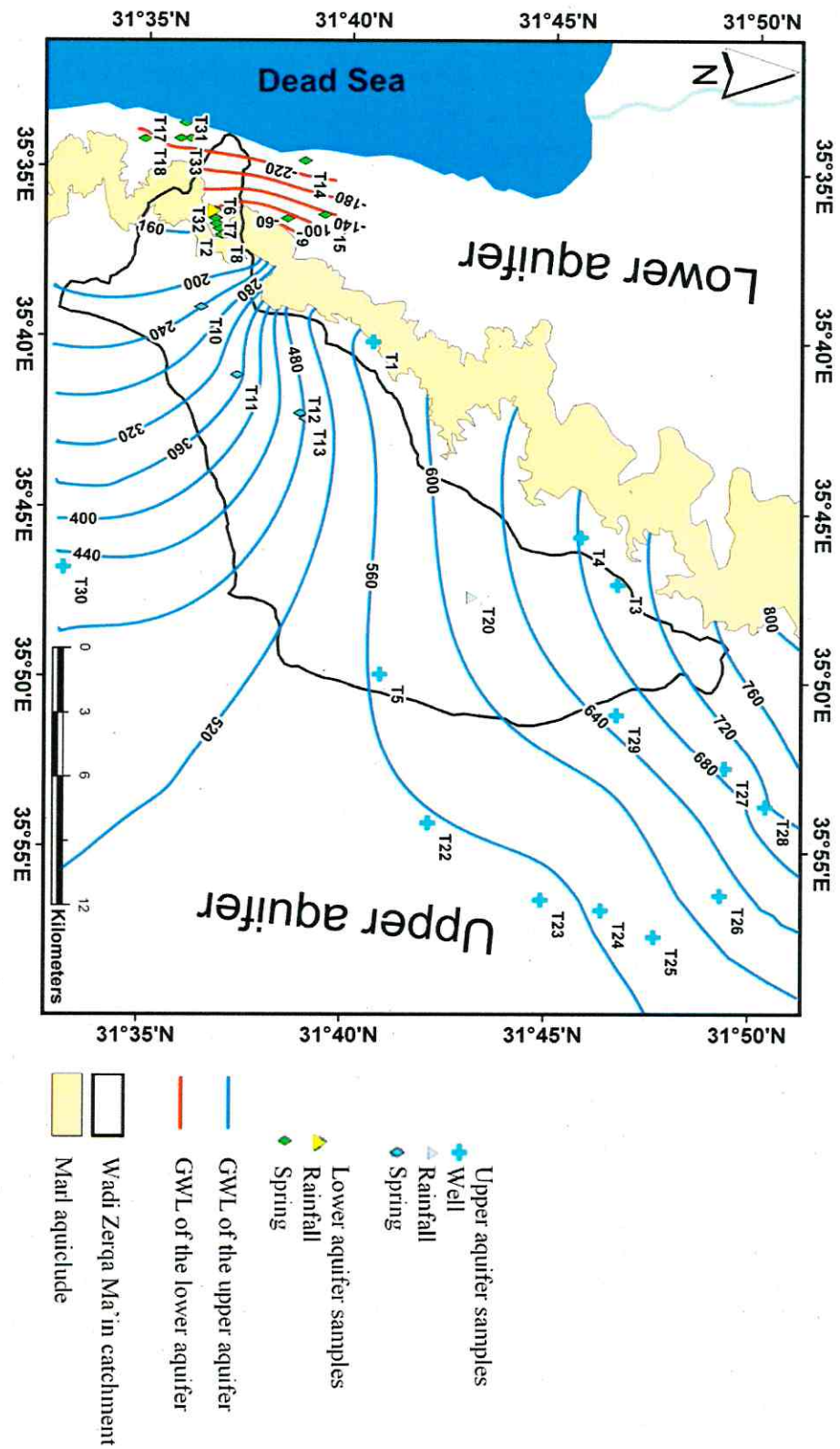
Fig. 1.4: Water samples locations and groundwater level of the upper and lower aquifer (2007). The water level measurements values are presented in Table 2.1 (Data of the upper aquifer wells: ministry of water and irrigation in Jordan 2007 (open file)).

12

1.2.2 Structural geology

The fault systems in Jordan have three main trends: 1) NW– SE, the oldest, that is parallel to the Red Sea and was generated simultaneously with Sea floor spreading (Johnson 1998). That system has been rejuvenated with clockwise rotation to become oriented WNW – ESE, and produced a shear belt along with 2) a WNW – ESE fault system, which is perpendicular to the Dead Sea transform fault. The major strike-slip fault of Wadi Zerka Ma'in catchment area belongs to this trend (Garfunkel & Ben-Avraham 1996). Later, this clockwise rotation changed gradually from NW – SE to N – S and led to the formation of 3) a NNW-SSE fault system that is parallel to the Dead Sea transform fault and is the youngest fault system in the study area (Niemi & Ben-Avraham 1997, Quennell 1958).

The regional Dead Sea transform fault experiences ~ 6 mm of strike slip motion per year (Klinger et al. 2000). It connects the divergent plate boundary along the Red Sea with the zone of plate convergence along the alpine orogenic belt in Turkey (Johnson 1998) (Fig. 1.5). According to Quennell (1958), the Dead Sea Rift valley was generated by two major horizontal movements with a total sinistral movement of 107 km and with a vertical down-throw of ~ 1500 m. These movements are not older than 14 Ma and not younger than 6 Ma. The Dead Sea represents a pull-apart zone in the Dead Sea transform fault (Bayer 1988, Niemi&Ben-Avraham1997).
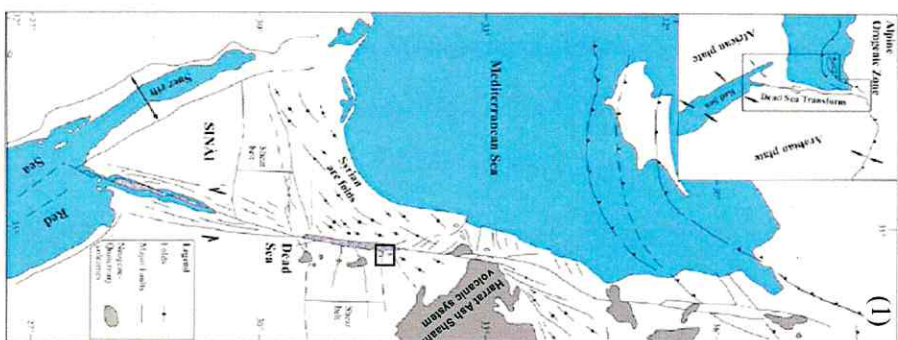
Fig. 1.5: Regional tectonic map after (Garfunkel & Ben-Avraham 1996 (1) and Johnson 1998 (2). The study area is located in the middle of the Dead Sea transform fault within shear belt zone of strike slip faults.

1.2.3 Dead Sea origin

In the post-Messinian a maximum ingression of the Mediterranean Sea occurred in the west and generated the Sadom Sea in the Dead Sea Rift Valley (Fig. 1.6). However, the Sadom Sea was connected to the Mediterranean Sea by the Yizreel Valley and therefore had 0 meter elevation above sea level (Horowitz 2001). Subsequently, the land between the Dead Sea Rift and the Mediterranean Sea was uplifted, denying further marine transgressions (Niemi & Ben-Avraham 1997). In the middle Pleistocene, the rift contained three lakes: Al Hula, Kinnert and Samara. However, ~ 100,000 years ago, the climate became more and more arid and caused the Lake Samara to shrink and be replaced by the more saline Lake (Lisan Lake) which was ~180 m below sea level (Horowitz 2001, Salameh & Farajat 2007).

The shrinkage of the Lisan Lake led to the formation of the Dead Sea Lake in a pull-apart zone of the Dead Sea transform fault. The Dead Sea lake had a water level of about - 400 m before 23,000 years, (Sneh 1996, Niemi & Ben-Avraham 1997). According to Salameh & Farajat (2007) the shrinkage of the Lisan Lake catchment area from ~ 170,000 km², to the recent Dead Sea catchment area (Fig. 1.7) of ~ 44000 km² was the main reason for that reduced lake level.

The catchment area shrinkage was a result of the eruption and spread of the basalt flows of Jabal Arab Druz, which together with the resulting deposition of thick rock debris and gravels blocked the pre-basalt drainage system (Lisan Lake catchment area) (Salameh & Farajat 2007) (Fig. 1.8). These basalt flows and volcanic eruptions together with Jabal Arab Al Drouz are called the Harat Al Sham Volcanic system (BGR 1999). After volcanic blocking, the Lisan Lacke catchment area was divided into four major catchment areas as follows
1) Wadi Al Sirhan (79608 km²).
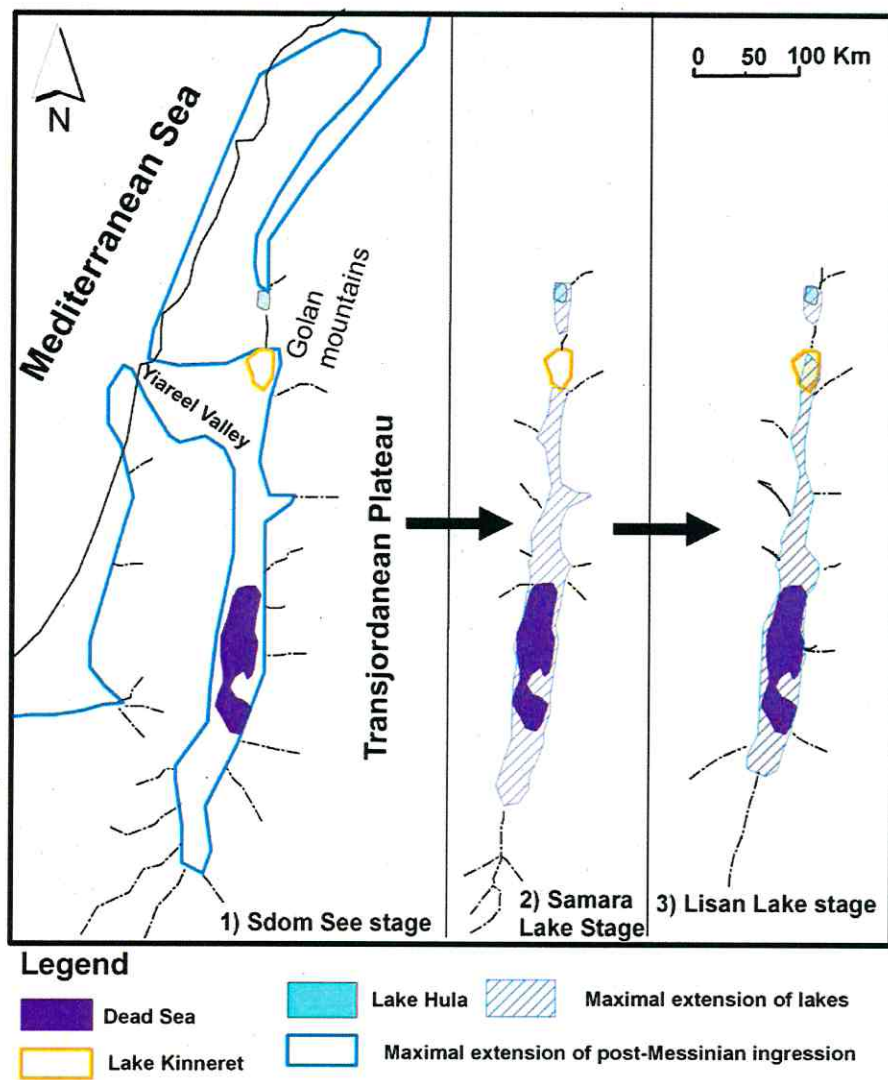
Fig. 1.6: Lisan Lake stages generation (modified after Horowitz 2001). After Sdom Sea stage three lakes were generated in the rift: Al hula, Kinneret and Samara Lakes.
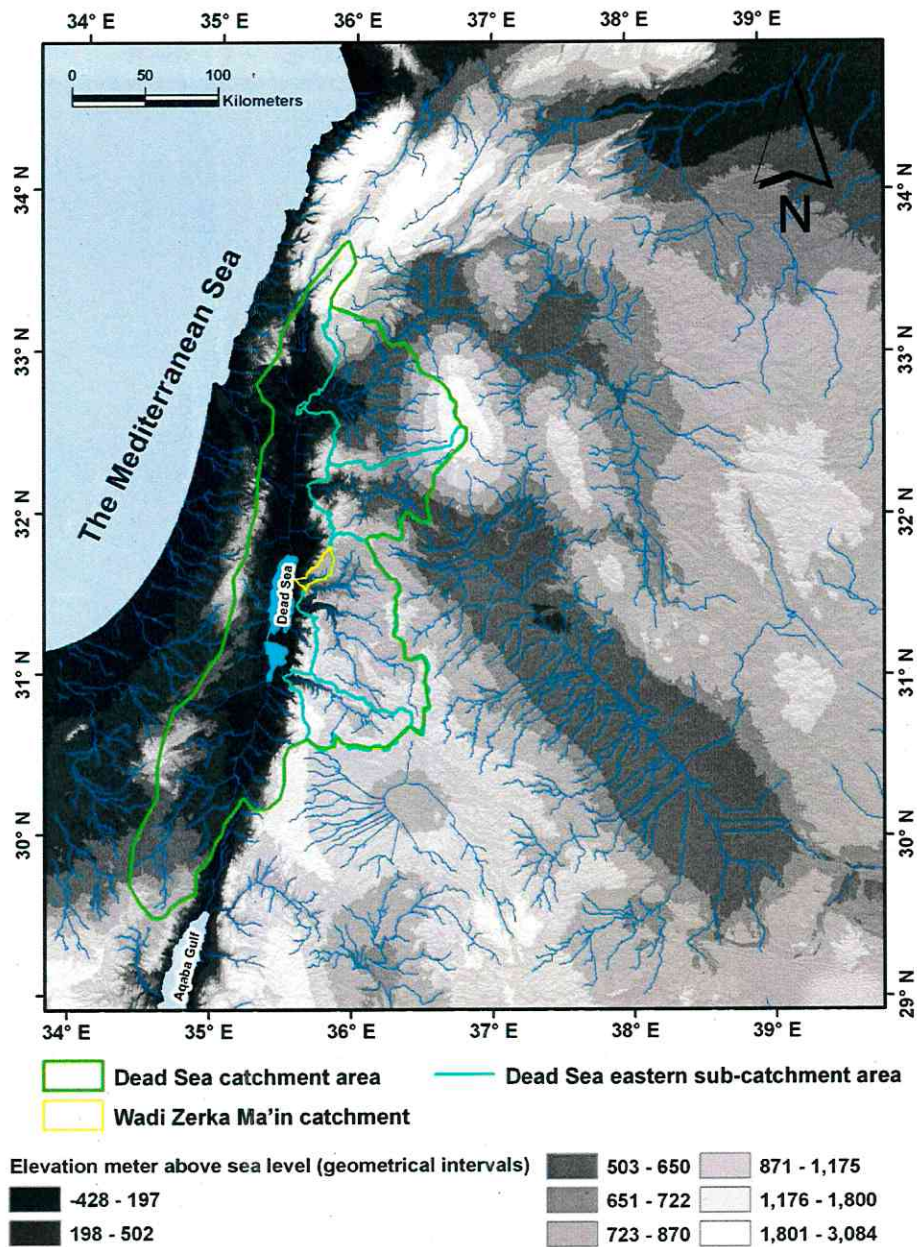
Fig. 1.7: The Dead Sea catchment area has an area of about 44000 km². There are 5 major subcatchment areas in the eastern of the catchment area (WGS 1984 Datum).
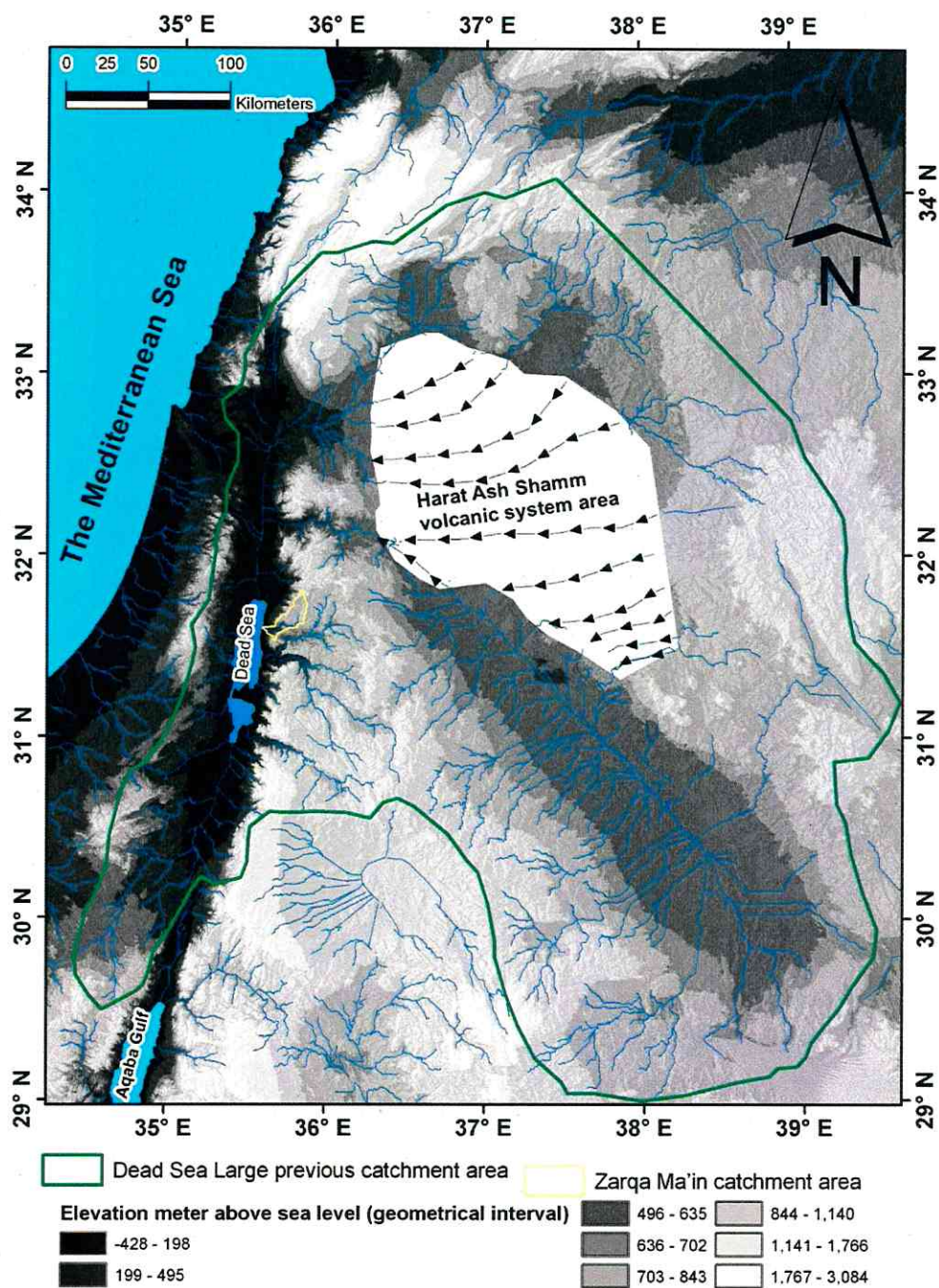
Fig. 1.8: Pre-basalt catchment area. The clipped area represents the Basalt of Harat Al Sham volcanic system including Jabal Arab Al Druz (WGS 1984 Datum).

2) Hammad (38237 km²).

3) Damascus (9570 km²).

4) Dead Sea (43629 km²) (Fig. 1.9).

1.2.4 Climatology

Climate is considered as one of the key factors for the groundwater recharging process as a result of its ability to control rainfall and the evaporation. The inequalities in the elevation, slope and aspect of the land surfaces cause variations in temperature, wind, cloudiness and precipitation. Therefore, the variance in the topography configurations causes climatic differences (Rushton & Ward 1979). The Dead Sea rift valley has strong orographic control over climatic parameters such as precipitation and temperature (Dayan & Morin 2006) and has thus divided the study area into two major topographic units:

1) The higher land on the top of the catchment area.

2) The lower land which is part of the Dead Sea rift valley.

The average maximum amount of rainfall in the high land reaches up to 600 mm/year while the minimum amount of rainfall in the low land reaches up to 200 mm/year (Fig. 1.10). The potential evaporation reaches up 1600 mm/year in the high land and 1980 mm/year in the low land (Salameh and Bannayan 1993). According to Koppen (1931), the catchment area of Wadi Zerka Ma'in is classified as an arid and semi arid region because of the potential evaporation exceeds the amount of precipitation. However, the upper part of the catchment area could be classified as a Mediterranean climate zone that is characterized by long, hot, dry summers, and short, cool, rainy winters (USDA 1993).

19
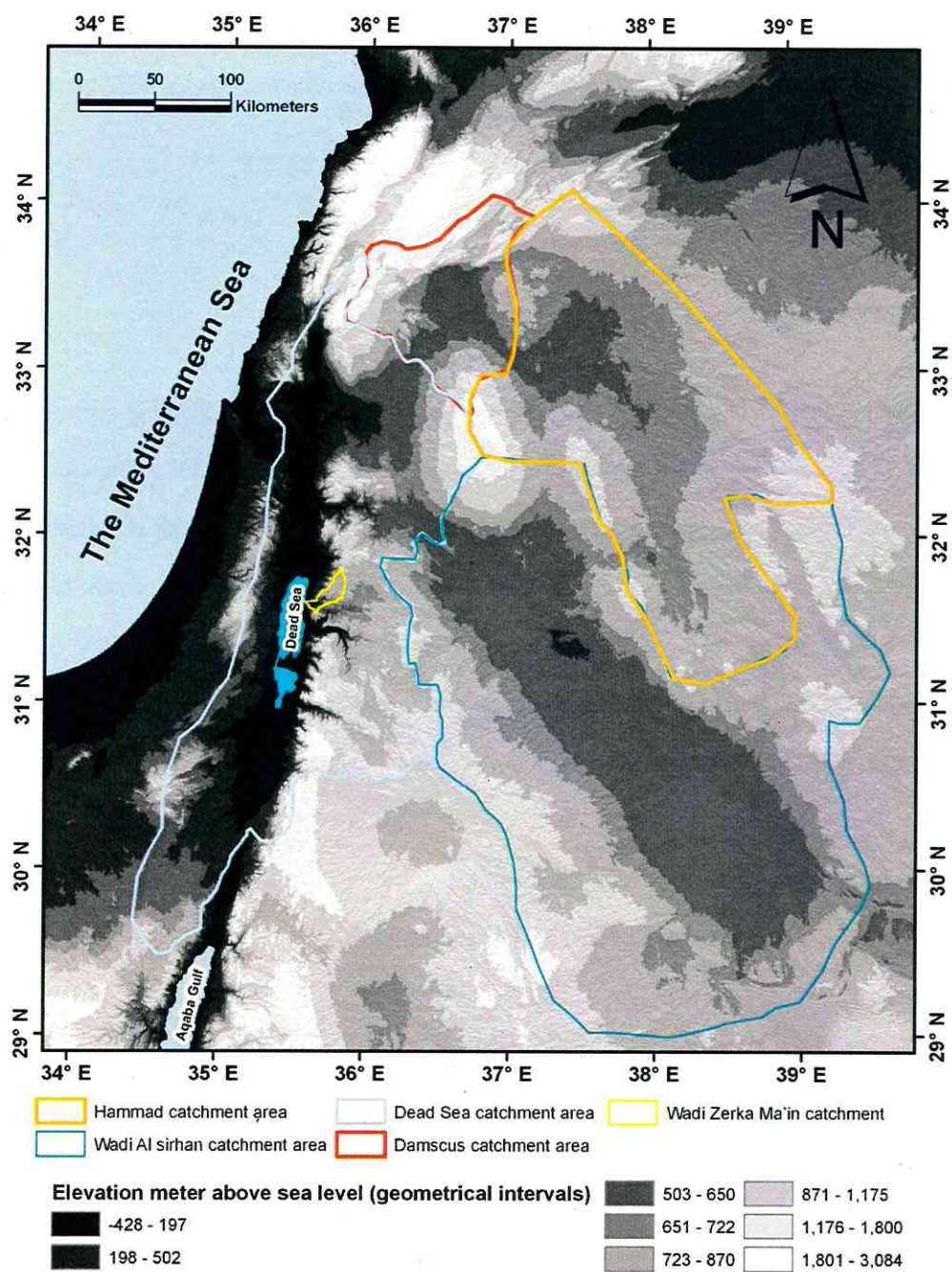
Fig. 1.9: Dead Sea, Wadi Al sirhan, Wadi Hammad and Damscus catchment area. The three catchment areas were one large catchment area before the late Pleistocene (WGS 1984 Datum).

20
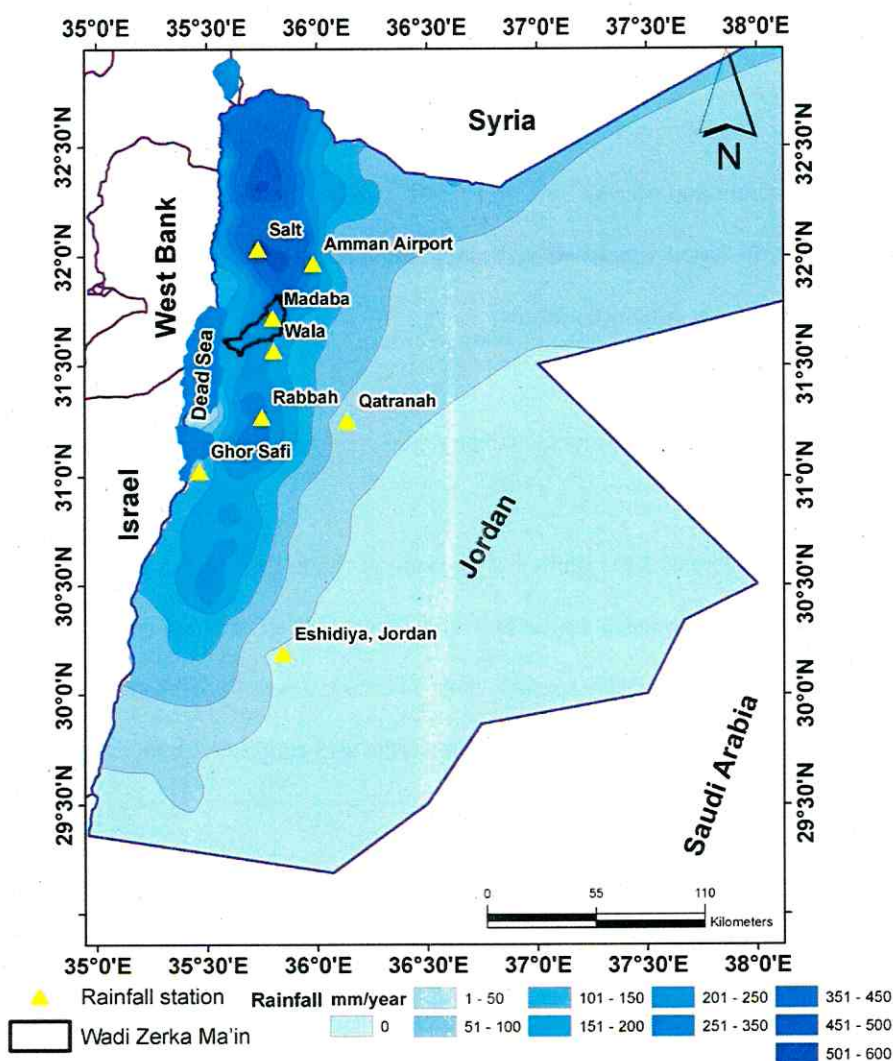
Station	Temp. C °	Relative humidity (%)	Wind speed (mph)	Elevation meter above sea level	Potential evaporation mm/year
Amman Airport	10.8	70.4	2.7	721	2000
Ghor Safi	18.6	59.9	0.5	-420	4000
Madaba	10.4	70.2	3.2	763	3000
Qatranah	10.6	65.3	2.5	792	4400
Rabbah	10.1	70.4	1.8	905	2000
Salt	10.6	68.9	2.4	777	2000
Wala	12.6	61.2	2.3	499	3000

Fig. 1.10: Rainfall map of Jordan (average 1990-2008) (WGS 1984 Datum). The highest amount of rainfall is found in the high land in North West of Jordan. The sudden change of the rainfall at the Western border of Jordan is due to the topographic dropping of the Dead Sea rift valley (Data: Department of climatology in Jordan).

21

1.2.5 Land cover

Land cover is the physical material on the surface of the earth that includes land use (including infrastructure and plants), soil, water and barren rocks (Fisher et al. 2005). It is a principal input to GIS-based watershed hydrologic models (Semmens et al. 2006). The land cover of the studied area is defined as follow:

1) City area represents about 7% while the country side area represents about 16%.

2) The Mediterranean forests have limited abundance in the higher land, where the average amount of rainfall per year reach up to 500 mm, and have an area of about 2% of the catchment area. Scrub plants are also sparsely distributed and cover 4% of the catchment area. The limited vegetation and the forest cover are due to the arid condition of the catchment area (USDA 1993) (Fig. 1.11).

3) Barren rocks cover 30 % of the study area and are described in detail in the geology description (Chapter 1.2.1).

4) Barren and semi-soil, which covers about 40% of the study area, is the product of the interaction among the six soil-forming factors: barren rocks, climate, vegetation and soil fauna topography, humans and time (Scheffer and Schachtschabel 2002).

Arid and semi arid region soils have unique circumstances that distinguish them from humid regions. They have a low level of organic matter, weak to moderate profile development and low biological activity (Dregne 1976). As the study area is situated within these climate zones, the soil profiles show a depth of maximum 150 cm in the plateau area, in the upper part
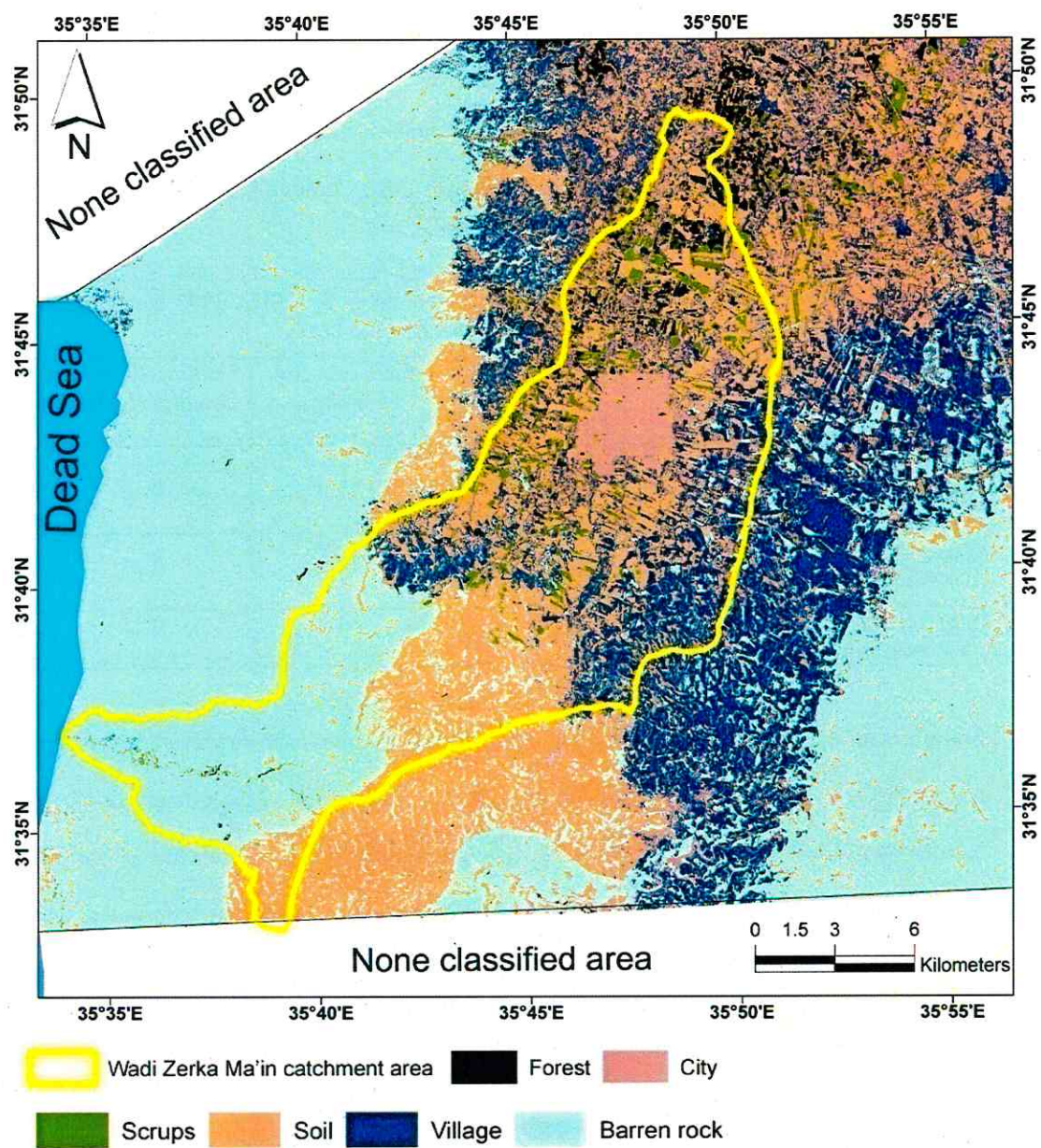
Fig. 1.11: Land cover of the study area. The urbanized area is condensed in the upper part of the study area.

23

of the catchment area, and minimum 50 cm in the high slope area at the sides of the wadi. The lower part of the catchment area has thin soil layers, up to 10 cm, or only barren rocks (USDA 1993, Cordova 1994). The soil texture of the study area (Tab. 1.2) is clay in the high land and silty clay and silty clay loam in the lower part (Shadfan 1982, Cordova 1994).

Tab. 1.2: Soil textures units and some of their physical parameters. The soil samples were taken from the top of 50 cm. The sample analyses were taken by USDA 1993 data base and were used for the supervised classification for Middle infra red bands.

Soil texture	Average thickness	Particulars Percent (%)			Field capacity (mm/dm)	Saturated hydraulic conductivity (m/d)
	m	Clay	Silt	Sand		
Clay (100 samples)	174	55-60	35-40	5-10	15.5	0.12
Silty clay (800 samples)	100	40-50	45-60	5-10	14.5	0.09
Silty clay loam (500 Samples)	150	35-40	45-55	15-20	14.0	0.15

Soil plays an important role in facilitating or restricting rainfall water downward movement toward the groundwater table (Santanello et al. 2007). Soil texture is the primary driver in calculations of soil hydraulic behaviour. However, the direct field measurements of the soil hydraulic properties, for both local and regional case studies, are often time-consuming and expensive (Hwang 2004). Each soil texture unit has homogenous hydrological parameters. Therefore, a soil texture map is a useful tool to deduce such soil hydrological properties (Bormann 2010) and to have a spatial distribution for the soil hydrological prosperities by considering that each soil texture unit has homogeneous hydrological parameters (Santanello et al. 2007). Silicified limestone rocks are found beneath the clay soil texture. Silty clay and silty clay loam are found at the sides of the wadi and their source is the sandstone rocks that are outcropping together with the erosion product from the limestone (Fig. 1.12) (Cordova 2004).
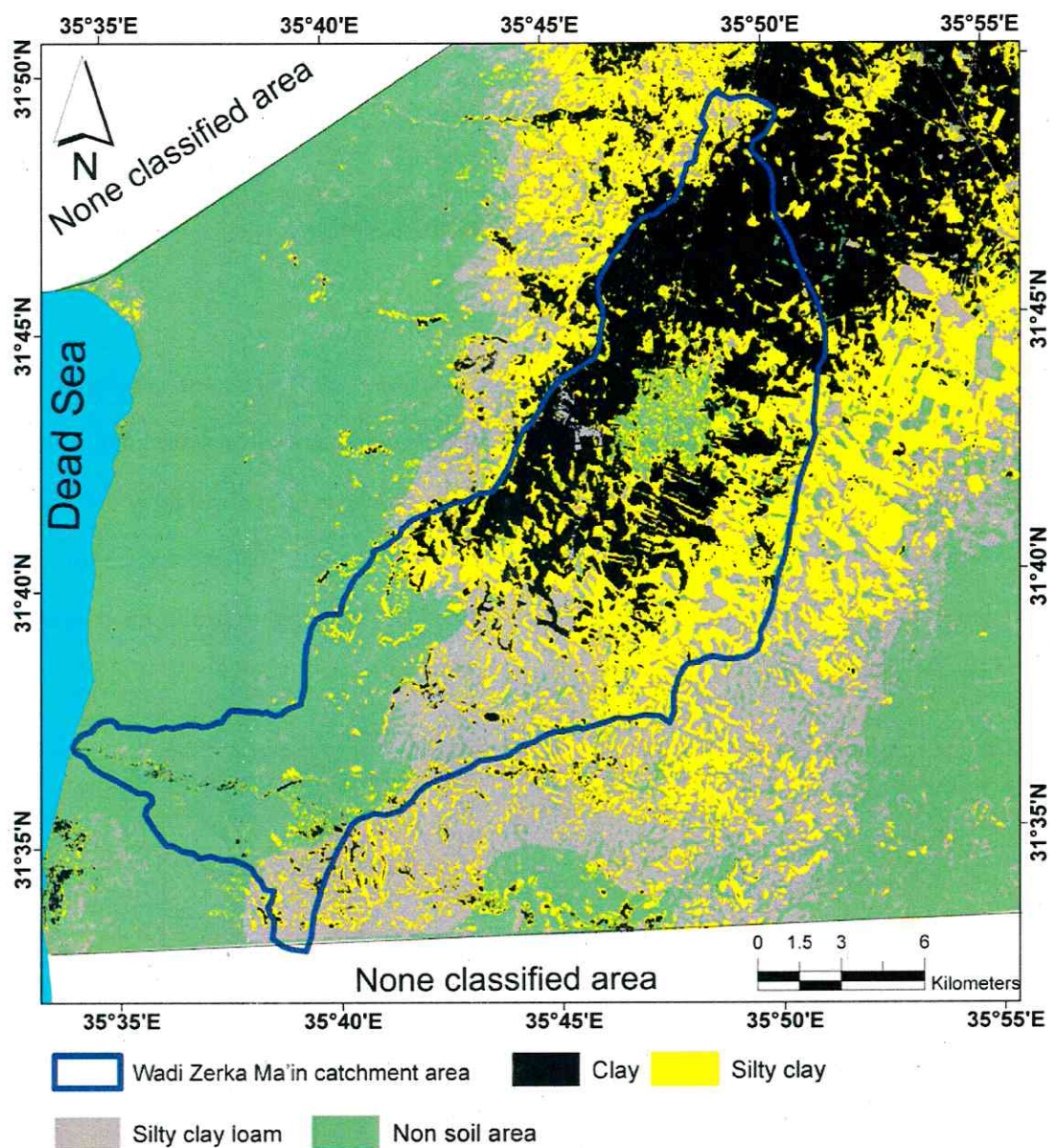
Fig. 1.12: Soil texture map of the study area. The upper part is covered mainly by clay texture where there is a highest amount of rainfall and the area is flat. The lower part is covered mainly by rocks where the lowest amount of rainfall occurs (USDA 1993).

25

Chapter 2

Methodology

2.1 Structural geology evaluation

2.1.1 Drainage network

Drainage networks respond rapidly to structural changes. The automated generation of drainage networks from digital elevation models (DEMs) is a powerful analytical function in geographic information systems (GIS). Remote sensing methods offer a vast array of DEMs with different resolutions to choose from (Gong et al. 2009, Wang & Yin 1998). Therefore, an integrated approach that combines remote sensing and GIS was used to extract the drainage network of Wadi Zerka Ma'in catchment area (Fig. 2.1).
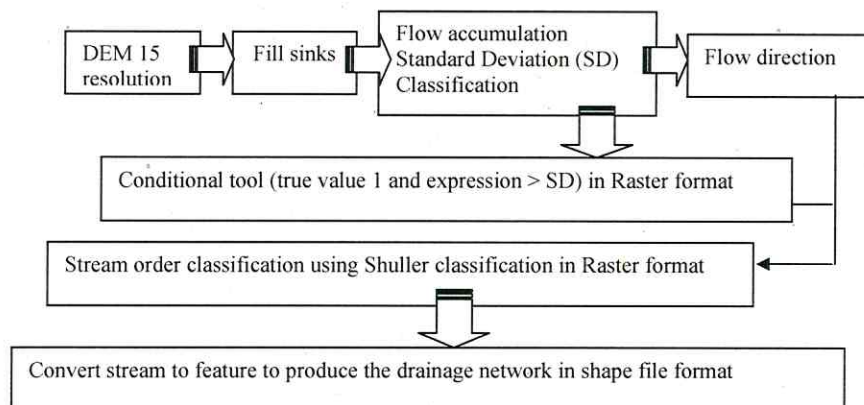
Fig. 2.1: Flow chart of extraction of the drainage network form DEM using GIS.

Two different DEM resolutions were used:

1) A DEM of 30 m resolution that covers the regional area and was downloaded from: http://asterweb.jpl.nasa.gov/gdem.asp.

2) A DEM of 15 m resolution (Fig. 2.2) that was produced from 2 scenes of ASTER

(Advanced Spaceborne Thermal Emission and Reflection Radiometer) images.

Interrelationships between topography and near-surface structure are often recognizable (Wilson & Dominic 1998). Topography can be parsed automatically by manipulating land-surface heights within elevations arrayed in DEMs. From a functionality perspective, GIS techniques can efficiently achieve that process through a variety of data visualization approaches, patterns and spatial analyses (Wang et al. 1998, Iwashi & Pike 2007).

The two DEMs were inserted in the GIS. According to the extension hydrology in the ArcGIS 9.2 software, the drainage network was extracted regionally and locally (Fig. 2.2). The first step was removing the holes in the DEMs and then using a D8 flow grid algorithm (O'Callaghan & Mark 1984). This algorithm estimates the flow direction possibilities at each cell towards the 8 neighboring cells. The least cost algorithm was used to connect the stream flow directions in order to generate a continuous network of streams (Shahzad et al. 2009, Shahzad & Gloaguen 2009). Geometrical classification and hillshade effects were then computed for the raster elevations to parse and visualize the topography using the spatial analyst extension in the ArcGIS 9.2 software.

2.1.2 Stream profile analysis

Stream profile analysis are a useful tool in structural geology and geomorphology as a diagnostic indicator of factors such as stages of landscape evolution, tectonic uplift or subsidence, variations in rock resistance and base level changes (Phillips & Lutz 2008). It is a tool to aid understanding of tectonic–climatic–topographic interactions since the river incision into bedrock is a response to tectonic, lake or sea level, and climatic forcing (Whipple & Tucker 1999). According to Whipple and Tucker (1999) the topographic profile of a stream is controlled by the following equations:
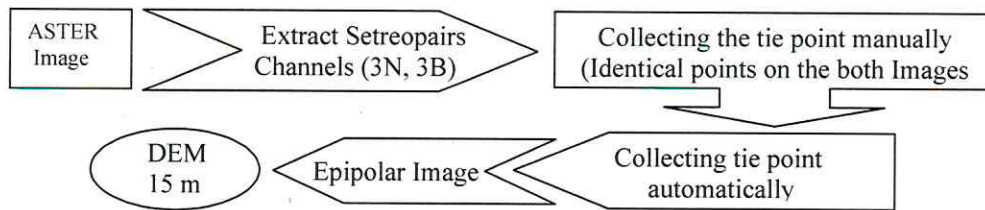
A) Simplified workflow for DEM extraction from ASTER image by using Geomatica V10.3 software.
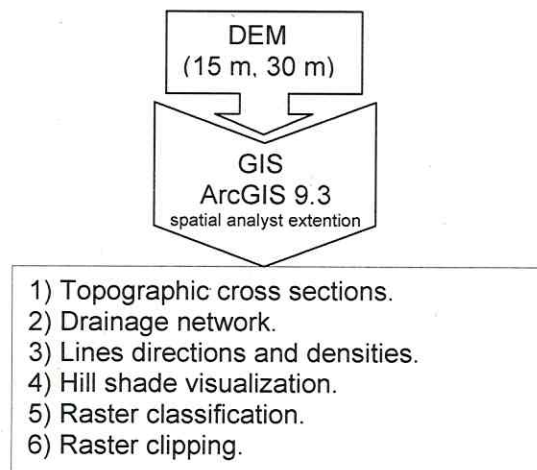
B) Simplified workflow for application of GIS in DEM.

Fig. 2.2: An integrated approach of remote sensing and GIS for drainage network extraction.

$$\frac{dz}{dt} = U - KA^m S^n \quad \text{(1)}$$

where dz/dt denotes the rate of change in the topographic elevation of a river during time. U is the uplift rate of the landmass, A is the catchment drainage area, S is its slope and K is its erodibility coefficient. The constants of m and n depend on basin hydrology, hydrologic geometry and the predominant erosion process. During steady state dz/dt is zero. Therefore the previous equation can be expressed as:

$$S = k_s A^{-\theta} \quad \text{(2)}$$

where the river steepness index k_s equals (U/K) and the concavity index θ equals (m/n). By combining the two equations (1) and (2) we get the equation:

$$U = k_{sn}^{\ n} K \quad \text{(3)}$$

Where k_{sn} is the normalized steepness index (Whipple & Tucker 1999).

2.1.3 Stream gradient index

The stream gradient index (Hack 1973) is defined as:

$$SL = (\Delta H / \Delta L)\, L \quad \text{(4)}$$

Where SL is the stream gradient index, $\Delta H / \Delta L$ is the gradient of the stream reach where the index is computed (ΔH is the drop in the topographic elevation of the reach and ΔL is the length of the reach) and L is the total stream length from the drainage divide to the center of the reach.

2.1.4 Basin asymmetry and similarity (hypsometry plot)

Two methods exist to evaluate the basin asymmetry: the transverse topographic symmetry factor method (T) and the asymmetric factor method (AF). An asymmetric factor (AF) can be applied over a relative large catchment area (Keller & Pinter 2002). Wadi Zerka Ma'in has a

29

small catchment area, therefore a transverse topographic symmetry factor (T) was applied, which evaluates the amount of asymmetry of a river within a catchment area and the variation of this asymmetry. The catchment area midline is the line of symmetry for the catchment. Mathematically, T denotes the ratio of the distance from the catchment area basin midline to the River (Da) and to the catchment area border as follow:

$T = Da/Dd$ (5)

The factor value varies from zero to one, which represents the minimum and the maximum value. Hypsometry refers to the distribution of the land area at different elevations. It has generally been used to infer the stage of geomorphic development and to study the influence of tectonics on topography (Hurtrez et al. 1999). The hypsometric curve is a plot of relative height (h/H) versus relative area (a/A) where:

(h) is the topographic elevation of a given location on the river.

(H) is the total topographic elevation.

(a) is the measurement (in km^2) of the area that is higher in elevation than the point of measurement.

(A) is the total area of the catchment.

Shahzad and Gloaguen (2009, 2010) developed TecDEM, a Matlab-based software for estimating and plotting stream profile analysis. TecDEM was used to estimate, extract and visualize stream profiles for the study area by using the 15 m DEM that was extracted from the Aster stereopair. The drainage network density (Dd) is defined as the ratio of the sum of the total stream length divided by the drainage catchment area (Knighton 1998). It is a spatial measurement of the drainage network geometry because it represents the degree of dissection of the drainage basin by surface streams (Keller et al. 1999). The spatial analyst extension in ArcGIS 9.2 was used to produce a drainage density map for the study area.

2.2 Groundwater chemistry analysis

Twenty-one water samples from wells and springs and two rainfall samples were collected during 2007 and 2008. For completion, another ten groundwater wells samples were included from Al Sawarieh (2005). The physiochemical parameters (EC, pH, temperature and Eh) were measured at the sampling sites by using a tetragon probe for measuring the EC value, a standard-hydrogen electrode was applied for measuring the redox value and pH-electrode (Calomel) for pH value. The pH probe was calibrated with buffer solution pH 4 and 7.

The coordinates of the samples and the elevation of the springs that representing the groundwater level were measured by a GPS instruments (Garmin 70) with a resolution of -/+10 meters. The groundwater levels in the wells were measured by the technical staff of ministry of water and irrigation (open file 2010).

The samples (60 ml bottles) were filtered (0.45 μm; cellulose-acetate) onsite. Water samples for cations and trace elements were acidified by adding 1 ml of 6 M HCl. Major ions were analyzed in the laboratory of the Helmholtz Centre for Environmental Research - UFZ (Germany) by inductively coupled plasma atomic emission spectrometry (ICP-AES) and using matrix adjusted standard solutions for calibration (Appelo & Postma 2005).

Ba, Cs, Rb, Y and U were analyzed by inductively coupled plasma mass spectrometry (ICP-MS) together with rare earth elements (REE). The detailed procedure for preparing REE analyses is described by Möller et al. (2006).

HCO3 was determined in the field by sulphuric acid titration. The standard H_2O–CO_2

equilibration method was used for the determination of isotope ratios of $^{18}O/^{16}O$ and $^2H/^1H$ in water by isotope ratio mass spectrometry (IRMS) with a delta S (Finnigan MAT) analytical precision of 0.1‰ (Epstein et al. 1953). The results of measurements are presented by delta notations δ18O and δ²H relative to the Vienna Standard Mean Ocean Water (V-SMOW).

2.3 Groundwater recharge modelling

Computed hydrological modelling is a primary technique for sustainable management of the water resources (Bier 2007). It is closely connected to GIS and remote sensing (RS). RS could provide multi-temporal and multivariate data of the land surface. GIS offers big capabilities of storage, manipulation and convergent analysis of the land surface data (Saraf et al. 2004). That synergism between GIS and RS technologies is a major advantage in the use of an integrated approach in the hydrological modelling (Trotter 1991). Therefore, an integrated approach of remote sensing and GIS was used to supply the hydrological model by the needed land surface data. Geomorphologically and geologically Wadi Zerka Ma'in catchment area is considered as a heterogeneous area (Salameh 1997, Shawabekeh 1998).

The hydrologic response unit (HRU) is a concept in the hydrological modelling and a prerequisite for hydrological modelling of heterogeneous cases (Flügel 1997). According to that concept, the area is subdivided in spatial distributed entities where each entity has spatial physiographic properties (Flügel 1997). Therefore, the catchment area within a physical boundary of groundwater modelling is divided by using the FeFlow 6 software to super mesh (Fig. 2.3, Fig. 2.4). The triangles of the finite elements of the super mesh will represent those entities while the needed spatial physiographic properties will be extracted by RS and attributed by the GIS.

2.3.1) Extraction physiographic characterisations layers of the study area

2.3.1.1) Elevation, slope and aspect

Digital Elevation Models (DEMs) are a type of raster GIS layer that represents any part of the world as a georeferenced regular arrangement of cells. In a DEM, each cell has a value corresponding to its elevation. DEMs analyses are widely used for modelling surface
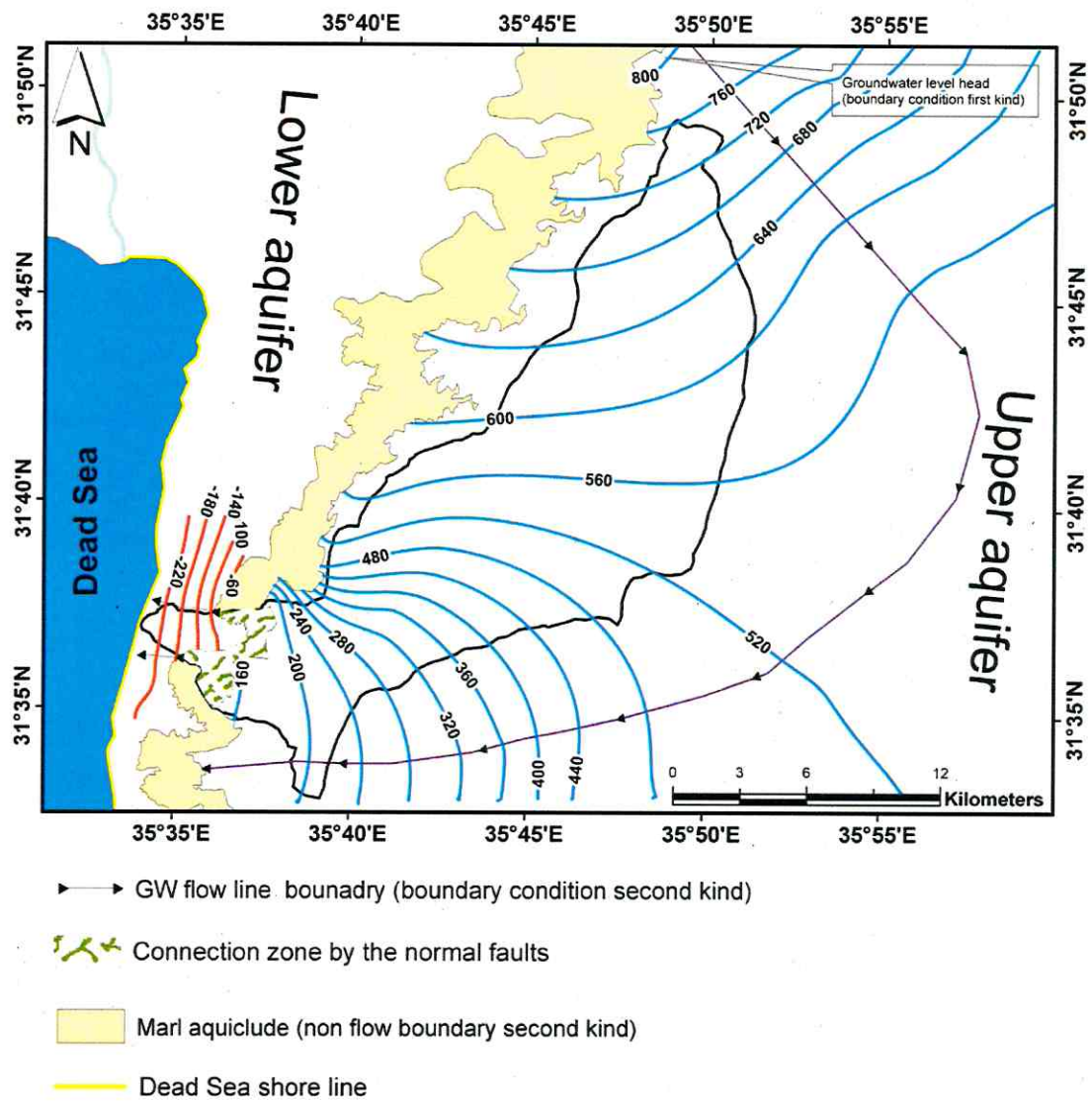
Fig. 2.3: A physical boundary of the groundwater flow of Wadi Zerka Ma'in catchment area.
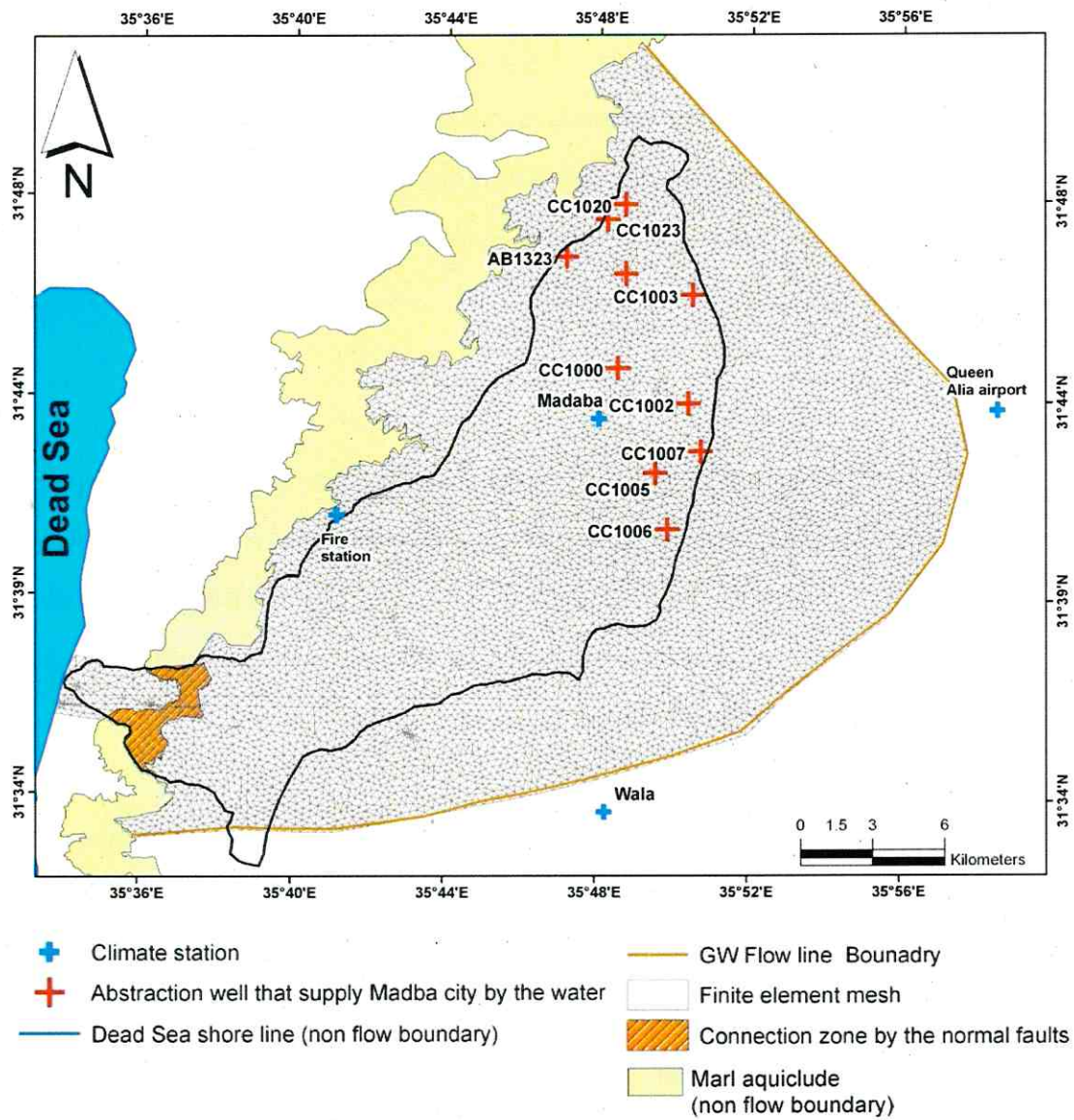
Fig. 2.4: Finite element mesh for the modelled area. Climate station of Ghour Al Safi locates south of the displayed area (see Figure 1.12).

hydrology. Those analyses include the automatic delineation of catchment areas, drainage networks extraction, slope angle estimating and slope aspect measuring. The accuracy of a DEM, which is able to replicate the hydrological reality of a catchment, is determined by the cell size (McMasteret 2002). Therefore, a high resolution DEM of up to 15 m was obtained from Advanced Space-borne Thermal Emission and Reflection Radiometer data (ASTER) (Fig. 2.5).

Runoff modelling is one of cardinal components in any groundwater recharge modelling (Bier 2007). Slope angle and slope aspect calculations are an integral part of any runoff modelling. As the slope angle increases, the velocity of surface runoff increases. On gentle slopes, water may temporarily pond and later infiltrate while on steep mountain sides, water tends to move downward more rapidly (Pruski 2002).

Owing to the irregular slope aspect, the runoff takes place in different directions. Components of both slope aspect and angle control the velocity and the volume of the runoff (Maidment 1993). The slope aspect and angle could be easily estimated using ArcGIS 9.3 with the spatial analyst extension. The used algorithm is the quadratic surface algorithm (Srinivasan and Engel 1991). Figure 2.6 and 2.7 show the slope aspect and angle.

2.3.1.2) Land cover classification

GIS technology has a remarkable capacity to store, retrieve, manipulate and display vast quantities of spatial and attributed data that are used in the hydrological modelling. However, some of the data which have a large spatial distribution must be obtained accurately from landsurface, such as the land cover data. This problem could be overcome by satellite remote sensing, such as ASTER images (Kam1995). Therefore, an integrated approach of remote

A)

B)
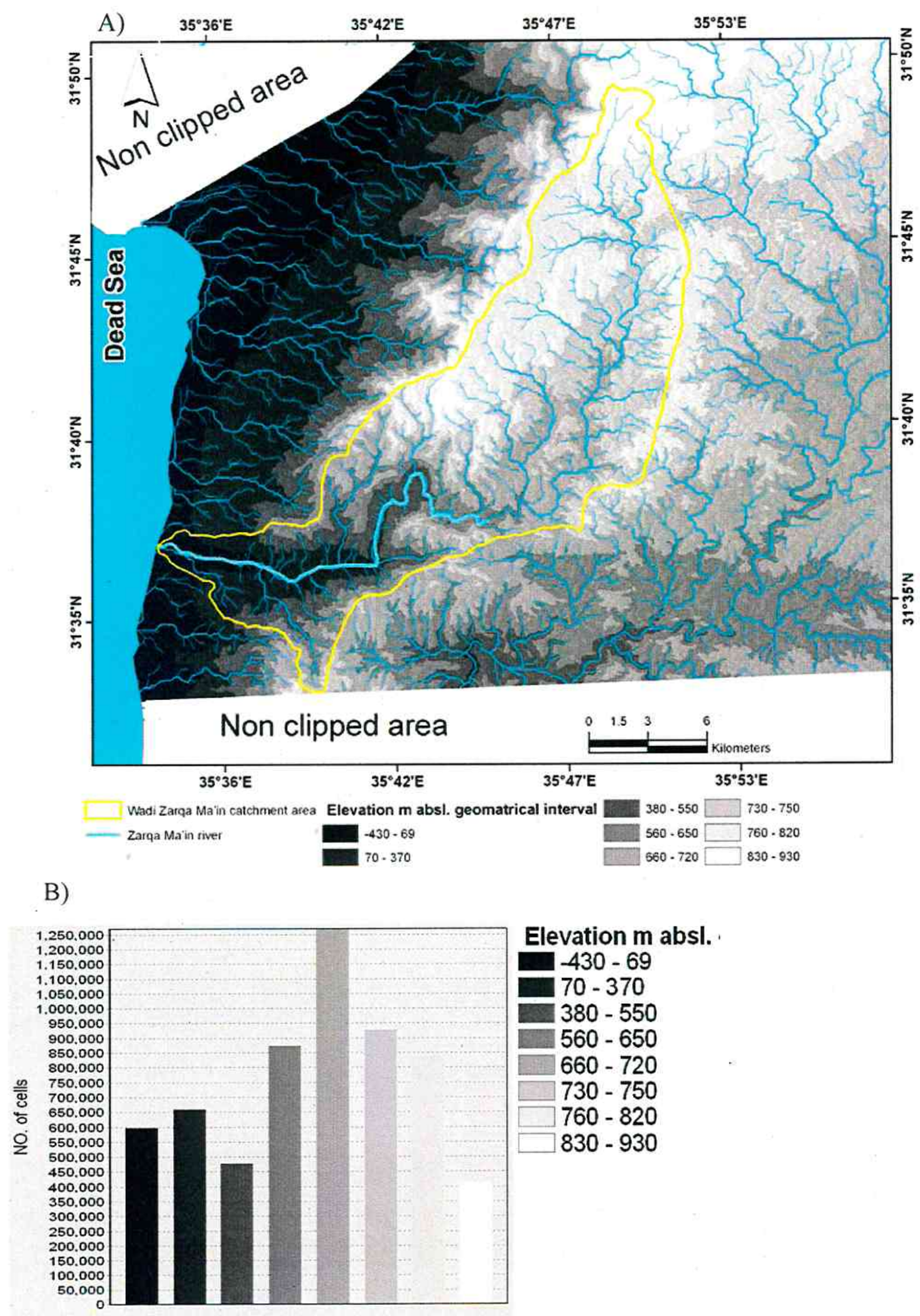
Fig. 2.5: DEM of the study area. A) The drainage network of the study area runs directional from the North to the West. B) Histogram of the elevation of the study area.
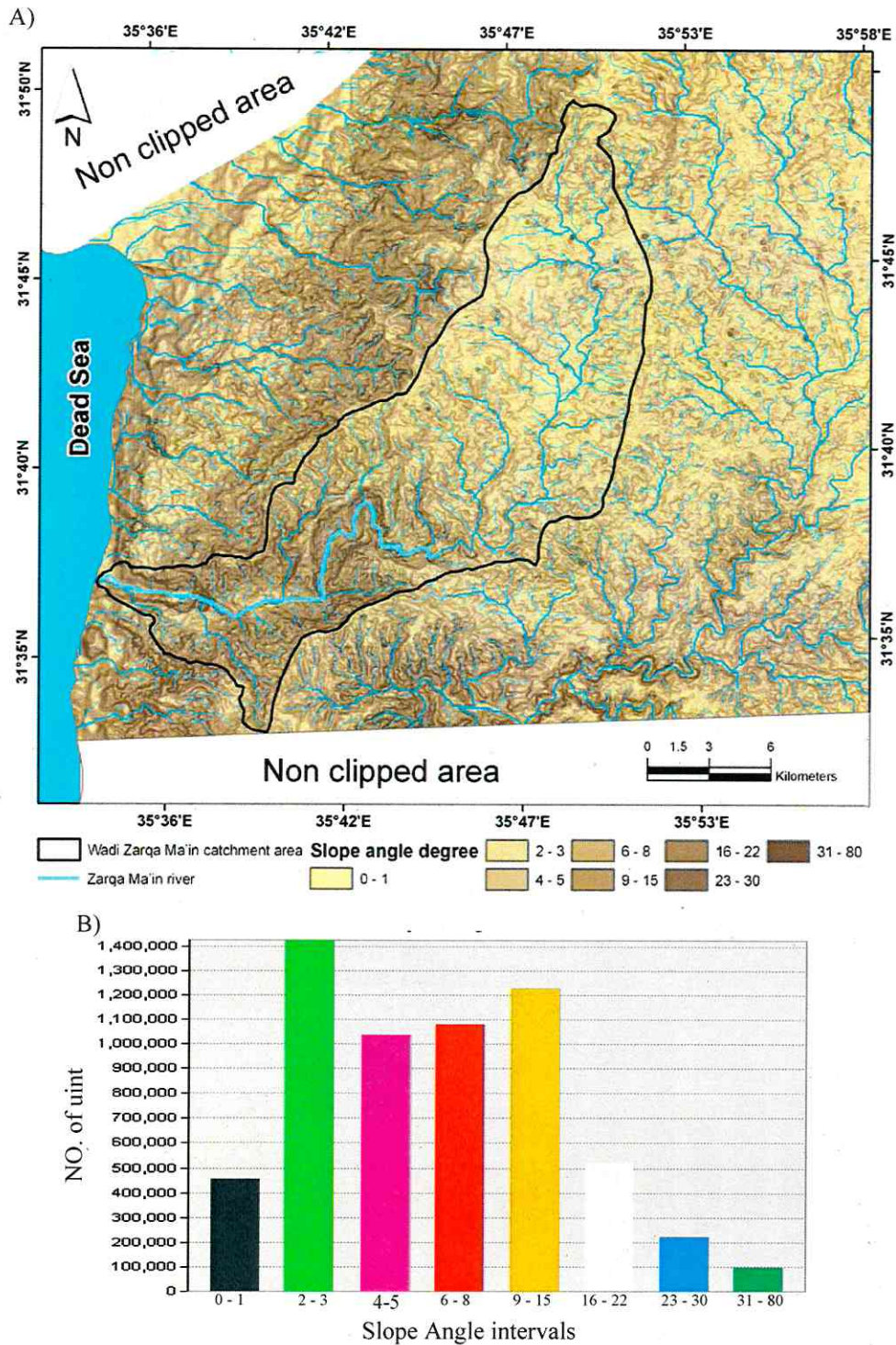
Fig. 2.6: A) Spatial distribution of slope in the study area. B) Frequency distribution of slope.
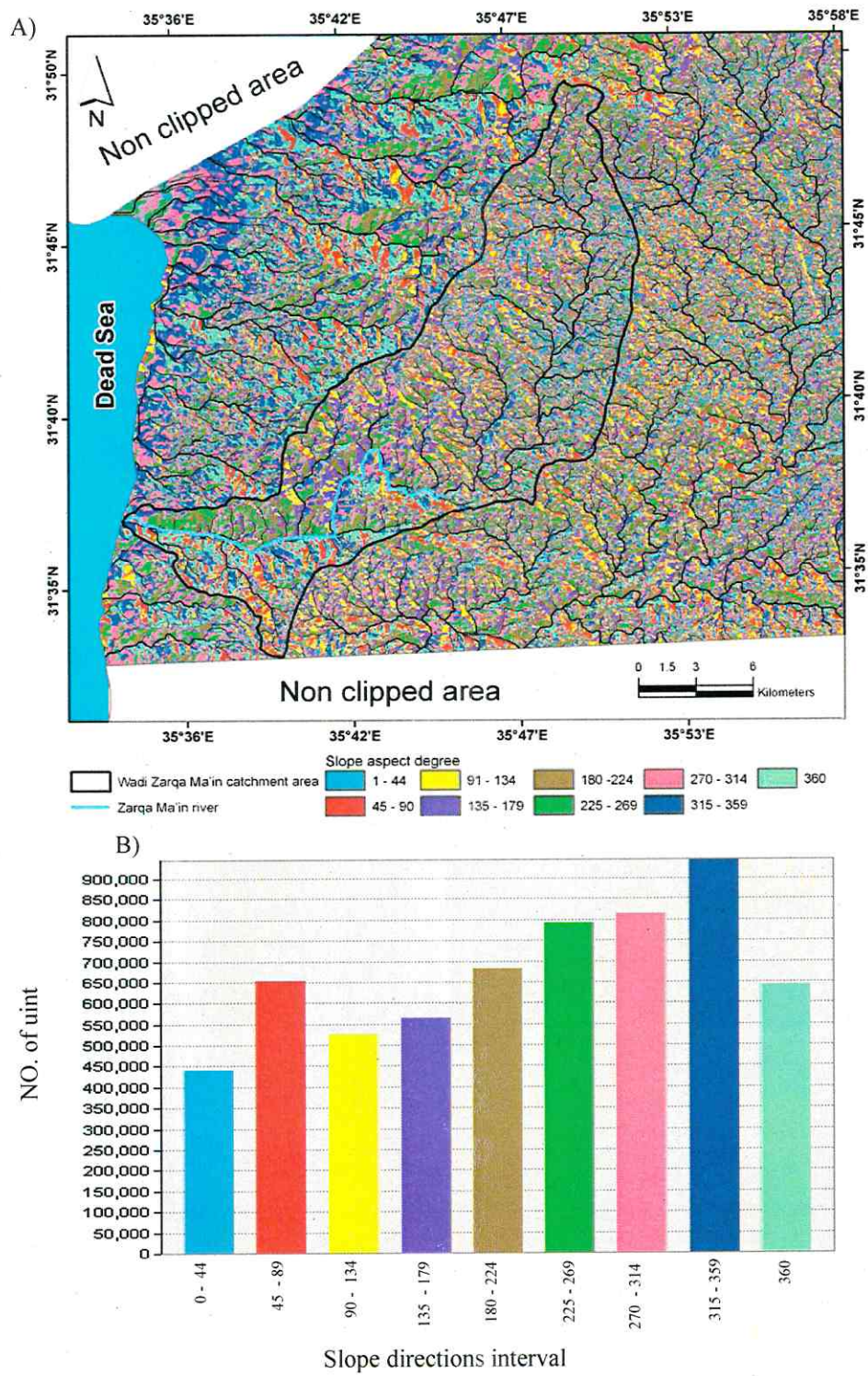
Fig. 2.7: A) Spatial distribution of aspect in the study area. B) Frequency distribution of slope.

sensing (RS) and geographic information system (GIS) was used to feed the model with the land cover data (Fig. 2.8). Supervised classifications of visible bands were performed to investigate the landuse while the supervised classifications of mid infra red bands were done to investigate the soil texture units.

2 Scenes georeferenced ASTER Image. 2005
(14 bands)

ArcGIS 9.2 Software

Clipping the region of interest from the scenes.

Envi 4.1 Software

1) Visible bands extraction (Fig. 2.9).
2) Middle infra red bands extraction (Fig. 2.10).

Supervised classification to make landuse map in raster format.

1) Converting the raster landuse map to a vector map.
2) Clipping Middle infra red band by soil vector layer.

Supervised classification to make soil textures map.

Fig. 2.8: Flow chart for extracting the landuse and the soil texture maps according to integrated approach of remote sensing and GIS.
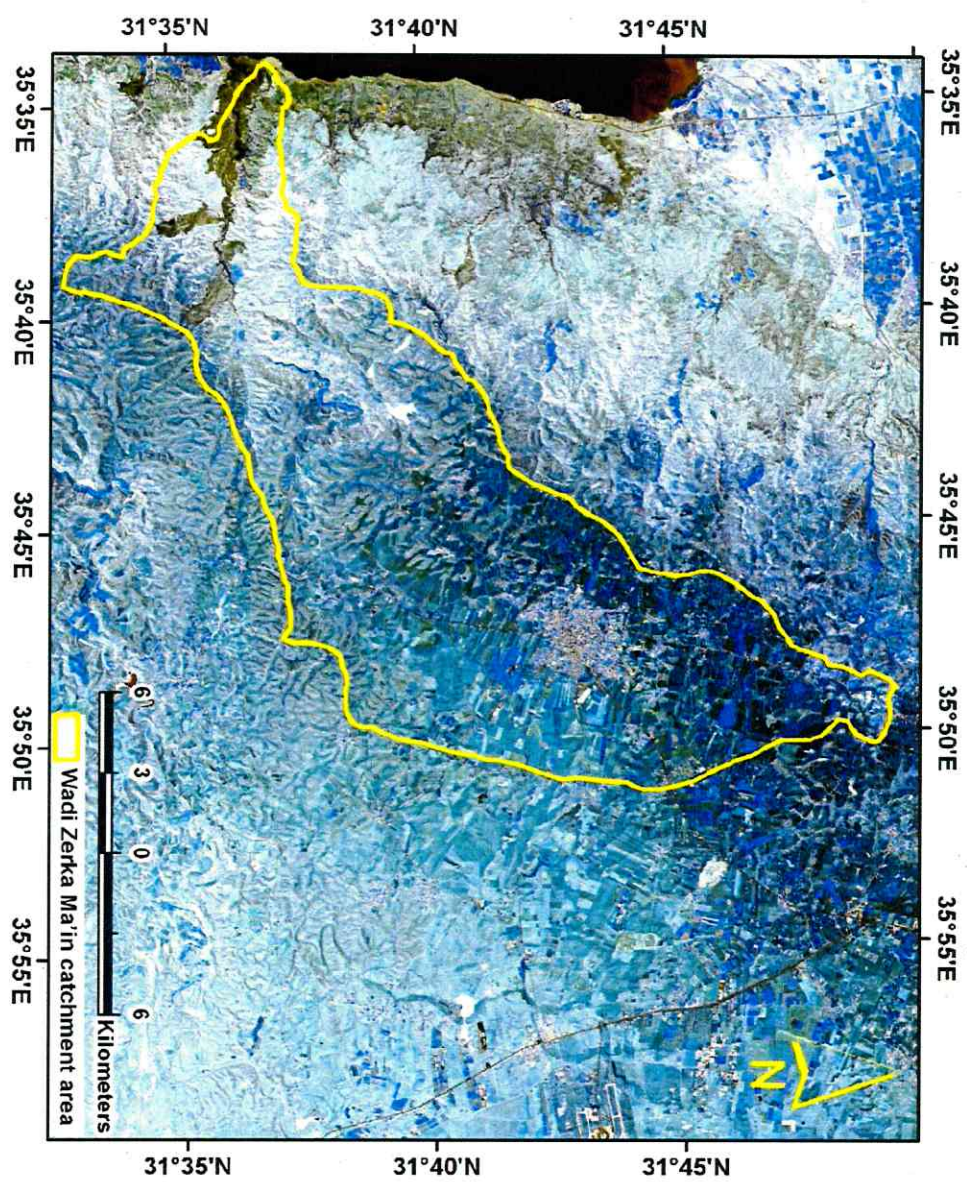
Fig. 2.9: Visible bands of the ASTR image of the study area.

Wadi Zerka Ma'in catchment area

31°35'N 31°40'N 31°45'N

35°35'E 35°40'E 35°45'E 35°50'E 35°55'E

9 3 0 6
Kilometers

N

42
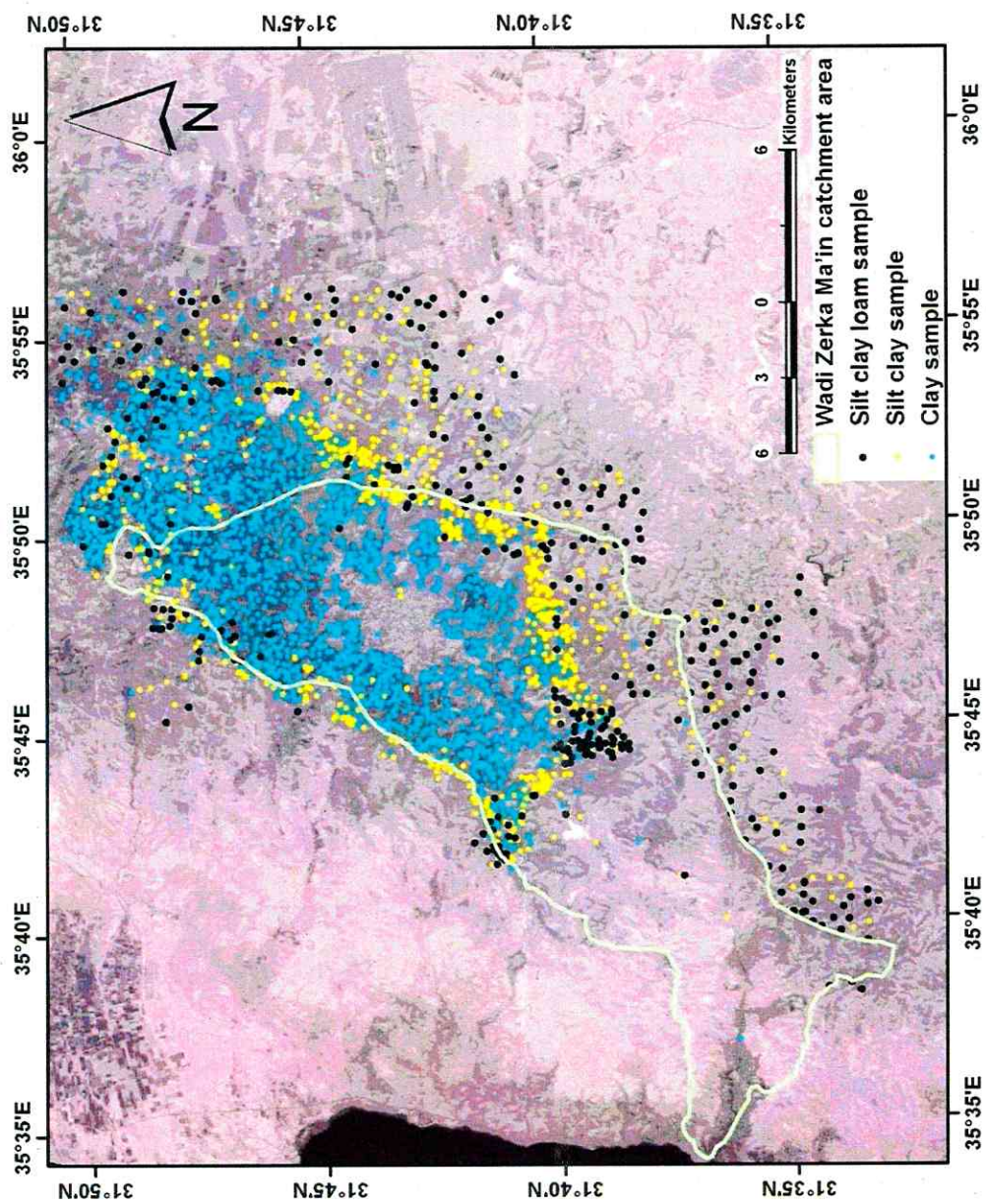
Fig. 2.10: Middle infra red bands of the ASTR image of the study area with superimposition of USDA 1993 samples.

2.3.1.3) Overlay physiographic characterisation layers and its super mesh

Overlay physiographic layers are one of the most common processes in GIS during hydrological modelling. It could create new layers and attributes relations by overlaying the physiographic layers (Coroza et al. 1997). According to the hydrologic response unit (HRU) concept, the heterogeneous catchment area is subdivided into cells where each cell is a homogonous unit of elevation slope, aspect and angel degree, soil texture, landuse class and climatological parameters. The super mesh was converted to HRUs by using the overlay method in GIS (Fig. 2.11). The climatological parameters were supplied for each HRU by the hydrological model software itself.

2.3.2) Hydrological modelling

A water balance equation is one of the most common methods to estimate the direct groundwater recharge of a catchment area. It has the advantages of being easy to apply and accounts for all the water entering the hydrological cycle. The method is essentially a book-keeping procedure which estimates the balance as follows:

$$Gr = P - Ea + \Delta S - Ro \qquad (6)$$

Where Gr = recharge; P = precipitation; Ea = actual evapotranspiration; ΔS = change in soil water storage and Ro = run-off. Five climate stations were used to obtain the available daily rainfall amount and the other climatological data that JAMS (Jena Adaptable Modelling System) software. The stations are: Queen Alai airport, Madaba, Main fire station, Wala and Ghour Al safi stations (Meteorological Department 2010, USDA 1993, Thornthwaite & Mather 1955). The spatial variability of the groundwater recharge is an important consideration, especially if the case study is heterogeneous geomoprhologically and climatologically such as the wadi Zerka Ma'in catchment area (Flügel 1997). Most of groundwater recharge estimation methods do not consider the spatial heterogeneity of the
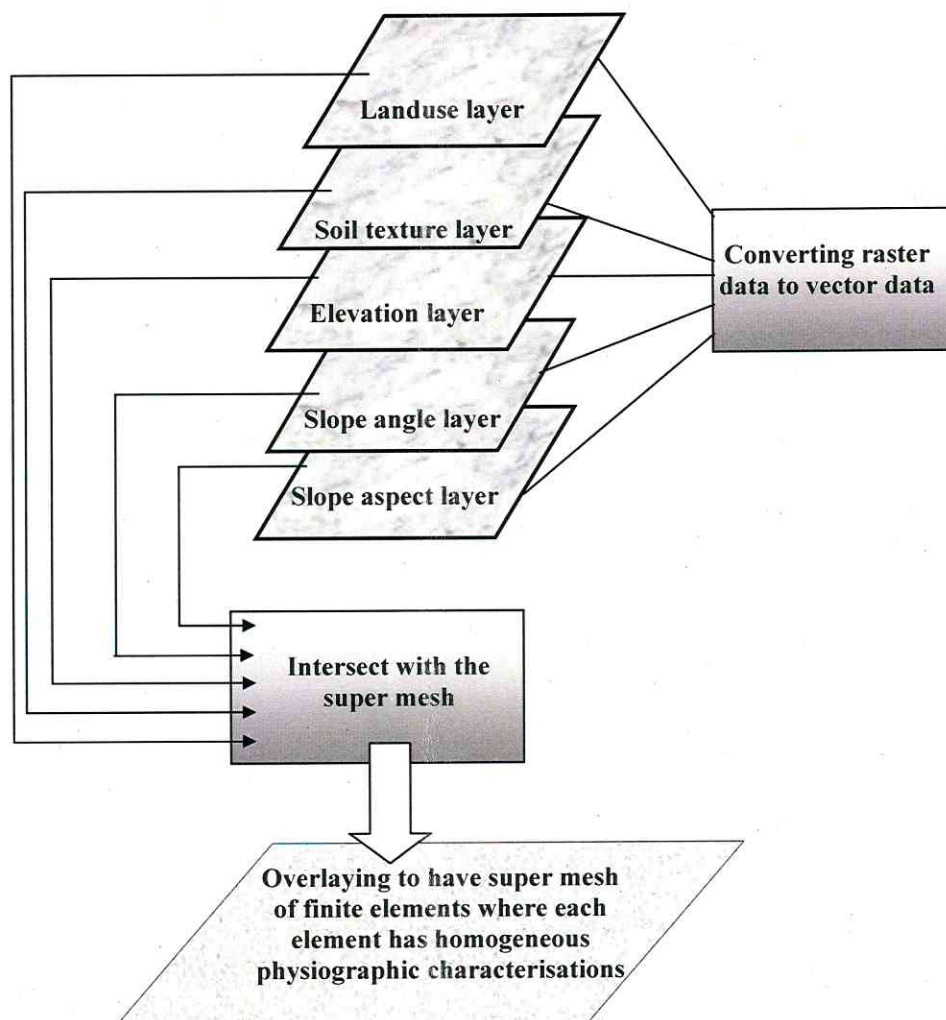
Fig. 2.11: Flow chart for generating HRUs by using the overlay method in GIS. The raster data of the soil, elevation and slope were converted to vector data in form of shape files before applying the overlaying method by using ArcGIS software.

45

catchment areas (Cook et al. 1989). However, the HRU method considers the heterogeneity of the catchment by subdividing the area into triangles, where each triangle is a homogenous unit of physiographic parameters, and then estimates the groundwater recharge accordingly. Hence, the catchment area is modelled not as one homogenous spatial unit.

Kralisch and Krause (2005) developed the Jena Adaptable Modelling System (JAMS) that use the Hydrological unit response HRU through the water balance estimation. However, JAMS was developed according to the Object Modelling System (OMS) that considers each model component and each item in the water balance equation as independent modules. These modules are coupled by a standardised software interface, JAVA software in case of JAMS, to achieve maximum platform independence (Kralisch et al. 2005). Accordingly, the main technical advantages of using JAMS software as HRUs modelling software are:

- The hydrological process simulation runs technically independently from the spatial representation of the HRUs. This causes a fast speed for simulation running proportionally to other software which uses the spatial representation during the hydrological simulation.

- JAMS has a capacity to use largely different configurations of the spatial and temporal data during the hydrological simulation.

- The climatological parameters that are recorded by the climate stations have the ability to distribute automatically and interpolate to all the HRUs.

- The result of the hydrological simulation could be represented by a GIS that has a capacity to store, manipulate, and analyses spatially.

2.3.2.1) Regionalization of climatic data

Regionalization of the five climate stations data was carried out by JAMS for HRUs of the study area. This generalization considering: 1) the distance between the climate stations and the HRUs and 2) the topographic elevation. It is achieved by the following steps:

1. Estimation of linear regression between the daily climatic data value and the topographical elevation of the stations. The coefficient of determination (r2) and the slope of the regression line (bH) of this relation is calculated assuming that the MW value is related linearly to the topographic elevation (H):

$$MW = a_H + b_H \cdot H \qquad (7)$$

The unknowns aH and bH are defined according to the Gaussian method of the smallest squares:

$$b_H = \frac{\sum_{i=1}^{n}(H_i - \overline{H})(MW_i - \overline{MW})}{\sum_{i=1}^{n}(H_i - \overline{H})^2} \qquad (8)$$

$$a_H = \overline{MW} - b_H \cdot \overline{H} \qquad (9)$$

The correlation coefficient of the regression is calculated according to the following equation:

$$r = \frac{\sum_{i=1}^{n}(H_i - \overline{H})(MW_i - \overline{MW})}{\sqrt{\sum_{i=1}^{n}(H_i - \overline{H})^2 \cdot \sum_{i=1}^{n}(MW_i - \overline{MW})^2}} \qquad (10)$$

2. Determining the stations which are closest to each HRU. The number of the stations, which needs to be entered during the parameterization, is dependent on the stations spatial network and on the position of the individual stations. The first step is to estimate the distance Dist(i) of each station to the area of interest:

47

$$Dist(i) = \sqrt{(RW_{stat(i)} - RW_{DF})^2 + (HW_{stat(i)} - HW_{DF})^2}$$

RW ... easting of the station i...n, or the HRU (DF)

HW ... northing of the station i...n, or the HRU (DF)

The stations with the closest distance to HRU are chosen from the distances calculated according to the equation above and are then used for potenzialization with the weighting factor pIDW. Accordingly, those distances are converted to weight distance wDist(i) where the influence of nearby stations increase and the more distanced stations decreased.

3. By using Inverse Distance Weighting (IDW) the weightings of the stations are determined dependent on their distances to each HRU. The IDW-method is used to consider the horizontal variability of the station data. The estimation is carried out according to the following equation:

$$W(i) = \frac{\left(\frac{\sum_{i=1}^{n} wDist(i)}{wDist(i)} \right)}{\sum_{i=1}^{n} \left(\frac{\sum_{i=1}^{n} wDist(i)}{wDist(i)} \right)} \qquad (12)$$

4. The calculation of the data value for each HRU with the weightings is estimated in the previous steps (Kralisch et al., 2005 Fugel et al. 1997 and Kralisch & Krause 2005, http://www.geogr.uni-jena.de/jamswiki/index.php).

2.3.2.2) Water balance modules

2.3.2.2.1)   Evapotranspiration: the   potential   evapotranspiration   and   the   actual evapotranspiration of the soil layers were estimated according to the Penman-Monteith

method (Monteith 1965) for each HRU that attributed to the requested data by using an overlay method in GIS. However, because the estimation is complicated and time-consuming, it was out sourced into the pre-processing part of the modelling. The only parameter that is used in the estimation and extracted during the modelling is the soil moisture. Two evaporation values are estimated for each day as a time period, a day value and a night value. This distinction is important because of the net radiation balance. The estimation for the day and for the night was done and then summed together.

2.3.2.2.2) Soil Water

The soil water module of JAMS software consists of two components: A) infiltration and evapotranspiration (process units) and B) storage units (middle pore, large pore storage and depression storage). The infiltration estimation is done by applying the following empirical equation:

$$Inf = (1 - soil_{sat}) \cdot maxINF \; [\text{mm/d}] \quad (13)$$

Where maxINF is in mm/d and is defined by the user. The relative saturation deficit of the soil (1 - soil$_{sat}$) is estimated according to the maximum filling storage of the middle and large pores as follow:

$$soil_{sat} = \frac{(MPS_{act} + LPS_{act})}{(MPS_{max} + LPS_{max})} \; [-] \quad (14)$$

Where MPS$_{act}$, MPS$_{max}$ ... actual, maximum filling of the middle pore storage.

LPS$_{act}$, LPS$_{max}$ ... actual, maximum filling of the large pore storage.

When the amount of water that infiltrates is more than the maximum infiltration rate (maxINF) the surplus water is converted to surface runoff. Jamas software considers the effect of the surface gradient at two gradients mainly as follow:

1) Surface gradient greater than 80% then only 25% of the precipitation is infiltrated.

49

2) Surface gradient less than 80% only 60% of the precipitation is infiltrated.

The infiltrated precipitation is routed to the middle pore storage and the large pore storage. The influx in the MPS (MPS$_{in}$) is the result of the infiltrated precipitation (Inf) against its relative storage content (ΘMPS) and a calibration coefficient (Dist coef) that is entered by the user. Mathematically, MPSin is represented by the following equation:

$$MPS_{in} = Inf \cdot \left(1 - e^{\left(\frac{-1 \cdot Distcoef}{\Theta MPS}\right)}\right) \ [\text{mm}] \qquad (15)$$

The infiltrated amount of precipitation water that is not absorbed by the MPS is received by the large pore storage (LPS$_{in}$):

$$LPS_{in} = Inf - MPS_{in} \ [\text{mm}] \qquad (16)$$

The value of the calibration coefficient ranges between zero (when no water can flow into the MPS) and infinite. The discharge from the MPS is represented by the evapotranspiration (ETP), which is calculated from the current storage filling of the MPS and the potential ETP.

The percolation water movement (perc) runs in the LPS and is therefore dependent on the amount of the large pores. To estimate the amount of that water, the runoff component needs to be estimated. The runoff is estimated against the relative saturation of the soil (soilsat), the actual large storage content (LPSact) and a calibration coefficient (LPSout) as follow:

$$LPS_{out} = \left(soil_{sat}\right)^{LPSout} \cdot LPS_{act} \ [\text{mm}] \qquad (17)$$

The following allocation of the LPS runoff in the vertical and lateral (inter) flow direction is carried out against the slope and a user specific calibration factor (LatVertDist) which can take values between zero and infinite. Accordingly, the following two equations are estimated: $\quad inter = LPS_{out} \cdot (\tan(\text{Slope}) \cdot LatVertDist) \ [\text{mm}] \qquad (18)$

$$perc = LPS_{out} \cdot (1 - \tan(\text{Slope}) \cdot LatVertDist) \; [\text{mm}] \quad \text{(19)}$$

(Kralisch et al., 2005 Fugel et al. 1997 and Kralisch & Krause 2005, http://www.geogr.uni-jena.de/jamswiki/index.php).

2.3.2.2.3) Runoff

The retention mechanisms of the runoff were described by the other soil water module. Therefore with this module only the HRUs influxes and discharges are allocated. The routing of the runoff generation is divided into:

A) Lateral routing: where the HRU could have several influxes but only one discharge. The order of the HRUs, as receiver, is specified by the topologic ID of the HRU dataset that was generated by the overlay method in GIS. By that data set, it is also specified which HRUs finally drain as receiving stream.

B) Reach routing: This is for the flow phenomena in the channel and the calculation of the rapidity of flow according to Manning and Strickler equation (Gauckler 1867). Jamas software applies this equation as follow:

1) Extracting the runoff retention coefficient (Rk). According to the following equation:

$$Rk = \frac{v}{fl} \cdot TA \cdot 3600 \; [-] \quad \text{(20)}$$

The parameter (TA), which needs to be set, is the routing coefficient. It measures the travel time of the discharge which moves from the channel to the runoff after the precipitation event. The parameter v is the stream's rapidity flow and fl is the flow length.

2) Calculating the rapidity of flow (v_{new}). Where (M) is a roughness factor, (I) is the slope of the river bed and (Rh) is the hydraulic radius as follow:

$$V_{new} = M \cdot Rh^{\frac{2}{3}} \cdot I^{\frac{1}{3}} \; [\text{m}^3/\text{s}] \quad \text{(21)}$$

51

The hydraulic radius (Rh) is estimated from the cross section of the river part where the water flows through (A), flow passage (q), the rapidity of flow (v) and the width of the river (b) as follow:

$$Rh = \frac{A}{b + 2\frac{A}{b}} \ [m] \qquad (22)$$

$$A = \frac{q}{v_{init}} \ [m^2] \qquad (23)$$

The initial rapidity (v_{init}) of flow is assumed to be 1 m/s, which is then iteratively matched with the new calculated rapidity of flow (v_{new}) until the deviation of both speeds are less than 0,001 m/s. Finally, the discharge of the particular river part (q_{act}) is calculated with the generated runoff retention coefficient (Rk) as follow:

$$Discharge = q_{act} \cdot e^{\left(\frac{-1}{Rk}\right)} \ [m^3/s] \qquad (24) \qquad \text{(Kralisch et al. 2005 Fluegel et al. 1997}$$

and Kralisch & Krause 2005, http://www.geogr.uni-jena.de/jamswiki/index.php).

2.4 Groundwater flow modelling

2.4.1 Three dimensional geological model and discretization

A three-dimensional (3D) geological model is the basis for creating a 3D hydrogeological model. It represents the geometry of the hydrogeological units that have the exact geometry of the geological layers (Zhang et al. 1997). The detailed borehole data of the wells in the study area is limited. Therefore, the 3D geological model was done through constructive interpolation of geological cross sections, by using the GMS 6.5 software, instead of using only limited boreholes data.

Topographical cross sections were generated from DEM by ArcGIS 9.3 using spatial analyst extension, which then were converted to geological cross sections and calibrated by the limited actual borehole data. However, boreholes data were extracted from the geological cross sections and inserted in the GMS 6.5 software to build the cross sections and make the constructive interpolations (Fig. 2.12), (Fig. 2.13). The geological layers, of the 3D geological model, were unified into three hydrogeological units and clipped according to the hydrogeological boundaries by the FeFlow software 6.5 (Fig. 2.14).

The discretization of the hydrogeological units were done by FeFlow 6 with the finite element method that considers the concaved hydrogeological boundaries of the studied area (Trefry & Muffels 2007). The total discretized area is about 611.25 km^2 with 15936 elements. It was considered having more small elements within the fault zones for representing the hydrogeological heterogeneity. The detailed hydrogeological parameters of the hydrogeological units are described in section 1.2.1 (page 10).

Formation symbol

- URC
- MCM
- AHP
- ASL
- WG
- WSL
- FHS
- NL
- KS
- Dr+Mn
- Ul
- IN
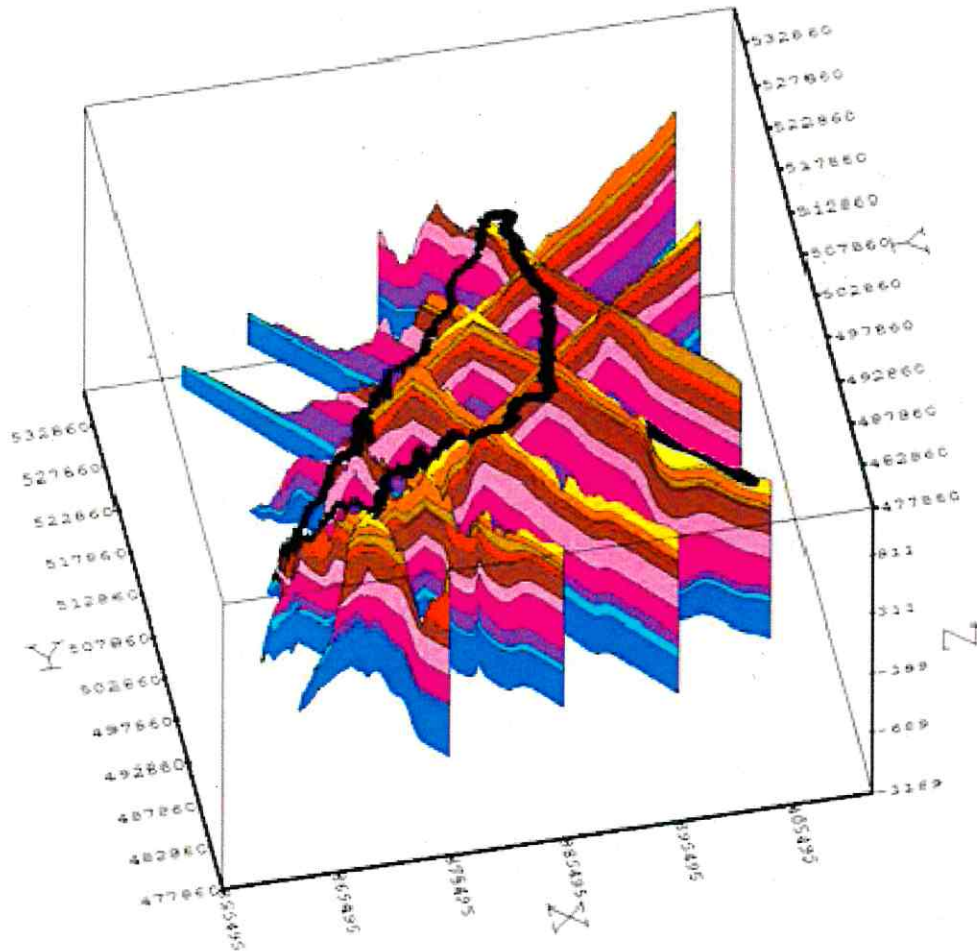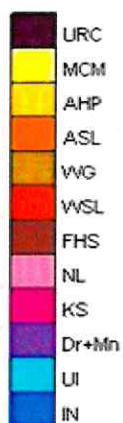
Fig. 2.12: Automatic cross sections generated from the 3D geological model. The black line, at the top of the formations, indicates for the catchment area brooder.

Formation symbol

■	URC
■	MCM
■	AHP
■	ASL
■	WG
■	WSL
■	FHS
■	NL
■	KS
■	Dr+Mn
■	UI
■	IN
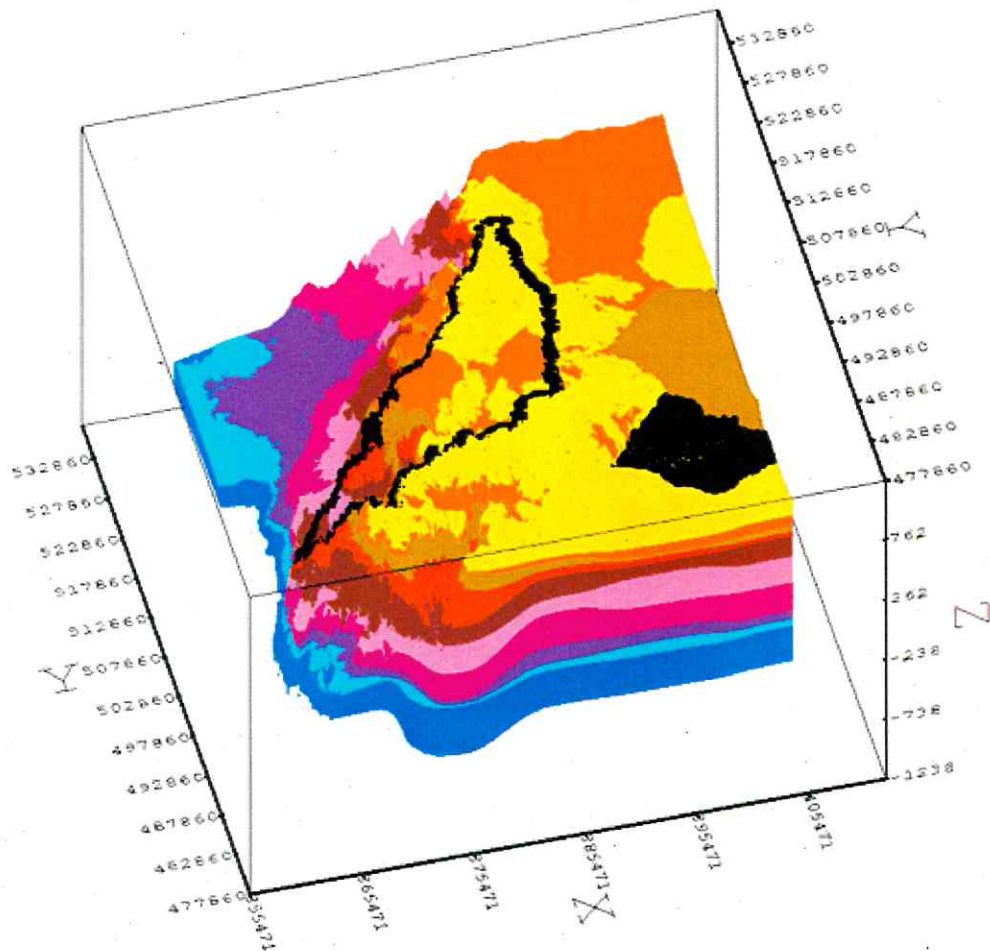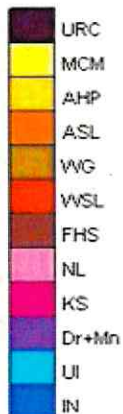
Fig. 2.13: Constructive 3D geological model by using GMS 6.5 (the vertical and horizontal coordinates are in meters). The black thick line, at the top of the formations, indicates for the catchment area brooder.

55
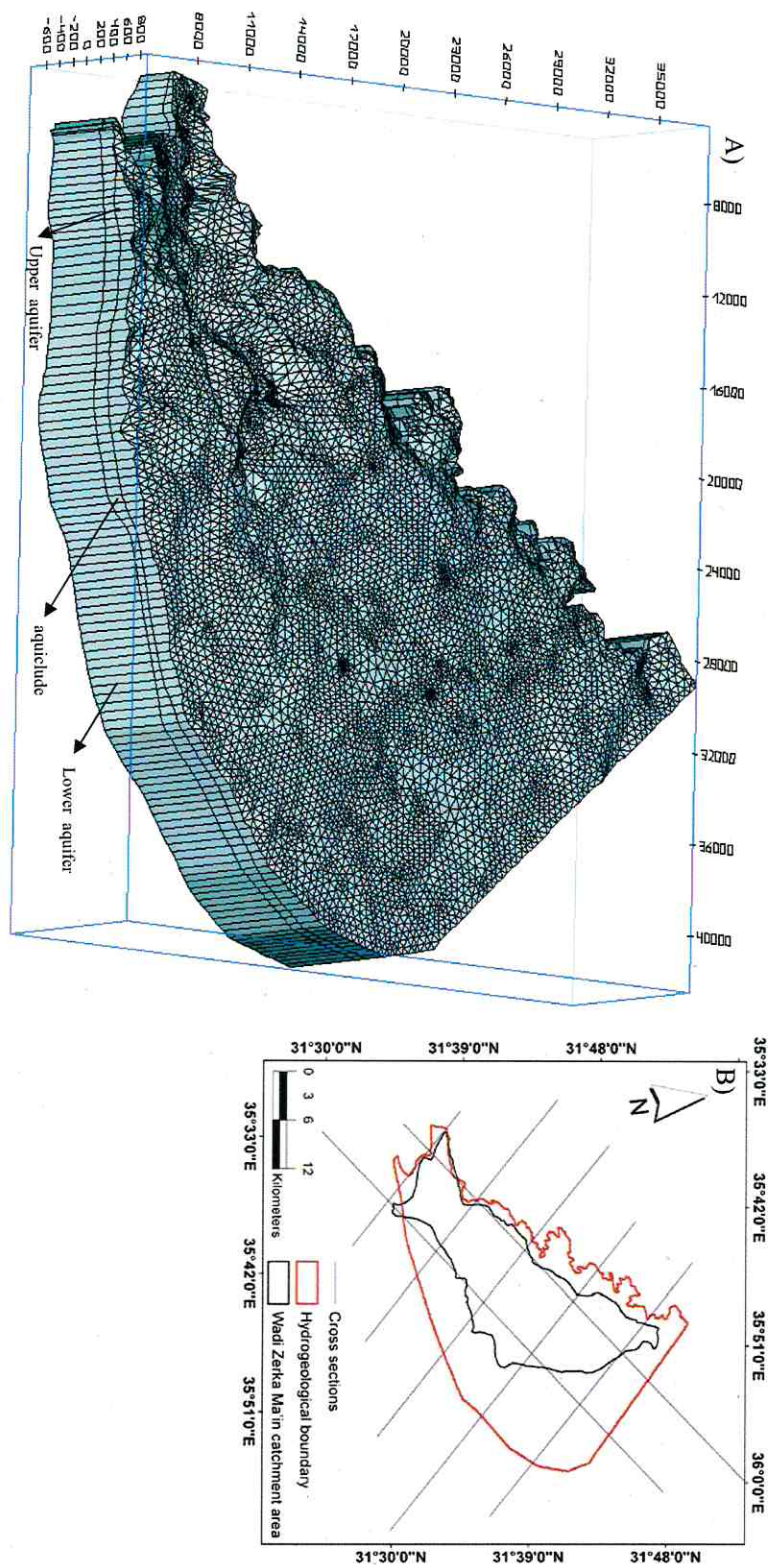
Fig. 2.14: A) Vertical and horizontal discretisation of the 3D geological model. B) The 3D geological model was clipped by the hydrological boundaries and the geological layers were unified to three hydrogeological units and discritized to finite elements by using the FeFlow 6.5 software. Numerical groundwater modelling was done only for the upper aquifer (see fig. 3.26). However, the lower aquifer was included only in the model geometry.

Groundwater flow within an aquifer is governed by the hydraulic head, which is a combination of water pressure, elevation and velocity (Fitts 2002).

Darcy's law describes the groundwater flow as $Q = K \cdot I \cdot A$; where Q is the volumetric flow rate (or discharge), A is the area that the groundwater is flowing through, I is the hydraulic gradient and K is a constant of the hydraulic conductivity (Fig. 2.15). The hydraulic gradient is defined as the different difference in the hydraulic heads divided by the flow length. Porosity and permeability are a component of hydraulic conductivity.

Groundwater flow in faulted aquifers is considered as one of the most complex groundwater systems because of the different heterogeneous hydraulic conductivity zones as well as the hydrologic barriers and conduits between the hydrogeological units that are generated during the faulting process (Allen & Michel 1999, Smith et al. 1990). Therefore, numerical groundwater modelling was used to estimate and generate the hydraulic conductivity zones.
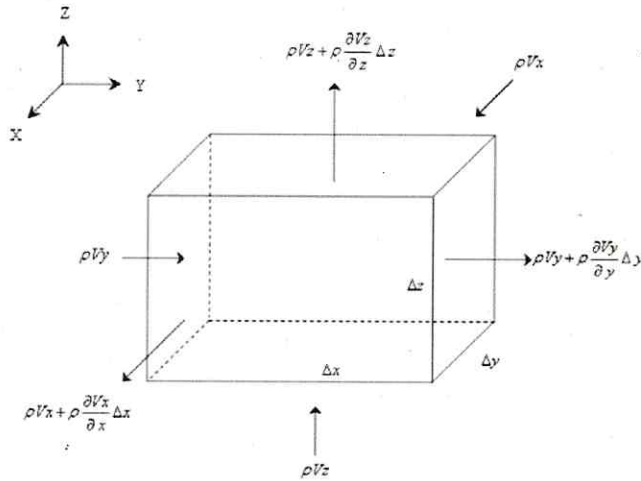
1) $v = \dfrac{Q}{A} = -K\left(\dfrac{dh}{dl}\right)$

2) $\dfrac{\partial v_x}{\partial x} + \dfrac{\partial v_y}{\partial y} + \dfrac{\partial v_z}{\partial z} = 0$

3) $\dfrac{\partial}{\partial x}\left(K_x \dfrac{\partial h}{\partial x}\right) + \dfrac{\partial}{\partial x}\left(K_y \dfrac{\partial h}{\partial y}\right) + \dfrac{\partial}{\partial z}\left(K_z \dfrac{\partial h}{\partial z}\right) = 0$

The velocity components in the x, y and z directions have been denoted as V_x, V_Y, V_z respectively.

Where A represents the area, V the velocity, Q the discharge, K the hydraulic conductivity, h the hydraulic head and l distance length.

Equation 1 represents the net mass flow per unit time through the cube.

Equation 2 (Darcy's law) represents the relation between the velocity and potentiometric gradient.

Equation 3 represents the substitutions of the two equations.

Fig. 2.16: Groundwater flow equations at steady state (modified after Freeze and Cherry 1979).

2.4.2 Groundwater flow model boundaries

The boundaries of a groundwater flow model determine the simulated flow domain. That domain should be expanded horizontally and vertically to coincide with the hydrogeological boundaries of the aquifer, and should also consider the physical conditions and directions of groundwater flow (Anderson & Woessner 2002). According to the partial differential equations of the groundwater flow, there are three types of boundaries that are used to simulate the flow (Tab. 2.1) (Anderson & Woessner 2002 and Trefry & Muffels 2007).

Tab. 2.1: The three common mathematical boundary conditions specified in mathematical analyses of groundwater flow systems (Franke et al. 1987)

Boundary kind and name	Formal name
Kind 1 (Specified head)	Dirichlet
Kind 2 (Specified flow)	Neumann
Kind 3 (Head-dependent flow)	Cauchy

In the study area, there is a groundwater head (first kind boundary) over the top of the catchment area (Fig. 2.17) with a length of 3.16 km where the hydraulic head is 800 m (absl.). A groundwater flow line with a length of 23.63 km was considered as boundary (second kind boundary); the extent of the meandered bed line of the aquiclude layer with a length of 62.14 km was considered as non-flow boundary (see figure 2.3).

59
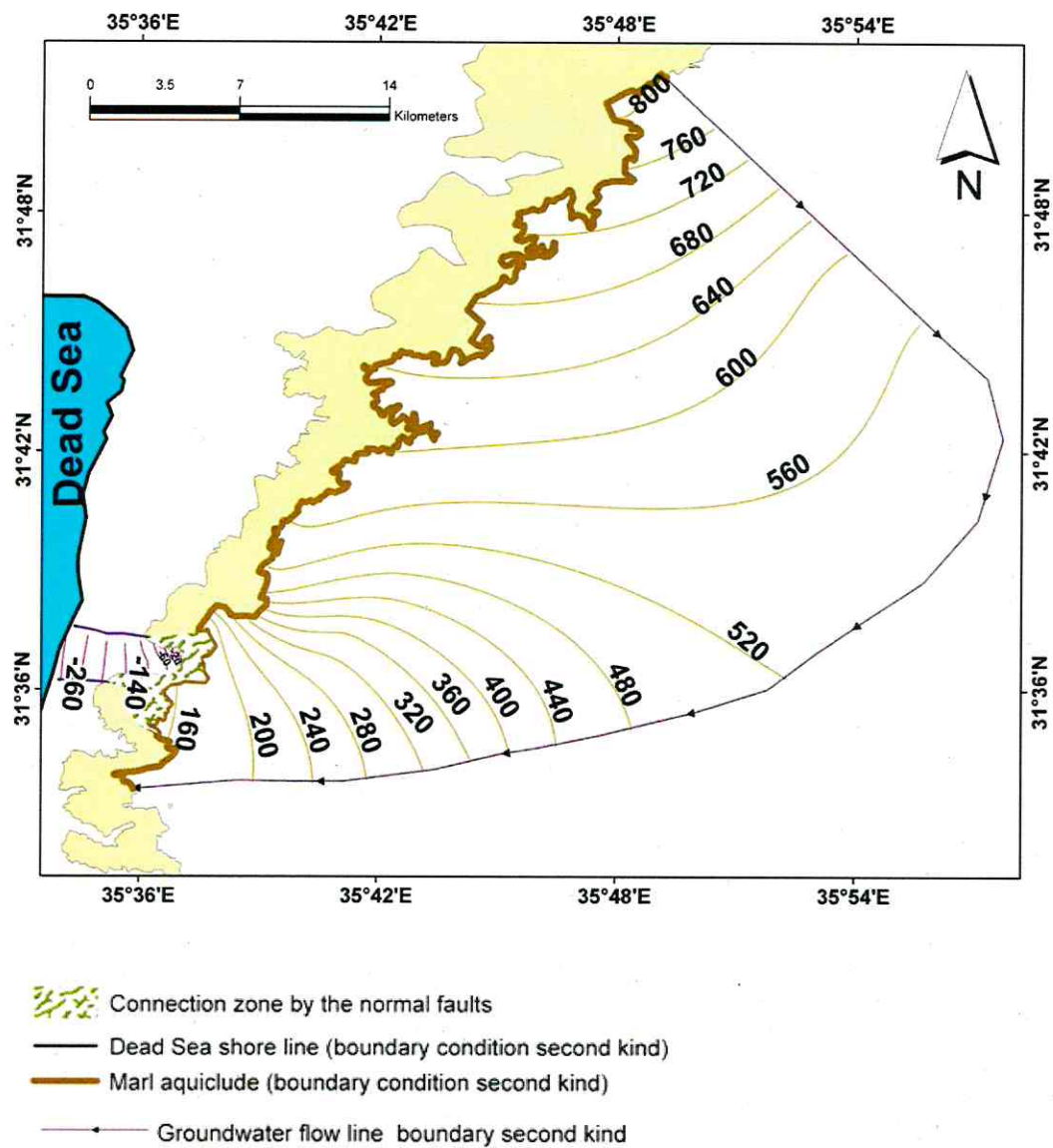
Fig. 2.17: Boundary conditions of the groundwater flow model. The details descriptions of the boundary conditions are in figure 2.3.

Chapter 3

Results and discussions

3.1 Structural geology

Studies of extensional basins in arid to semiarid regions have demonstrated that changes in fault geometries divide the earth surface into geomorphic and tectonic segments, characterized by different surface processes (Hilley et al. 2003 and Burbank & Anderson 2008). A Wadi is a depression in earth surface plains that could be associated with fault geometry. The study of the fault geometry includes two aspects: (1) types of displacement of rocks blocks and (2) tectonic expressions of faulting (Burbank & Anderson 2008). These aspects could be investigated through the geomorphic expressions of faulting. Therefore, the geomorphology of the faulted catchment area was studied in order to determine the type of the major and minor fault systems as follow:

3.1.1 Drainage network and fault directions

The study area is a part of the Dead Sea Rift Valley that is considered as an active tectonic region (Shtober-Zisu et al. 2008). In tectonically active regions the drainage network reflects the interaction between surface processes and the growth and propagation of underlying faults (Ribolini & Spagnolo 2008). Figure 3.1 shows that the drainage network directions of Wadi Zerka Ma'in catchment area follow the NNE-SSW fault system that is parallel to the Dead Sea transform fault, and the WWN-EES fault system that is normal to the Dead Sea transform fault. However, the effects of the NW-SE faults are limited and found mostly in the upper part of the catchment area.

The drainage density of a catchment indicates the landscape dissection and runoff potential. A

61
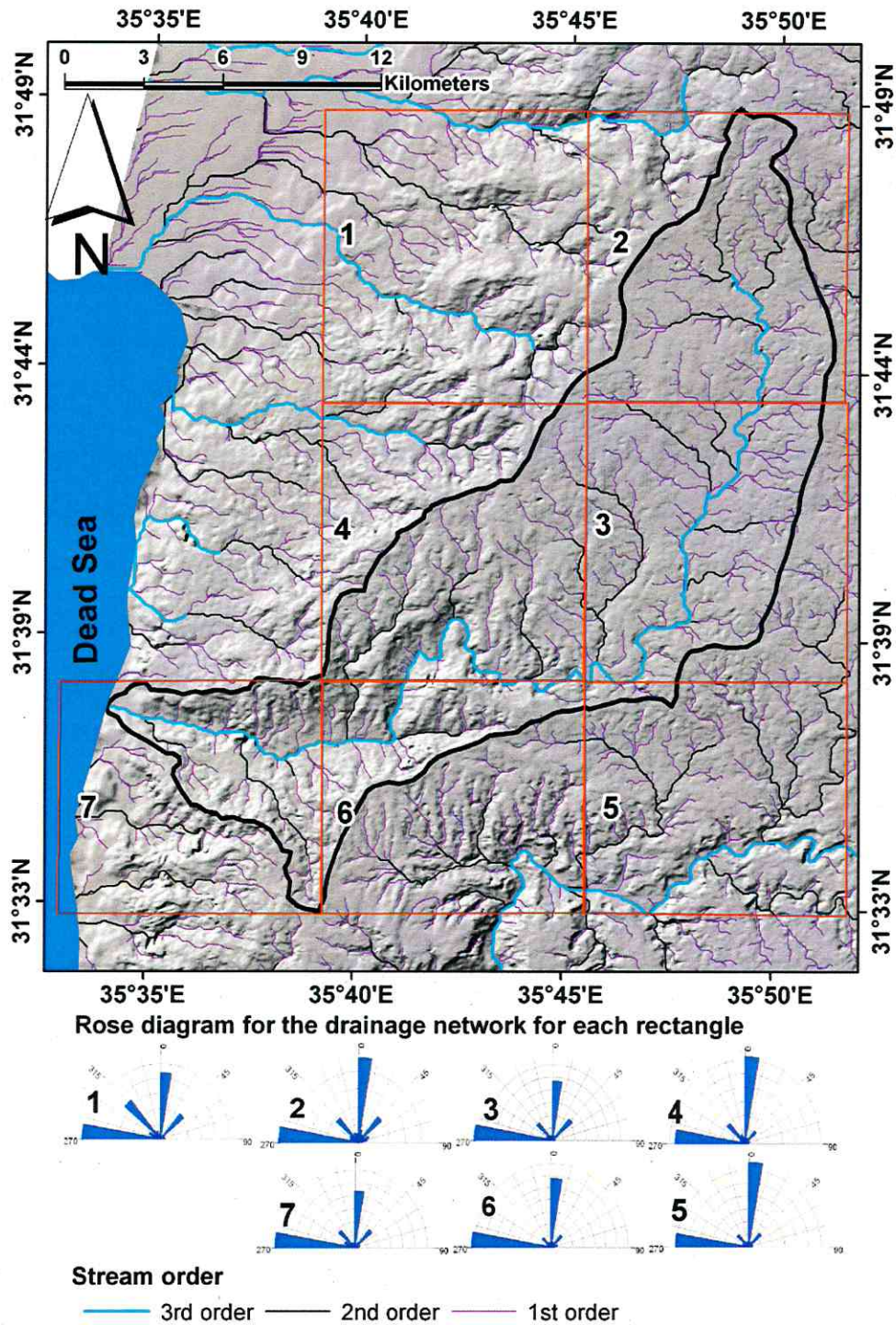
Fig. 3.1: Drainage network directions in the study area. The study and the surrounding areas were divided into 7 rectangles. The rose diagrams were generated for each rectangle alone and for all the streams orders.

low value of drainage density indicates a highly permeable landscape, with a small potential for runoff. A high value of drainage density indicates a highly dissected surface (Dinesh 2008). In tectonically active areas like the Dead Sea Rift Valley, faults are the generators of that dissected surface (Burbank & Anderson 2001). Hence, the highest drainage density directions in the studied area have the same directions as the fault systems, NNE-SSW and WWN-EES (Fig. 3.2). Drainage density value is between 1.6 to 2.8 km/km² for these directions. This indicates that the drainage network was generated simultaneously with the NNE-SSW and WWN-EES fault systems and is under structural control along these trends.
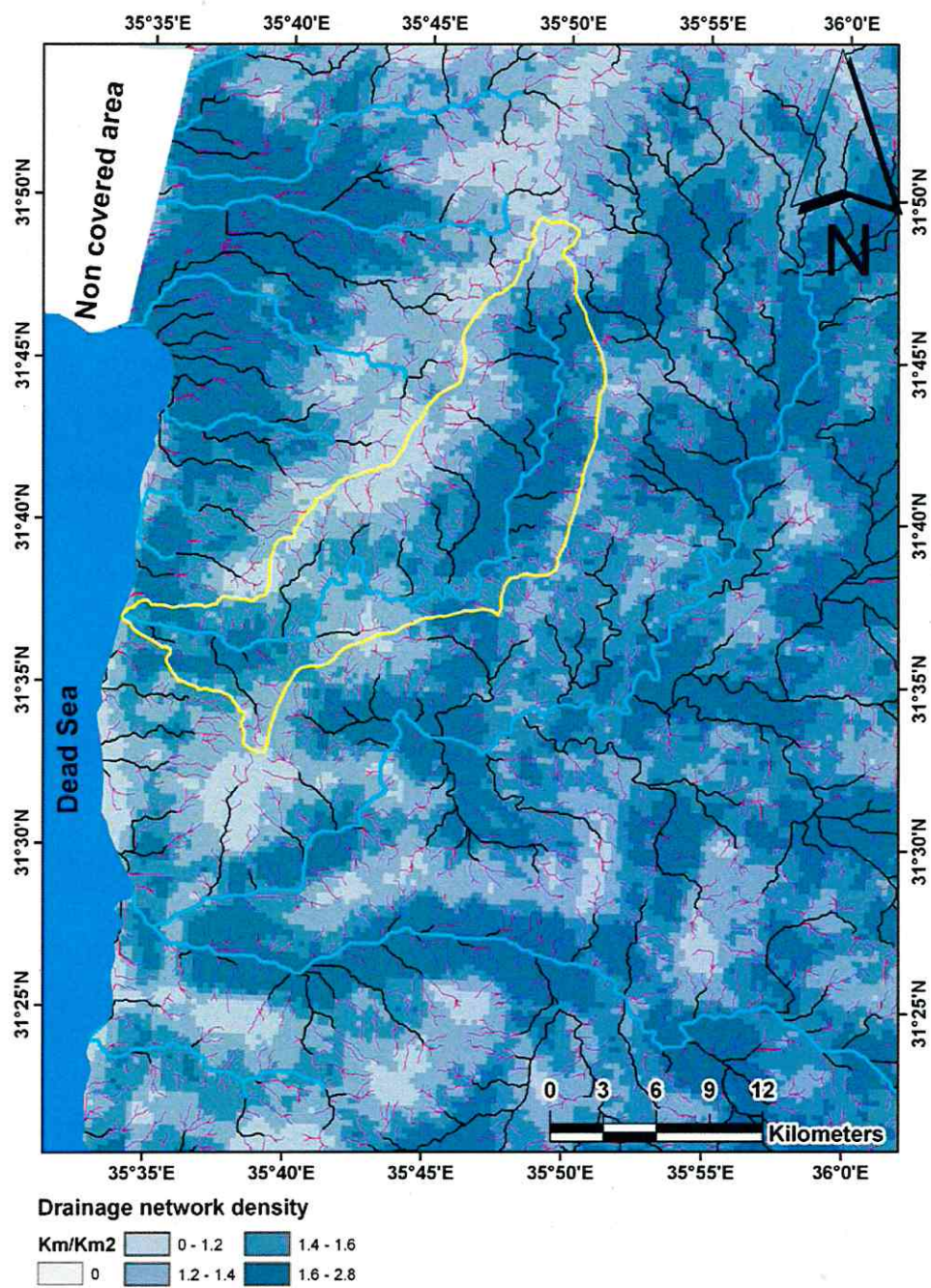
Fig. 3.2: Drainage network density in the study area. The basin asymmetry has a reflectance on the drainage density in the upper part of the catchment area where the north west of the catchment area has a higher density than the north east part.

3.1.2 Influence of a regional strike-slip faulting on the Zerka Ma'in River profile

The regional strike–slip fault of Wadi Zerka Ma'in cuts through the middle and lower parts of the catchment area and is associated with normal faults (Fig. 3.3). Therefore, it is considered as a transtensive strike-slipe fault. A knickpoint is a steep reach in a stream topographic profile that creates localized sharp incision (Gardner 1983). It is a response either to the resistance differences of lithological layers to the denudation process, a reaction to fault displacement, or a disequilibrium steepening in response to a relative base level fall (Tucker & Slingerland 1994, Bishop et al. 2005). Two normal faults are located in the Wadi Zerka Ma'in River with two complimentary kinckpoints at different distance as follow: (Fig. 3.4 and Fig. 3.5). The first one is located at a distance of 34 km from the source, with a vertical lowering of 250 m. The second is located 44 km from the source with a vertical lowering of
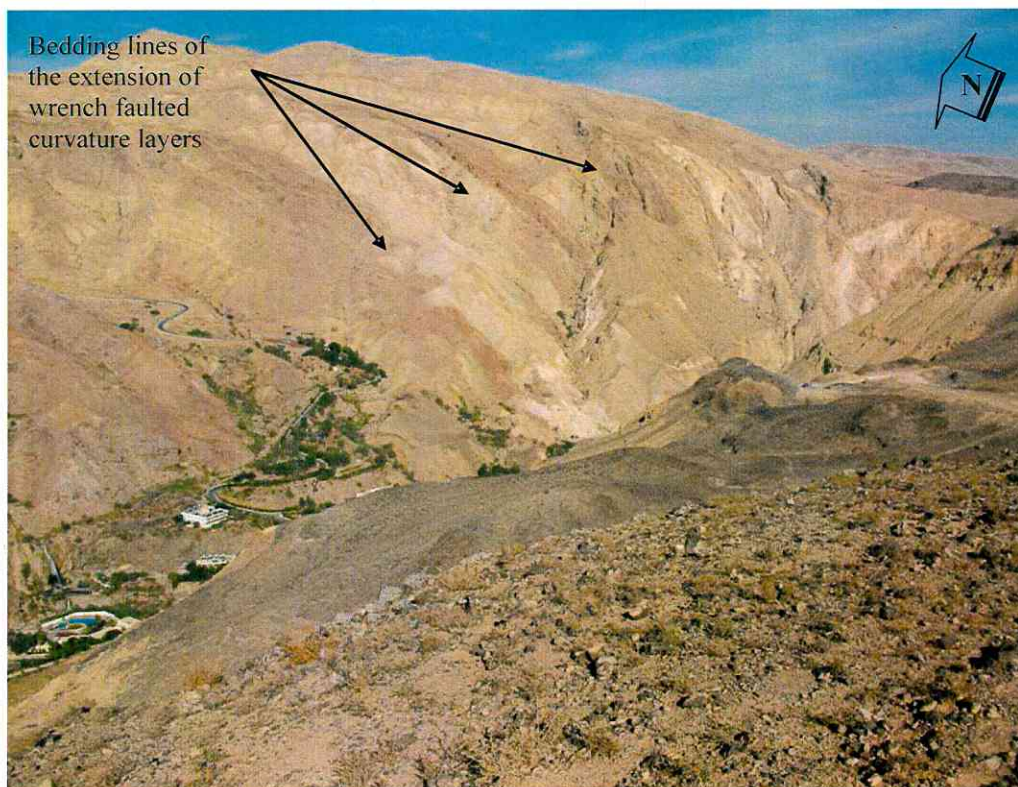
Fig. 3.3: Photo of the lee of wrenched faulted curvatures layers at Wadi Zeka Ma'in. Photo taken from N 31° 36′ 28.61″ E 35° 37′ 09.32″.

65
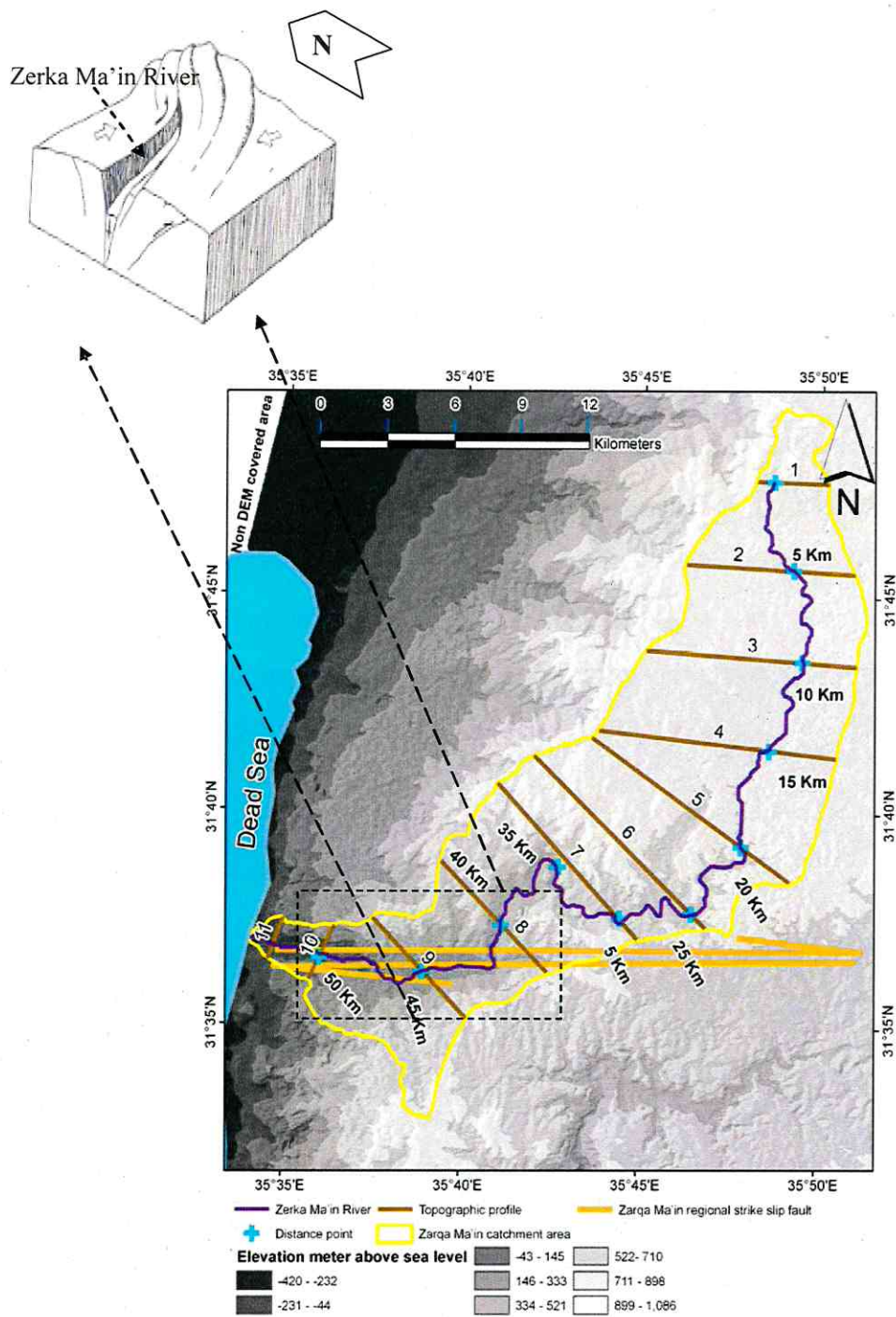
Fig. 3.4: Location of the topographic profiles and transstensional zones in the Wadi.
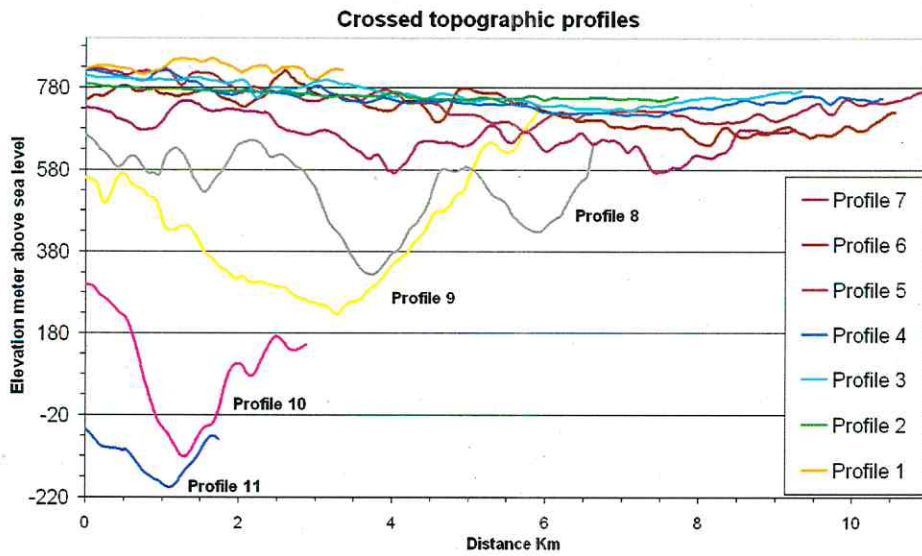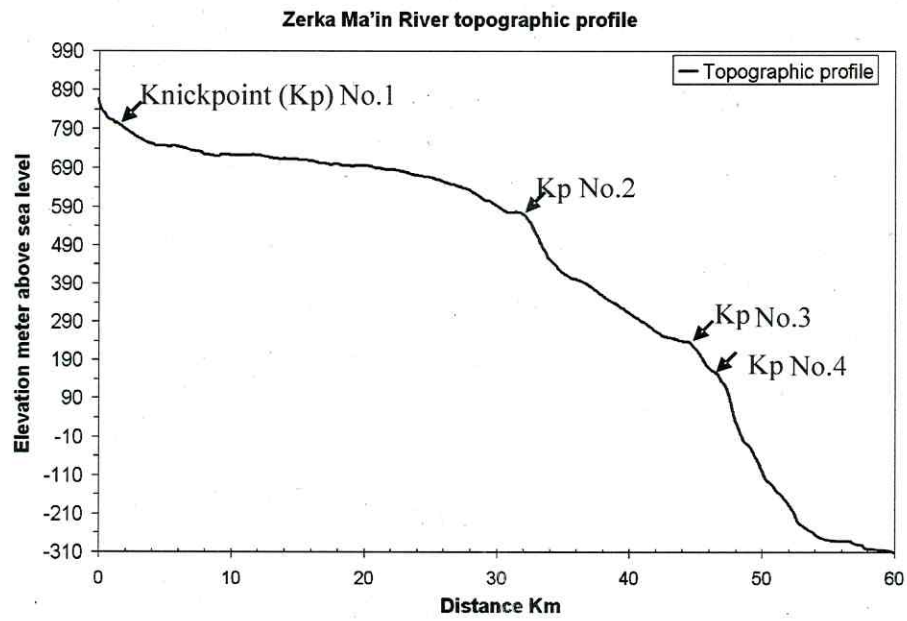
Fig. 3.5: Topographic profile of Wadi Zerka Ma'in. 1) Zerka Ma'in River topographic profile. 2) Crossed topographic profiles. The tow topographic droppings are the result of the negative (Tulip) structure.

67

100 m. The rapid drop of the Dead Sea water level after the Lisan lake stage enhanced river incision in the clastic sandstone units, so the second knickpoint developed as a result of disequilibrium with the Dead Sea water level.

Catchment areas that are influenced by uplifting processes are marked by a convex river profile and high steepness index (k_{sn}) values (Van der Beek et al. 2002, Knighton 1998). Figure 3.6 shows that the studied area has four steepness indices (ksn) that are generated in four stages as follows:

1) *ksn* = 0.73 with concavity index (θ) of 0.56 as a result of anticlinal uplift in the top of the catchment area.

2) *ksn* = 51.40 and θ = 1.74 as a result of the first knickpoint which is caused by the first normal fault.

3) *ksn* = 62.04 and θ = 1.54 as a result of the second knickpoint which is caused by the second normal fault.

4) *ksn* = 544.03 and θ = 1.18 as a result of river incision after the Lisian lake stage.

The Hack stream gradient (SL) index is a valuable tool for evaluating the vertical surface deformation component (Troiani & Della 2008). The sensitivity of the index to changes in the stream permits evaluation of the relationships between tectonic activity, rock resistance and topography (Keller et al. 2002). It was found that there are four major stream gradient indices that occurred with changing steepness indices. The effects of the normal fault in vertical deformation is shown by the SL = 994 and SL = 3092.

3.1.3 Catchment area hypsometry and asymmetry

The hypsometric curve is a dimensionless graph of area-altitude distribution. It describes the

68
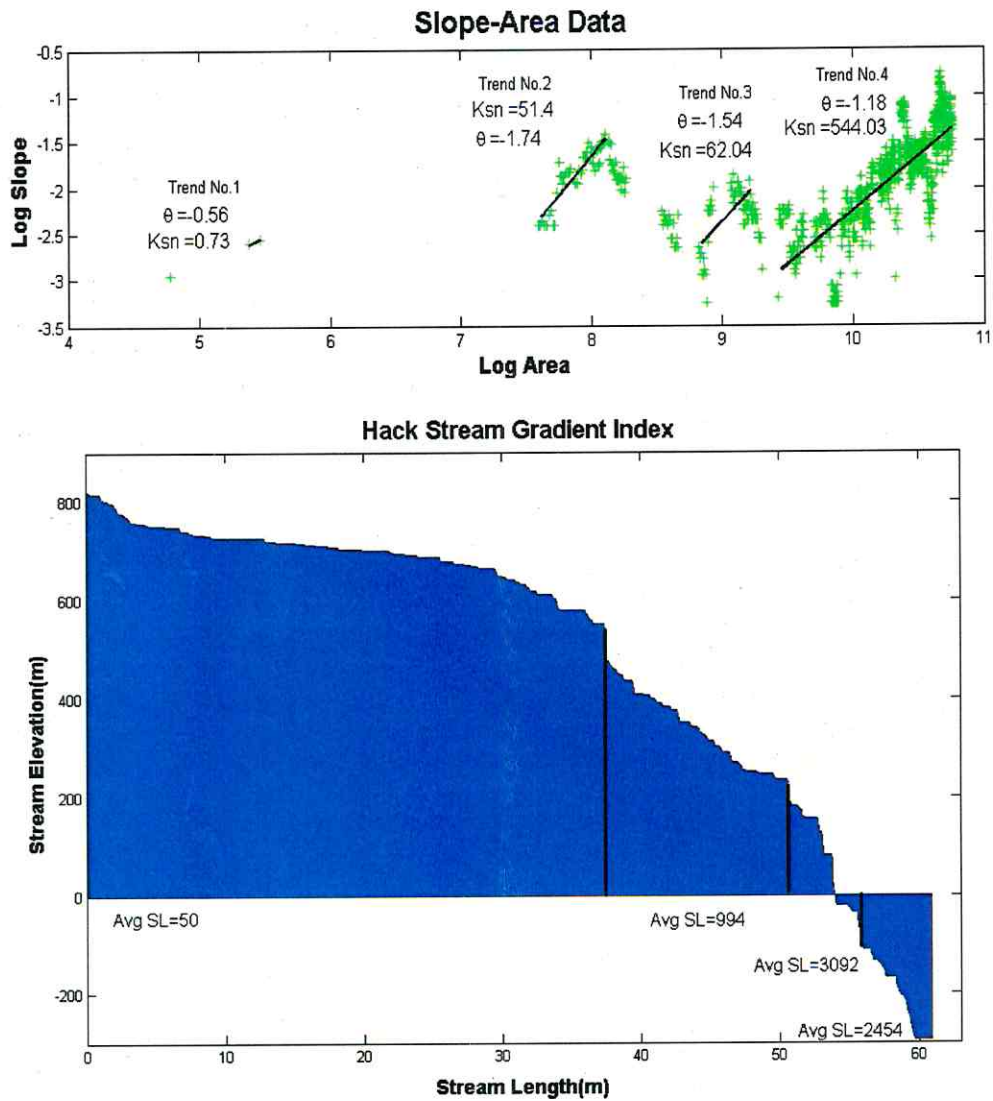
Fig. 3.6: Stream profile analysis of Wadi Zerka Ma'in River. 1) There are two knick points that located within the transtensional zone of the strike slip fault. 2) Four major trends in the log area/ log slope diagram. 3) Hack stream gradient index shows that there are three major gradient dropping.

69

total size of the catchment area relative to topography (Ohmori 1993). Runoff components are strongly related to the catchment area hypsometric form (Vivoni et al. 2008). A relatively less eroded (convex) catchment area that is dominated by subsurface processes shows higher total runoff. A relatively more eroded (concave) basin has less total runoff with a higher degree of surface response (Rodríguez-Iturbe & Rinaldo 1997). Furthermore, According to the geomorphic cycle a convex curve indicates a young stage and s-shaped curves a mature and old stage (Ohmori 1993).

Figure 3.7 A shows the hypsometric curve of Wadi Zerka Ma'in. The catchment area has a high convexity, indicating an early stage in the geomorphic cycle. The normal faults within the major strike slip fault led to an uplifting which generated the convexity. A high convexity land reflect the subsurface processes and generates high total runoff.

A transverse basin asymmetry vector denotes the direction and degree to which a river deviates from the basin mid-line. It creates important map-scale data for a neo-tectonic assessment and permits the delineation of geomorphic domains of stream migration that are related to tilted fault blocks (Garrote et al. 2006). Basins that are associated with wrench or transform faults are asymmetrical. The sense of basin asymmetry changes along the strike of transform faults (Ben-Avraham 1991). Figure 3.7 B and C show that the Wadi Zerka Ma'in catchment is a strike-slip faulted area that displays strong left asymmetry and is highly influenced by the NW- SE fault system, the oldest fault system in the region. The second major trend of the asymmetry arrows is parallel to the strike-slip fault of Wadi Zerka Ma'in and the third trend is parallel to the Dead Sea transform fault. Thus, the trends of the asymmetric arrows parallel those of the fault systems.
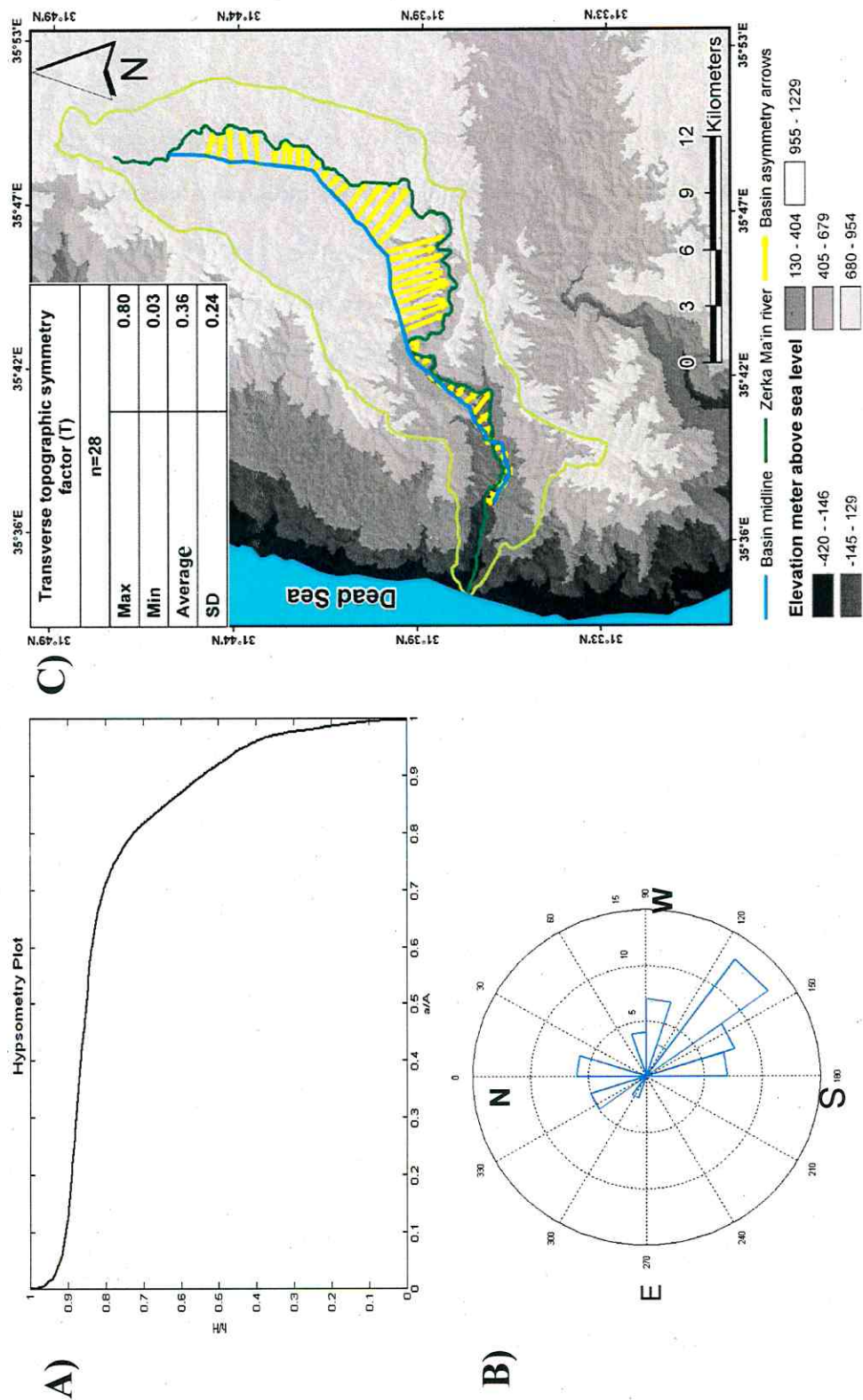
Fig.3.7: A) Hypsometry plot as an indicator of basin similarity. B) Basin asymmetry rose diagram. C) Basin asymmetry arrows.

3.2 Groundwater chemistry

Groundwater chemistry may reflect geological structures. Such structures may generate zones of hydrochemical anomalies according to changing of physiochemical parameters and acting as conduits between hydrogeological units that causing groundwater mixing (Guangcai et al. 2005). Because Wadi Zerka Ma'in is a faulted catchment area investigating its groundwater chemistry needs to to take into account the spatial distribution of the faults.

3.2.1 Groundwater genesis

The hydrogeochemical evolution of groundwater requires manipulation and classification of the hydrochemical data of groundwater samples (Domenico and Schwartz 1997). Table 3.1 shows the descriptive statistics for the concentrations of major cations and anions of the two aquifers groundwater samples (Tab. 3.2 and Tab. 3.3).

Tab. 3.1: Descriptive statistics, max., min., and mean values of physiochemical parameters and major chemical analysis of the groundwater samples. In general, EC and temp. values of the lower aquifer are higher than the upper aquifer.

Unit		EC (µS/cm)	TEMP. (°C)	pH	EH (mV)	HCO3 (mg/l)	CO3 (mg/l)	CO2 (mg/l)	Ca (mg/l)	Mg (mg/l)	K (mg/l)	Na (mg/l)	Cl (mg/l)	SO4 (mg/l)	NO3 (mg/l)
Upper aquifer	Min	572	18	7	97	120	0	0	39	15	2	26	41	14	9
	Max	1518	37	8	440	427	1	55	116	57	6	132	214	151	59
	Mean	911	28	7	362	274	0	14	74	29	4	52	86	55	28
	SD	304	6	0	173	93	127	114	20	13	1	29	52	43	17
Lower aquifer	Min	1073	16	6	-63	164	0	1	61	17	11	66	149	97	0
	Max	4001	58	8	471	430	3	455	386	58	70	638	1043	849	7
	Mean	2733	38	7	218	246	1	101	151	35	41	376	647	235	2
	SD	893	13	1	173	77	1	147	75	13	15	156	248	183	2

Plotting the chemical analysis of those in a Durove diagram (Fig. 3.8) shows that there are three groundwater genesis:

1) Earth-alkaline water predominantly bicarbonate (water group A) in the upper aquifer.

2) Earth-alkaline water predominantly sulphate (water group B) in the upper aquifer.

3) Earth-alkaline water predominantly chloride (water group C) in the lower aquifer.

Tab. 3.2: The coordinates and the water elevations of the samples (October 2007). The coordinates of the samples are in the Jordan Transverse Mercator (JTM) coordinate system was used for sampling.

Location name	Sample Symbol	X Coordinate	Y Coordinate	Water level (m asl.)	Type
Ein Almineaa	T1	373744	506151	577	Well
Ein Hamamat Main creek	T2	368469	499141	-17	Spring
Bar Alsbawi alarish	T3	385030	517267	699	Well
Bar Alfasalia	T4	382806	515585	682	Well
Bar Abdlatif abushuima	T5	389198	506494	565	Well
Ain Al Amir	T6	367598	498941	-91	Spring
Ein Ras Al shalal	T7	367986	498961	-68	Spring
Ein Main b g mix	T8	368775	499255	69	Spring
Ein Wadi Ahmara 1	T9	367988	502250	-92	Spring
Ein Mshra Aldaon 2	T10	372126	498317	239	Spring
Ein Shbieb	T11	375271	499954	346	Spring
Ein Mshra Aldawon 1	T12	377035	502816	474	Spring
Ein Source of Zerka Ma'in	T13	377288	503068	482	Spring
Ein Wadi Ahmara 2	T14	365298	503039	-256	Spring
Ein Wadi Ahmara 3	T15	367816	503940	-130	Spring
Ein Al Amira bmsa 1	T16	364248	497832	-247	Spring
Ein Al Amira bmsa 2	T17	364266	495747	-196	Spring
Ein Al Amira bmsa 3	T18	364266	495757	-196	Spring
Ein Almghara	T19	367986	498961	-86	Spring
Madaba station Rainfall	T20	385626	510657	615	Rainfall
Ma'in station Rainfall	T21	367631	498906	-91	Rainfall
Bar M. Al Fayez	T22	396108	508697	557	Well
Bar Hmaidi Al Fayez	T23	399704	513797	555	Well
Bar Qastel 15	T24	400188	516534	422	Well
Bar A. Abu Jnaib	T25	401434	518928	428	Well
Bar Harran Bakhit	T26	399508	521924	623	Well
Bar H. Salfiti	T27	393584	522131	690	Well
Bar Bsharat	T28	395371	523967	711	Well
Bar M. Nablsi	T29	391089	517232	652	Well
Bar Waleh 14	T30	384201	492097	458	Well
Ein S 1	T31	363523	497625	-303	Spring
Ein S 2	T32	368238	499018	-40	Spring
Ein S 3	T33	364242	497370	-253	Spring

Tab. 3.3: The value of physiochemical measurement and chemical analysis of the major ions (the symbol n.a means not analysed).

Unit	Sample	EC (µS/cm)	TEMP. (°C)	pH	EH (mV)	HCO3 (mg/l)	CO3 (mg/l)	CO2 (mg/l)	Ca (mg/l)	Mg (mg/l)	K (mg/l)	Na (mg/l)	Cl (mg/l)	SO4 (mg/l)	NO3 (mg/l)
Upper aquifer	T1	1056	19.9	7.8	440	150	0	0	65	42	2	78	160	107	31
	T3	572	18.5	7.5	393	120	0	2	39	15	3	30	58	29	29
	T4	596	23.9	7.9	416	129	0	0	49	16	3	29	53	48	26
	T10	1040	18.4	7.4	413	300	0	18	92	42	5	76	153	75	n.a
	T11	1518	31.9	7.0	400	381	0	55	94	57	6	132	214	151	9
	T12	575	24.9	7.9	419	236	1	5	52	24	3	32	57	31	22
	T13	700	24.1	7.3	316	215	0	16	61	29	3	42	71	33	29
	T22	1272	33.0	7.0	n.a	427	n.a	n.a	85	32	3	46	60	50	n.a
	T23	785	26.0	7.6	n.a	350	n.a	n.a	71	25	5	41	45	51	14
	T24	802	33.0	7.0	n.a	260	n.a	n.a	72	24	3	44	70	35	21
	T25	1072	34.0	7.3	n.a	261	n.a	n.a	72	24	3	44	70	35	55
	T26	810	35.0	7.0	n.a	284	n.a	n.a	73	25	6	45	65	26	37
	T27	700	36.0	7.4	n.a	300	n.a	n.a	77	21	3	26	41	14	33
	T28	928	37.0	7.3	97	320	n.a	n.a	100	22	6	40	70	18	59
	T29	677	25.0	7.4	n.a	238	n.a	n.a	66	17	2	38	45	35	21
	T30	1470	25.0	6.8	n.a	413	n.a	n.a	116	51	5	97	146	145	15
	T20	174	14.0	#	n.a	n.a	n.a	n.a	29	1	2	5	45	20	n.a
Lower aquifer	T5	1073	39.3	7.0	78	184	0	3	61	44	11	66	149	97	1
	T8	3740	18.3	8.3	413	195	3	1	386	57	44	406	696	849	2
	T2	2790	47.5	8.1	246	190	3	2	140	27	45	406	696	190	2
	T32	3260	31.9	7.0	0	363	0	58	155	41	50	459	840	251	0
	T9	3290	24.0	7.6	471	430	2	13	218	36	47	453	755	194	7
	T7	3020	57.5	5.9	6	289	0	397	150	31	47	444	746	184	1
	T6	3090	45.1	6.6	225	279	0	79	154	33	48	450	757	191	n.a
	T14	3660	16.0	7.6	329	317	1	12	153	51	58	551	934	327	n.a
	T15	4001	16.8	7.9	384	243	1	5	133	58	70	638	1043	329	n.a
	T16	2100	50.1	6.2	217	187	0	149	117	21	32	275	483	131	1
	T17	1655	54.0	6.0	264	199	0	229	93	17	25	204	372	115	n.a
	T18	3007	45.9	5.8	295	238	0	455	154	32	46	452	756	192	n.a
	T19	3028	39.0	6.5	400	252	0	86	155	33	46	457	767	196	n.a
	T31	1662	38.1	7.2	9	167	0	17	102	21	27	194	361	140	2
	T33	1614	39.3	7.8	-63	164	1	3	97	20	25	191	351	142	2
	T21	128	16.0	n.a	n.a	n.a	n.a	n.a	17	2	1	6	40	10	n.a

74
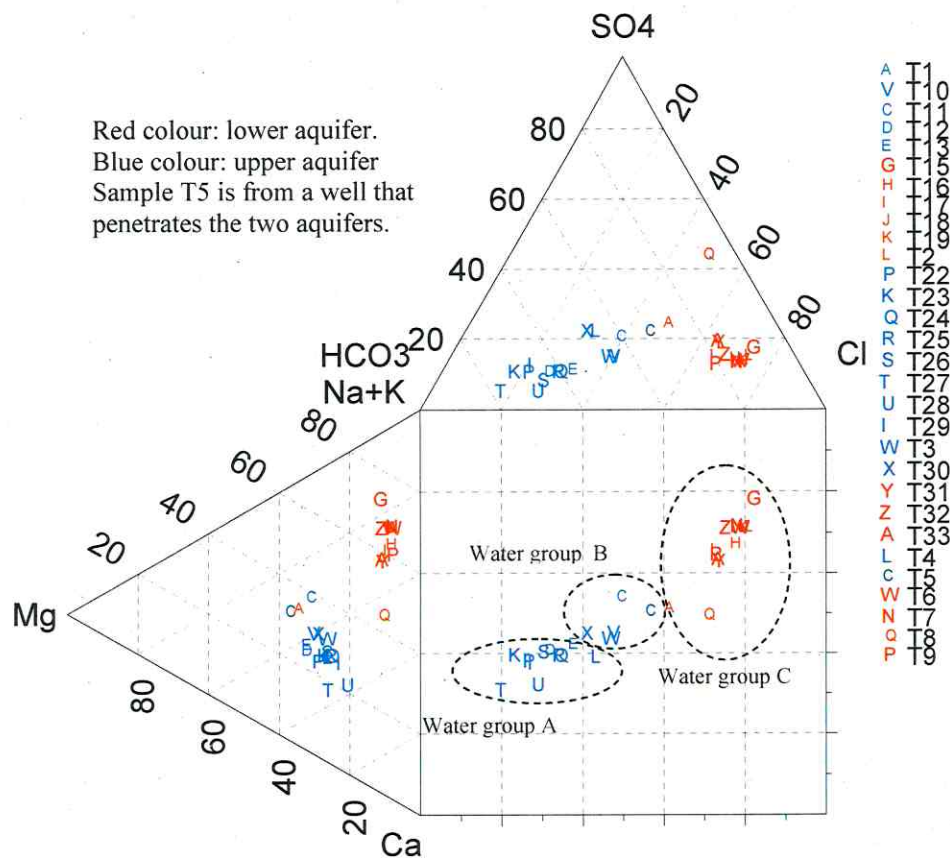
Fig. 3.8: Durov diagram showing three groundwater groups. The mixing group B is generating as a result of the groundwater mixing of the upper aquifer (water group A) and the lower aquifer (water group C).

The upper aquifer mainly consists of limestone with a silt and clay soil cover (Cordova et al. 2004). When rainfall is infiltrating in soil bicarbonate and carbonate have different sources: (a) carbon dioxide in the atmosphere dissolved in rainwater, (b) carbon dioxide in the pores due to microbial decay of organics metter, and (c) dissolution of carbonate minerals in soil. The process can be represented by the following equations:

$$CO_2 + H_2O \Leftrightarrow H2CO_3 \qquad (1)$$

$$CaMg(CO_3)2 + 2CO_2 + 2H_2O \Leftrightarrow Ca^{+2} + Mg^{+2} + 4HCO_3- \qquad (2)$$

$$CaCO_3 + CO_2 + H_2O \Leftrightarrow Ca^{+2} + 2HCO_3- \qquad (3)$$

(during rock percolation)
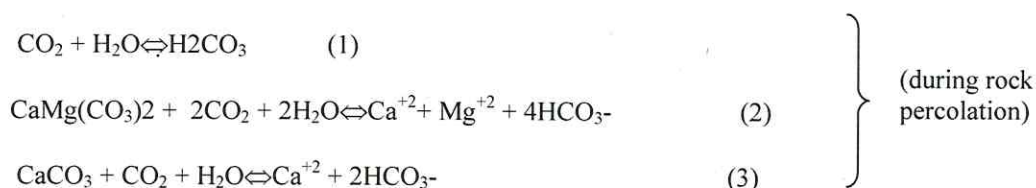
The predominantly bicarbonate earth-alkaline water (water group A) in the upper aquifer is generated as a result of this process. On the other hand, agriculture and urban areas may cause anthropogenic contamination leading to an increase of NO_3^- in the upper aquifer.

Calcite is the most common cement in sandstones However, the cement of the sandstone in the lower aquifer consists mainly of calcite, dolomite, gypsum, kaolinite and halite (Schneider et al. 1984) and has a significant influence on the groundwater chemistry expressed by an enrichment of Cl and SO_4 (water group C). The saturation indices (Tab. 3.4) show under- and oversaturaion with respect to calcite and dolomite, while halite and gypsum are in all cases undersaturated. Water group B represents a mixture between water groups A and C. This mixing is generated by the embedded normal faults of the major strike slip fault (Fig. 3.9). These faults are mainly in the middle reaches of the catchment area. They form a conduit for the confined Water group B represents a mixture between water groups A and C. This mixing is generated by the embedded normal faults of the major strike slip fault.

These faults are mainly in the middle reaches of the catchment area. They form a conduit for the confined groundwater in the lower aquifer to rise up to the upper aquifer. Accordingly, the

Tab. 3.4: Saturation indices of some minerals (# means not modelled).

Sample ID	Anhydrite	Aragonite	Barite	Calcite	Dolomite	Fluorite	Gypsum	Halite
T1	-1.96	0.28	0.17	0.43	0.95	-1.32	-1.72	-6.49
T3	-2.58	-0.27	-0.06	-0.12	-0.40	-1.72	-2.34	-7.32
T4	-2.29	0.37	-0.23	0.52	0.89	-1.61	-2.07	-7.39
T10	-1.99	0.35	0.10	0.50	0.92	-1.16	-1.75	-6.53
T11	-1.73	0.13	0.16	0.27	0.75	-1.36	-1.54	-6.19
T12	-2.50	0.58	-0.11	0.73	1.46	-1.61	-2.28	-7.32
T13	-2.43	0.05	-0.02	0.20	0.41	-1.37	-2.21	-7.12
T22	-2.10	0.00	#	0.14	0.28	-0.85	-1.92	-7.07
T23	-2.18	0.44	#	0.59	1.09	-1.29	-1.96	-7.17
T24	-2.28	-0.26	#	-0.12	-0.29	#	-2.10	-7.12
T25	-2.29	0.05	#	0.18	0.32	#	-2.11	-7.12
T26	-2.39	-0.19	#	-0.05	-0.12	#	-2.22	-7.15
T27	-2.61	0.25	#	0.39	0.66	#	-2.44	-7.58
T28	-2.45	0.28	#	0.42	0.65	#	-2.29	-7.18
T29	-2.31	-0.03	#	0.11	-0.01	#	-2.09	-7.35
T30	-1.64	-0.25	#	-0.11	-0.22	#	-1.42	-6.47
T5	-1.95	-0.13	-0.07	0.00	0.32	-0.61	-1.81	-6.64
T6	-1.42	-0.01	-0.13	0.12	0.06	-1.70	-1.32	-5.17
T14	-1.36	0.58	0.49	0.73	1.21	-1.57	-1.11	-4.93
T15	-1.42	0.67	0.39	0.82	1.53	-1.10	-1.18	-4.82
T16	-1.55	-0.61	-0.08	-0.48	-1.21	-2.14	-1.48	-5.56
T17	-1.62	-0.76	-0.14	-0.63	-1.49	-2.23	-1.59	-5.80
T18	-1.41	-0.89	-0.13	-0.76	-1.70	-1.88	-1.31	-5.16
T19	-1.45	-0.20	-0.12	-0.06	-0.33	-1.77	-1.30	-5.14
T31	-1.63	0.13	#	0.27	0.31	#	-1.48	-5.80
T33	-1.64	0.78	#	0.92	1.62	#	-1.49	-5.82
T8	-0.66	1.41	0.40	1.56	2.56	-1.48	-0.42	-5.21
T2	-1.43	1.29	0.01	1.42	2.63	-2.03	-1.34	-5.25
T32	-1.41	0.27	#	0.41	0.66	#	-1.23	-5.09
T9	-1.42	1.04	0.28	1.18	1.92	-1.31	-1.20	-5.12
T7	-1.34	-0.53	-0.19	-0.40	-0.99	-1.99	-1.33	-5.21

Formation Symbol

AHP		ASL		WG	
WSL		FHS		NI	
KS		Dr & Mn		UI	
BDS& IN					

Water movement

Piezometric GWL lower aquifer

GWL upper aquifer
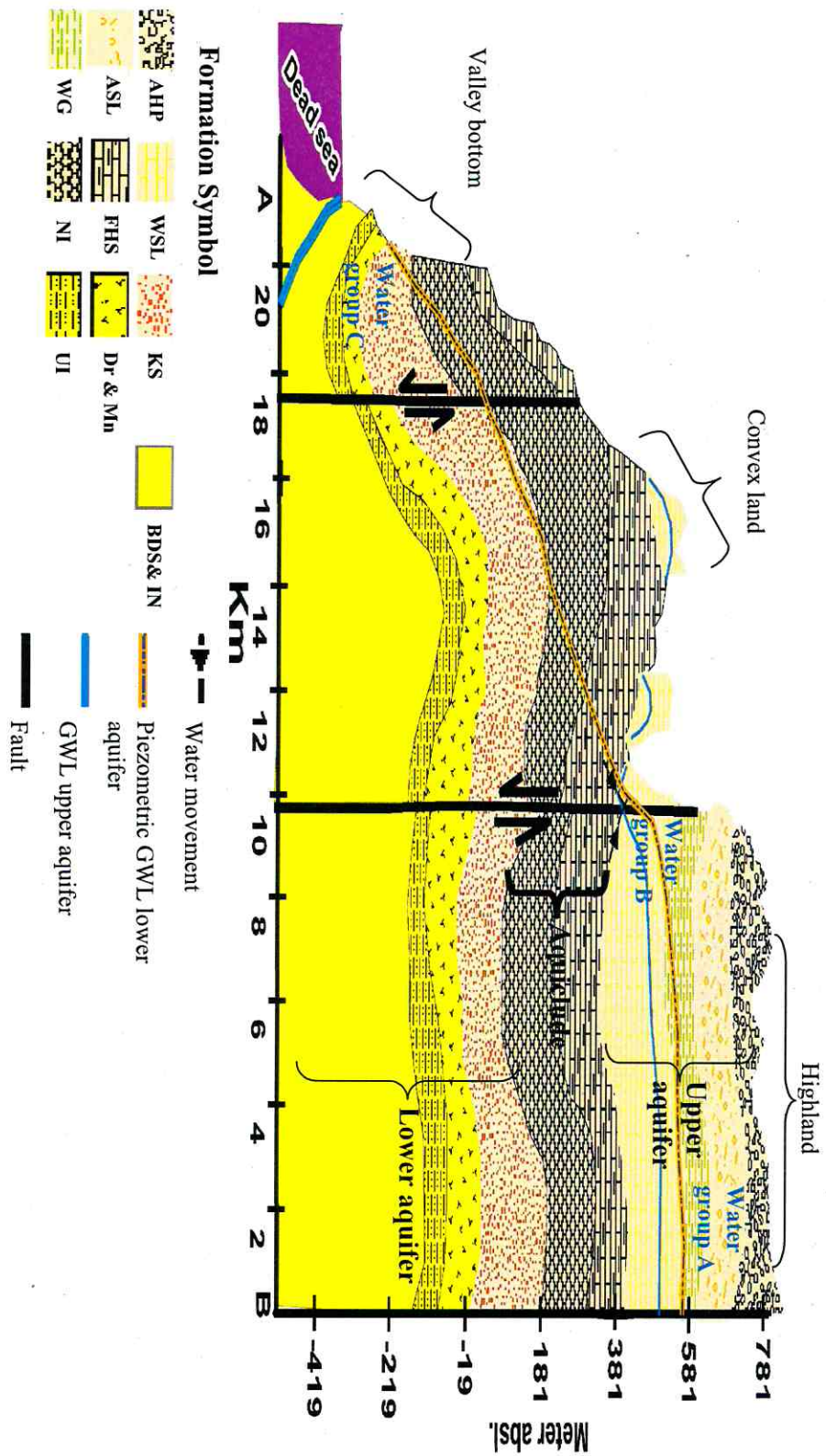
Fault

Fig. 3.9: Topographical and geological cross section in the study area. The piezometric groundwater of the lower aquifer (Margane et al 2002) is raised up into the upper aquifer by the embedded normal faults of the major strike slip fault zone. Hence those normal faults work as conduits between the two aquifers by passing the aquiclude layer.

78

groundwater of the two aquifers is mixed and produces water group B at the bottom of the upper aquifer. Water sample T5, which was taken from a well that pumps from two aquifers, is considered as an artificially mixed groundwater since the mixing is because pumping from the lower aquifer. Therefore, we will compare it to the natural groundwater mixed samples, the samples that were taken from the embedded normal faults zone.

As compared to many other dissolved ions, chloride is considered as a non-reactive ion and shows no changes along the water flow paths (Seiler et al. 2007). Figure 3.10 shows the correlation between the water level and the chlorine concentration in a logarithmic scale. It shows three cluster groups and hence is confirming that there are three water groups. However, water group B (sample T5) contains water which is pumped from two aquifers and is therefore an artificial groundwater mixture.

The outcrops of the upper aquifer are located within a high altitude area while the lower aquifer outcrops on the eastern side of the Dead Sea rift valley in form of low land. The upper aquifer receives an average amount of rainfall of approximately 300 mm/year, which is rapidly decreasing to about 100 mm/year in the western region, where the lower aquifer outcrops and discharges. However, an estimation by Khdeir (1997) indicates that only 8% of the rainfall infiltrates and recharge the groundwater.

The climate in the study area is arid to semi-arid with a high evaporation loss (Salameh 1993). Therefore, the remaining soil moisture in that area creates groundwater recharge enriched in heavy stable isotopes of ^{18}O and ^2H in comparison to the precipitation water (Allison et al. 1983). Stable isotope signature of $\delta^{18}O$ vs. δ^2H of the groundwater represents the climatic conditions of the recharging water. Therefore, in fossil groundwater, stable isotopes provide a record of paleoclimatic conditions that indicates under which climate condition the fossil

CI concentration versus water level
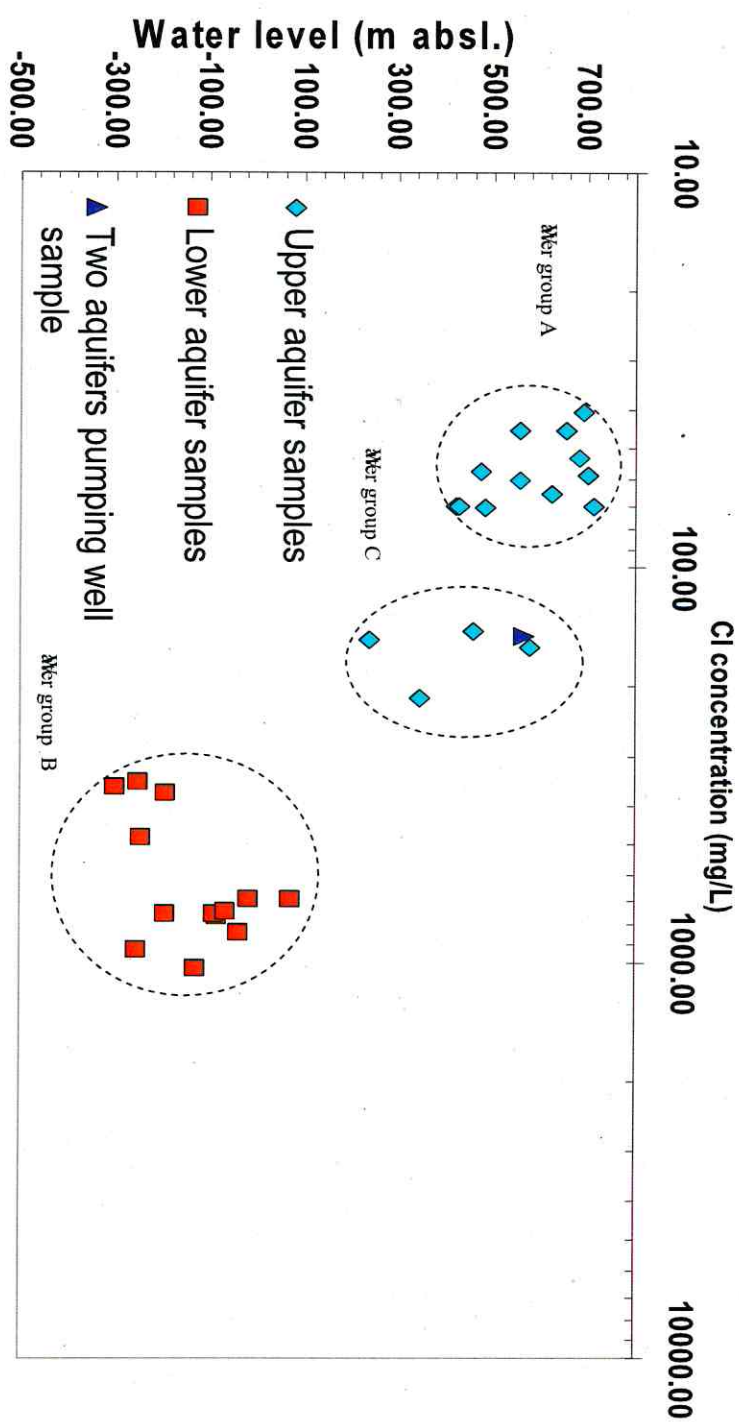
Fig. 3.10: The three groundwater groups have three groups of logarithmic scale chlorine concentration. The distinguishable difference between the chlorine concentration between the upper and the lower aquifer is related to the elevated concentration of halite cementing material in the sandstone of the lower aqifer (Shneider et al. 1984).

80

Figure 3.11 shows that the groundwater of the upper aquifer in comparison to rainfall in the highland is enriched in $\delta^{18}O$ and δ^2H values, which indicates the influence of evaporation before replenishing the aquifer. The groundwater of the lower aquifer show enriched $\delta^{18}O$ values compared to the groundwater of the upper aquifer. According to Bajjali (2001), the lower aquifer groundwater, which is fossil groundwater, was generated under higher temperatures than actual climatic conditions, resulting in enrichment with stable isotopes values relative to the upper aquifer. The two aquifers were recharged by rainfall of different climatic origin that led to a variation of $\delta^{18}O$ and δ^2H values within the same aquifer (Gat and Carmi 1970). However, a groundwater mixing line couldn't be drawn between samples of the upper aquifer (water group A), lower aquifer (water group C) and the mixed upper aquifer (water group B) because the two aquifers receive groundwater recharge of different climatic origin (Bajjali 2001, Gat & Carmi 1970). However, the high relief topography of the study area cause also a spatial variation in the stable isotopes signatures within the same aquifer. This variation makes them not useful as an indicator for the groundwater mixing.
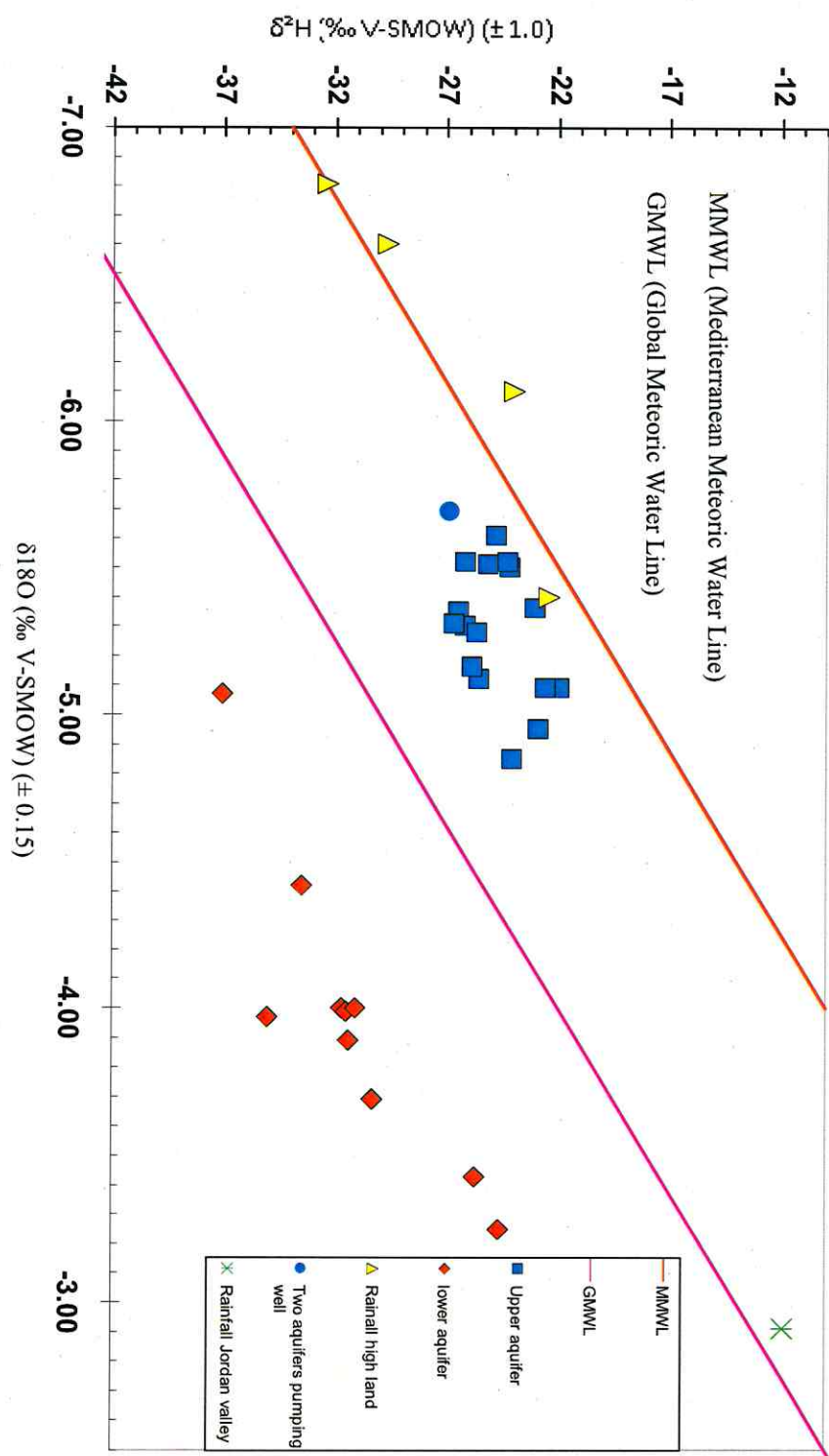
Fig. 3.11: Plot of δ²H versus δ¹⁸O of groundwater and rainfall samples. The two aquifers were recharging by rainfall water of different climate origins.

3.2.2 Trace elements, REE, and groundwater geochemical modeling

Trace elements were found in the groundwater with concentrations less than 10 μ mol/l which could be derived mainly from the host rocks, soils and anthropogenic contamination sources (Salbu & Steinnes 1995). The study area has limited industrial activities to be an anthropogenic source for the trace elements and the soil cover generated from the local outcropping rocks (Cordova 2004). Therefore, the trace elements abundance in the Wadi Zerka Ma'in (Tab. 3.5) aquifers mainly reflects the geochemical reactions between groundwater and the mineralogical component of the aquifer matrix which are continuously taking place along the water pathway (Salbu and Steinnes 1995, Pellig-ba 1996). These geochemical reactions are controlled by physicochemical parameters. The values of these parameters are strongly varying (Fig. 3.12) and hence lead to fluctuations of the trace elements. However, mineral dissolutions are the most common geochemical reactions that generate both major ions and trace elements (Appelo and Postma 2005, Naumov et al. 2009).

The rare earth elements (REE) lanthanide elements or lanthanides, are known in the periodic table from lanthanum (#57) to lutetium (#71), and also yttrium (#39), totalling 15 chemically similar elements that occur in many common rocks in small amounts (Johannesson 2005). Groundwater has REE patterns that closely mimic the REE patterns of the rocks through which they flow. The similarities between groundwater and aquifer rock REE patterns allow REE to be used as a tracer for groundwater-aquifer rock interactions (Johannesson et al. 1997). Similar to trace elements, the concentrations of REE (Tab. 3.6) are controlled by the physiochemical parameters and the mineralogical components of the aquifer matrix (Henderson 1984).

The fluctuations of trace elements, Rare Earth Elements (REE) and saturation indices were

Tab. 3.5: The chemical analysis of stable isotopes and trace elements of the groundwater samples (n.a. means not analysed).

Unit	Sample Symbol	δ ^{18}O (± 0.15)	δ² H (± 1.0)	F (mg/l)	Br (mg/l)	Ba (mg/l)	Sr (mg/l)	U (mg/l)
Upper aquifer	T1	-6	-25	0.8	n.a.	0.10	0.90	0.00
	T3	-5	-23	0.5	n.a.	0.10	0.40	0.00
	T4	-5	-22	0.6	n.a.	0.10	0.40	0.00
	T10	-6	-26	0.8	0.7	0.10	1.00	0.00
	T11	-5	-23	0.8	n.a.	0.10	1.40	0.00
	T12	-6	-24	0.6	n.a.	0.10	0.60	0.00
	T13	-6	-24	0.8	n.a.	0.10	0.70	0.0
	T22	-5	-27	n.a.	n.a.	n.a.	n.a.	n.a.
	T23	-5	-26	n.a.	n.a.	n.a.	n.a.	n.a.
	T24	-5	-24	n.a.	n.a.	n.a.	n.a.	n.a.
	T25	-5	-26	n.a.	n.a.	n.a.	n.a.	n.a.
	T26	-5	-26	n.a.	n.a.	n.a.	n.a.	n.a.
	T27	-6	-25	n.a.	n.a.	n.a.	n.a.	n.a.
	T28	-5	-27	n.a.	n.a.	n.a.	n.a.	n.a.
	T29	-5	-23	n.a.	n.a.	n.a.	n.a.	n.a.
	T30	-5	-26	n.a.	n.a.	n.a.	n.a.	n.a.
Lower aquifer	T2	-4	-31	0.40	2.30	0.10	3.30	0.00
	T5	-6	-27	2.40	n.a.	0.10	3.70	0.00
	T6	-4	-31	0.50	1.80	0.10	3.60	0.00
	T7	-4	-32	0.40	2.50	0.10	3.40	0.00
	T8	-4	-30	0.40	2.10	0.00	3.60	0.00
	T9	-4	-35	0.60	2.60	0.10	3.60	0.00
	T14	-3	-26	0.40	n.a.	0.10	3.80	0.00
	T15	-3	-25	0.90	3.00	0.10	3.60	0.00
	T16	-4	-34	0.40	n.a.	0.10	3.00	0.00
	T17	-5	-37	0.40	n.a.	0.10	2.60	0.00
	T18	-4	-32	0.40	n.a.	0.10	3.80	0.00
	T19	-4	-31	0.50	2.30	0.10	3.60	0.00
	T20	-7	-32	0.10	n.a.	0.00	0.10	0.00
	T21	-3	-12	0.10	n.a.	0.00	0.10	0.00
	T31	n.a.	n.a.	n.a.	1.70	0.10	3.00	0.00
	T32	n.a.	n.a.	n.a.	1.50	0.10	3.60	0.00
	T33	n.a.	n.a.	n.a.	1.70	0.10	3.00	0.00

Tab. 3.6: Descriptive statistics for Rare Earth Elements (REE) of the groundwater samples

Unit		La ng /l	Ce ng /l	Pr pg/l	Gd ng /l	Tb ng /l	Dy ng /l	Ho ng /l	Lu ng /l
Upper aquifer (n = 16)	Min.	<1	5	<1	<1	<1	<1	<1	<1
	Max.	5	733	2	2	20	3	<1	<1
	Mean	3	191	<1	<1	5	2	<1	<1
	Median	4	14	<1	<1	<10	2	<1	<1
	SD	2	361	<1	<1	10	1	<1	<1
Lower aquifer (n=4)	Min.	3	10	4	9	2	6	<1	<1
	Max.	34	66	12	28	6	32	<1	1
	Mean	18	31	8	16	3	18	<1	1
	Median	18	24	8	15	3	17	<1	1
	SD	15	24	4	8	2	11	<1	<1

Legend:

- ——— GWL of the upper aquifer
- ——— GWL of the lower aquifer
- ☐ Zarqa Ma'in catchment area
- ☐ Marl aquiclude

Physiochemical parameters

- ■ EC value
- ■ Temp. degree
- ■ pH value

	EC (μs/cm)	TEMP. (C⁰)	pH
Min.	572.00	18.40	50.78
Max.	4001.00	57.50	8.31
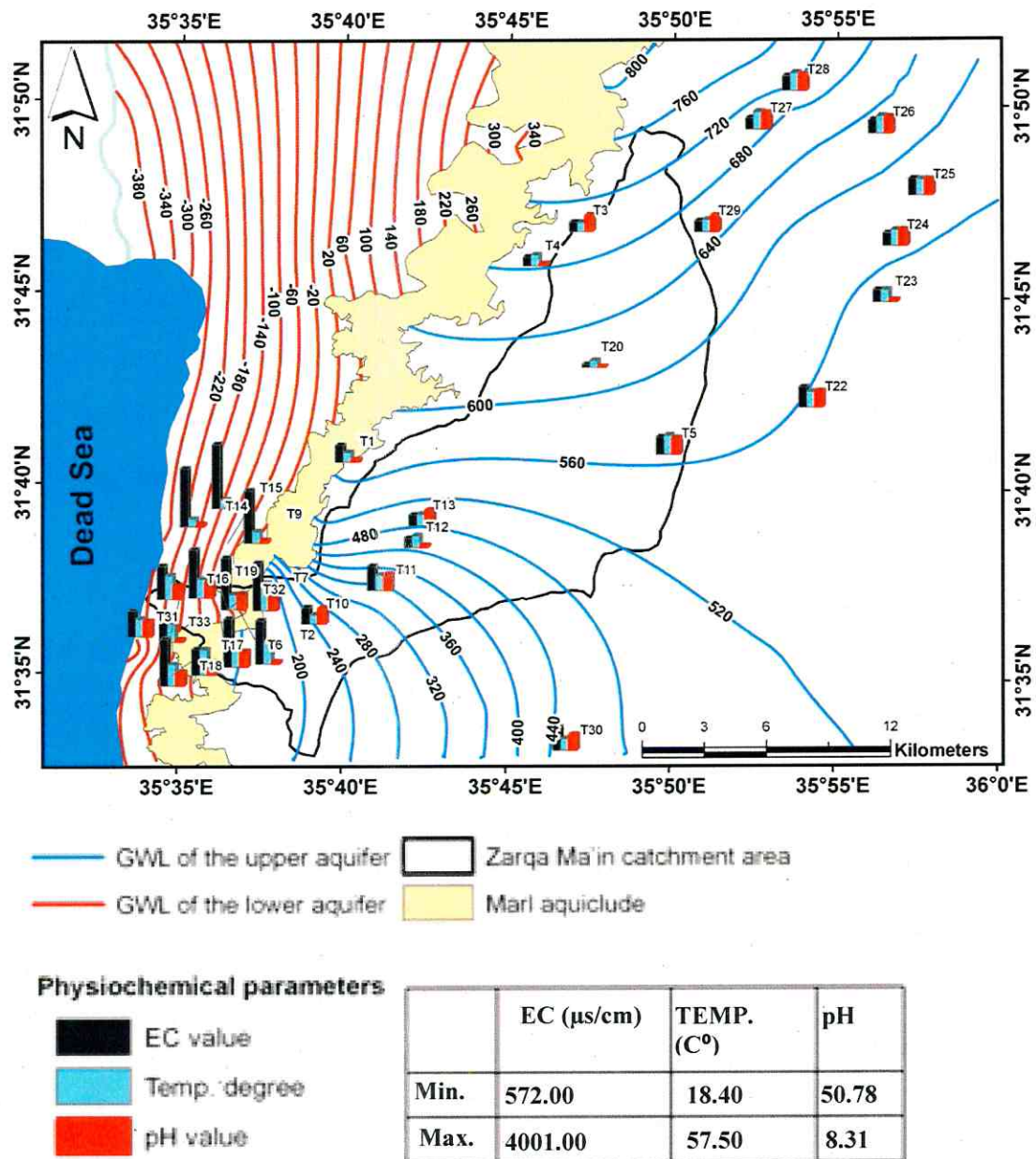
Fig. 3.12: Spatial distribution of the physiochemical parameters values of the groundwater. They have irregular variation even within the same aquifer.

85

studied along a specific groundwater flow path line (Fig. 3.13). Along the flow path line the physiochemical parameters in each aquifer are constant, which allows for easier patterns comparison.

Figures 3.14 A and B show the fluctuations of some trace element concentrations along the flow path line. In general, the lower aquifer is more enriched with trace elements than the upper aquifer. This is because the sandstone and its carbonates cement material offer different mineralogical sources for the trace elements. An exception is the uranium ion with high concentrations in the upper aquifer which comes from leaching of the phosphate layer at the top of the aquifer (Schneider et al. 1984). The trace element signature of water group B (the mixed groundwater) is located between the signature of water group A and water group C. For the saturation indices signature, the situation is similar (Fig. 3.15). Figure 3.16 shows that the groundwater of the lower aquifer is more enriched with REE than the upper aquifer. During the passage of the lower aquifer groundwater through the marly part of the embedded normal fault, intensive sorption for the REE is acting by the clay minerals that are found in the marl rocks (Setti et al. 2004). This process leads to dramatic decreasing of their concentration and as a result water group B has an independent pattern.

Hydrochemical modelling of the inter-aquifer groundwater mixing was performed in order to calculate the mixing ratio between the lower and upper aquifer. Groundwater sample T25 was chosen as representative for the upper aquifer (water group A) because it originates from the deeper part of the upper aquifer. Sample T33 was chosen as representative for the lower aquifer (water group C) because it comes from the top of the lower aquifer. The bottom of the upper aquifer and the top of the lower aquifer are expected to be near the direct mixing zone between both aquifers within the embedded normal faults. Groundwater sample T3 was chosen as a typical result of mixing of the two aquifers (water group B) because it comes
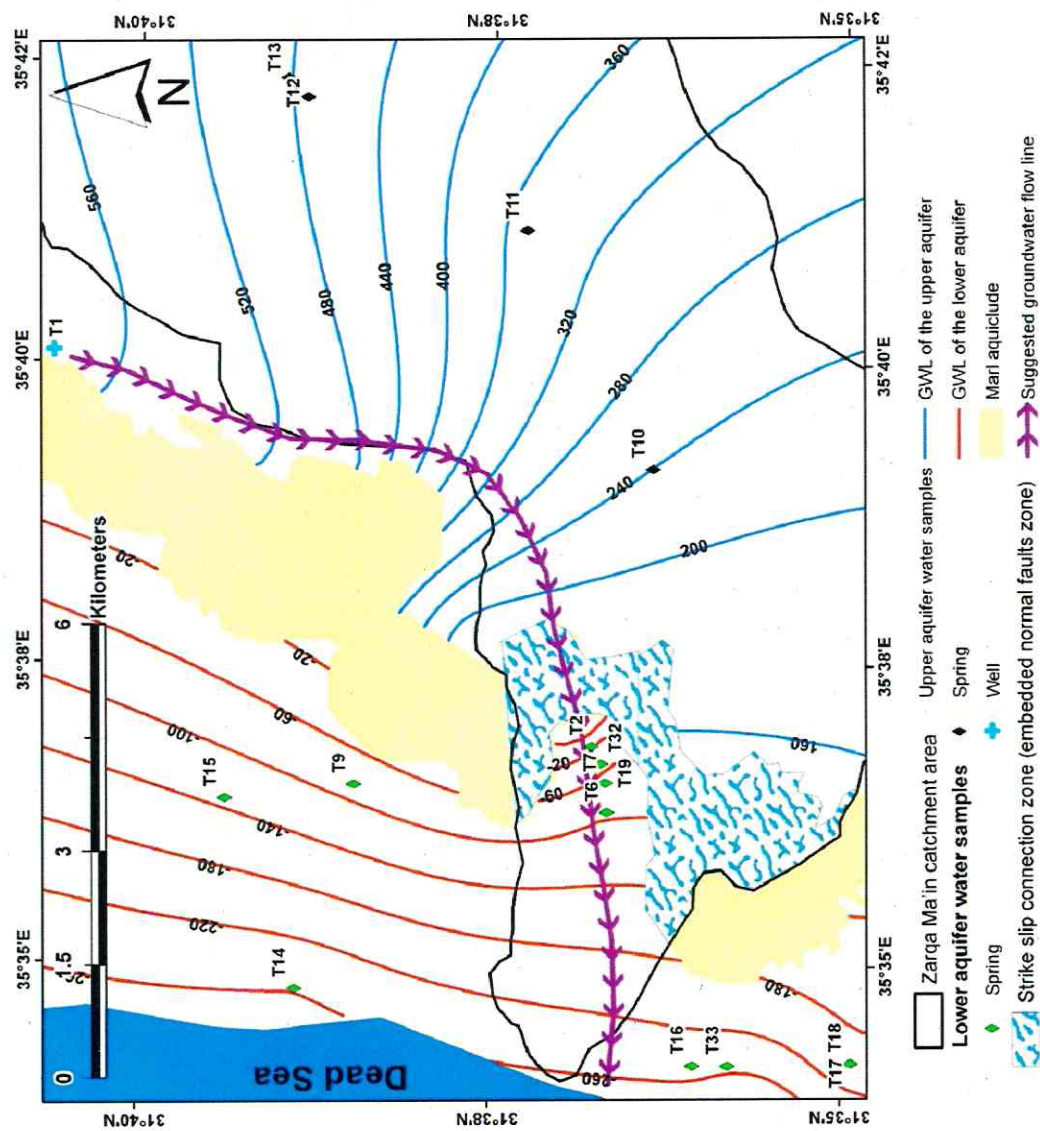
Fig. 3.13: The studied groundwater flow line. The samples T1, T12, T11, T10, T2, T32, T7,T6, T19, and T16 were considered to be along the same groundwater flow line which passes through the strike slip fault zone.
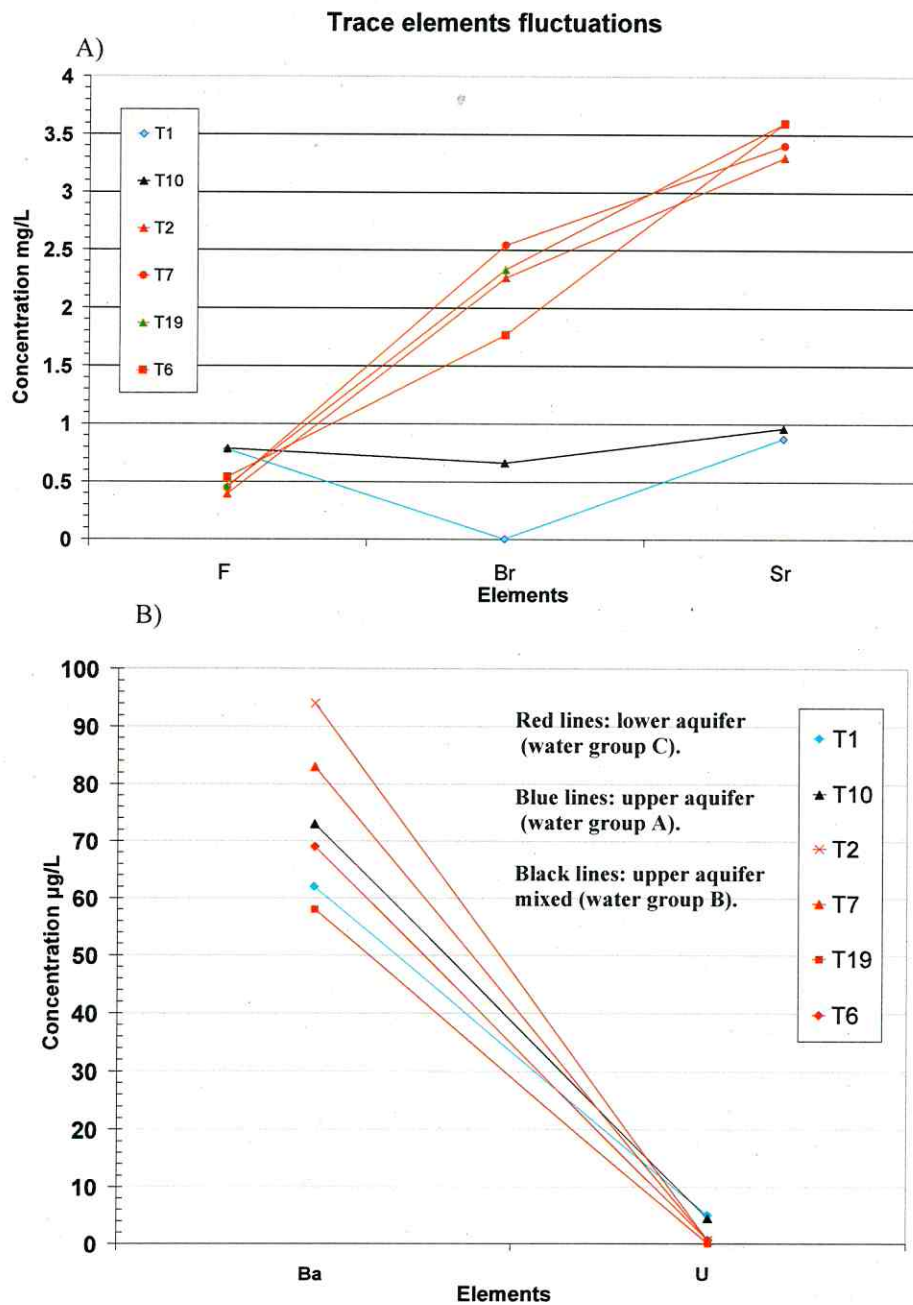
Fig. 3.14: A) The high concentration trace elements. B) The lowest concentration trace element. As of groundwater mixing, the trace elements signature of water group B locates between the signature of water group A and water group C.
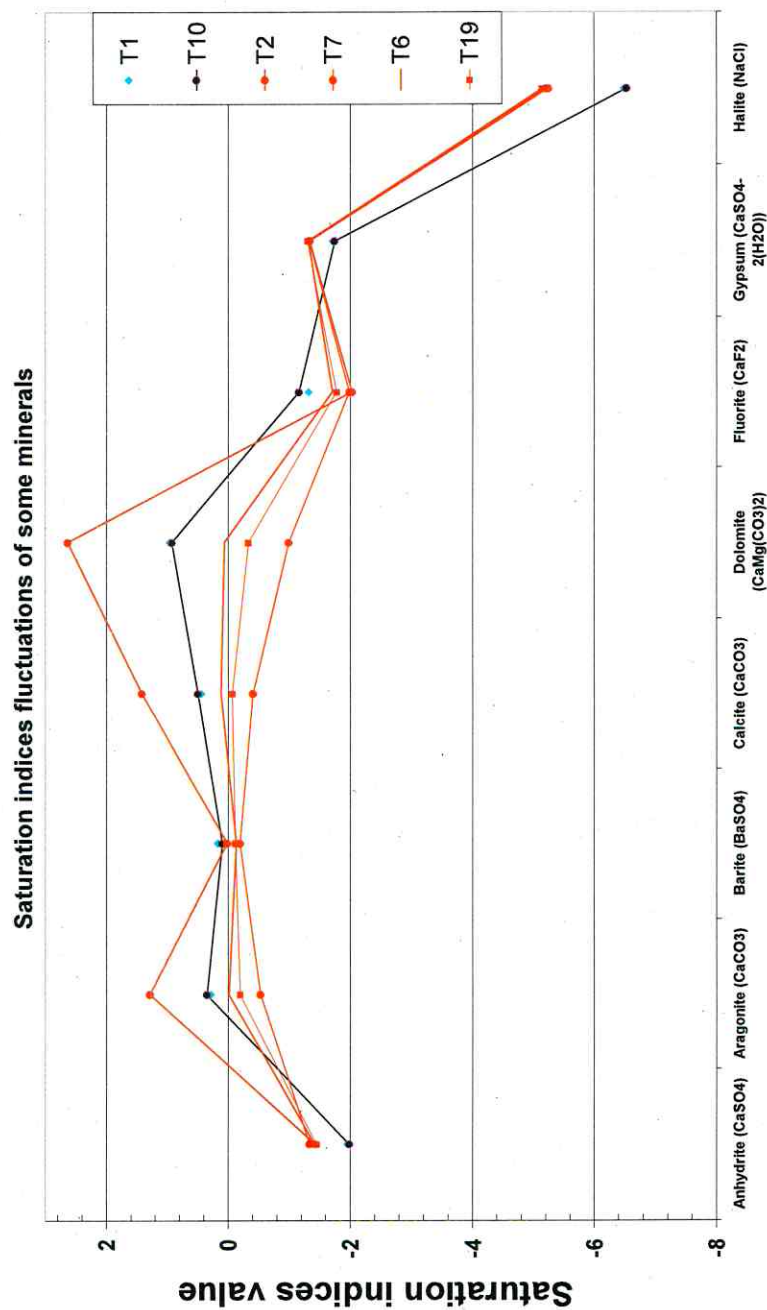
Fig. 3.15: Fluctuations of the saturation indices. The variations of the physiochemical parameters values lead to the intensive fluctuations of the mineral saturations indices even along groundwater flow line. Most of the minerals saturation indices of water group B locate between the ones of water group A and water group C.

89

REE, C1 Chonderite Normalized

Log REE, C1 chonderite normalized

REE
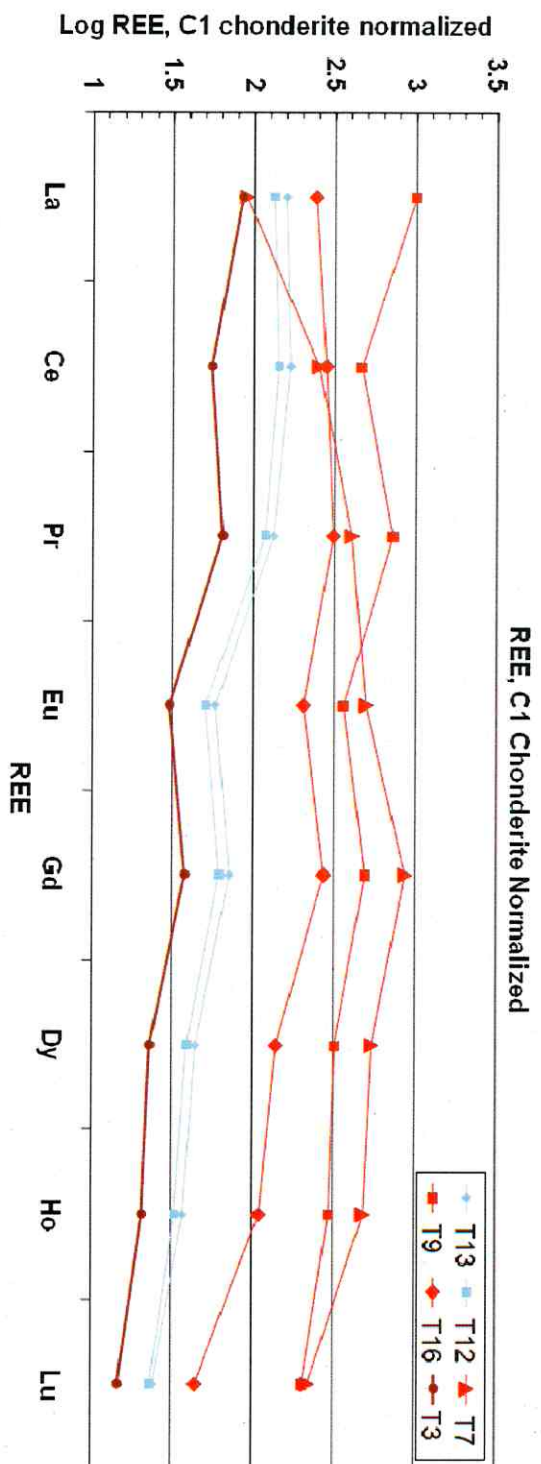
Red lines: lower aquifer (water group C).
Blue lines: upper aquifer (water group A).
Black lines: upper aquifer mixed (water group B).

Fig. 3.16: Fluctuations of rare earth elements (REE) of the groundwater samples. The three water groups have three independent REE signatures. The dramatic decreasing of the REE concentrations of the mixed groundwater (water group B) is due to the intensive sorption of them during the up ascending by the embedded normal faults in the marl aquiclude layer.

90

from the embedded normal fault within the major strike slip fault zone. The PHREEQ extension of the program code Aquachem was used to estimate the percentage of mixing (Tab. 3.7). It was found that water group B is mixed by 94% of the upper aquifer (water group A) and 6% of the lower aquifer (water group C). The mixing process degrades the water quality of the groundwater of the upper aquifer and is changing it from low sodium and salinity hazard to moderate salinity and sodium hazard (Fig. 3.17).

Tab. 3.7: The optimized mixing percent. T25 represents water group A, T33 represents water group C and T3 represent water group B the mixing zone. It was found that water group B is a result of mixing 94% of water group A with 6% of water group C.

Solution 1: T25				
Solution 2: T33				
Optimized sample: T3				
Contribution of sample 1	94%			
mg/l	Sample 1	Sample 2	Sample 3	Optimized
Na	43.90	191.00	29.62	52.73
K	2.74	25.30	2.95	4.09
Ca	71.94	97.10	39.08	73.45
Mg	23.50	20.20	14.83	23.30
Cl	70.30	351.00	58.42	87.142
HCO3	260.50	163.84	119.59	254.70
SO4	34.56	142.00	29.45	41.01
pH	7.30	7.84	7.47	7.33

C1   250   C2   750   C3   2250   C4

Sodium Hazard (SAR)

32

26

19   S4

13

6

0

100   1000

Salinity Hazard (Cond)

S3

S2

S1

Legend

A	T1
V	T10
C	T11
D	T12
E	T13
G	T15
H	T16
I	T17
J	T18
K	T19
L	T2
P	T22
K	T23
Q	T24
R	T25
S	T26
T	T27
U	T28
I	T29
W	T3
X	T30
Y	T31
Z	T32
A	T33
L	T4
C	T5
W	T6
N	T7
Q	T8
P	T9

Sodium (Alkali) hazard:
S1: Low
S2: Medium
S3: High
S4: Very high

Salinity hazard:
C1: Low
C2: Medium
C3: High
C4: Very high

Red color: lower aquifer.
Blue colour: Upper aquifer
Sample T5 is a well that
penetrate the two aquifers.

Fig. 3.17: The groundwater mixing is increasing the salinity and sodium hazard of the upper aquifer because the lower aquifer has a high and very high sodium and salinity hazard.

3.3 Groundwater recharge

Groundwater recharge is a critical factor for understanding the flow and the origin of the groundwater especially in these topographically complex catchment areas such as Wadi Zerka Ma'in catchment. The variations of groundwater recharge quantity to the water table owing to the variations in soil properties and thickness, fault and fractures hydrologic prosperities of geologic layers in the unsaturated zone and climatic factors. However, the last two factors vary strongly in Wadi Zerka Ma'in as a result of being a faulted catchment area and locate within the Dead Sea rift valley (Domenico & Schwartz 1997, Fitts 2002).

The major strike slip fault that bounds the middle and the lower part of the catchment area and hence generate fractures and minor faulted zones in addition strong orographic spatial control on climatic parameters by the Dead Sea rift that divided the catchment area into major units high land and lower land where the elevations reach up 1000 and 420 meter above sea level respectively. Therefore, a hydrological modelling that considers the hydrological heterogeneity of the Wadi Zerka Ma'in catchment area is needed to estimate and understand the groundwater recharge as a result of the structural setting of the Wadi.

Direct groundwater recharge is the water added to the groundwater reservoir in excess of soil-moisture deficits and evapotranspiration by direct vertical percolation through the vadose zone (Lerner et al. 1990). The chosen hydrogeologicl boundaries of the arid catchment area of Wadi Zeka Ma'in consider the direct groundwater recharge type.

However, the arid catchment areas have on average a potential of evapotranspiration that exceeds the rainfall. Therefore, direct groundwater recharge generates occasionally on rainfall events of high concentration, accumulation of rain water in depressions and streams, and the

ability of rain water to escape evapotranspiration by rapid infiltration through the soil media and percolation through cracks, fissures, or pores of the rocks (De Vries et al. 2002).

According to daily observations of five climate stations, the average rainfall and temperature for the last 30 years of the studied area are presented in Figures 3.18 and 3.19. They show that the rainfall average of the studied area decreased in the last 28 years from 275 mm/year to 100 mm/year while temperature increased from 24.8 to 26.8 degree. Such local climatic change affects the runoff and the evapotranspiration, and therefore the groundwater recharge (Bouraoui et al. 2009). To evaluate that effect, a hydrological modelling was done according to JAMS software in three steps as follow:

A) An initialization period.

B) Parameter calibration, parameter optimization and sensitivity analysis for the soil water module were progressed by using the available data.

C) Parameter validation was carried out by running the model with the complete 28 years.

Figure 3.20 shows that the potential evaporation mostly exceeds the actual evaporation; therefore, groundwater recharge occurs occasionally. The local climate change for the last 28 years has led to increased evapotranspiration potential from 130 mm/month to 148 mm/month; as a result of increased temperature with the subsequent decrease in groundwater recharge due to increased actual evapotranspiration.

The simulated hydrograph of Wadi Zerka Ma'in River for the last 28 years (Fig. 3.21) shows that the flash flood of the river has decreased from 37.5 m³/s to less than 2 m³/s, as a

94
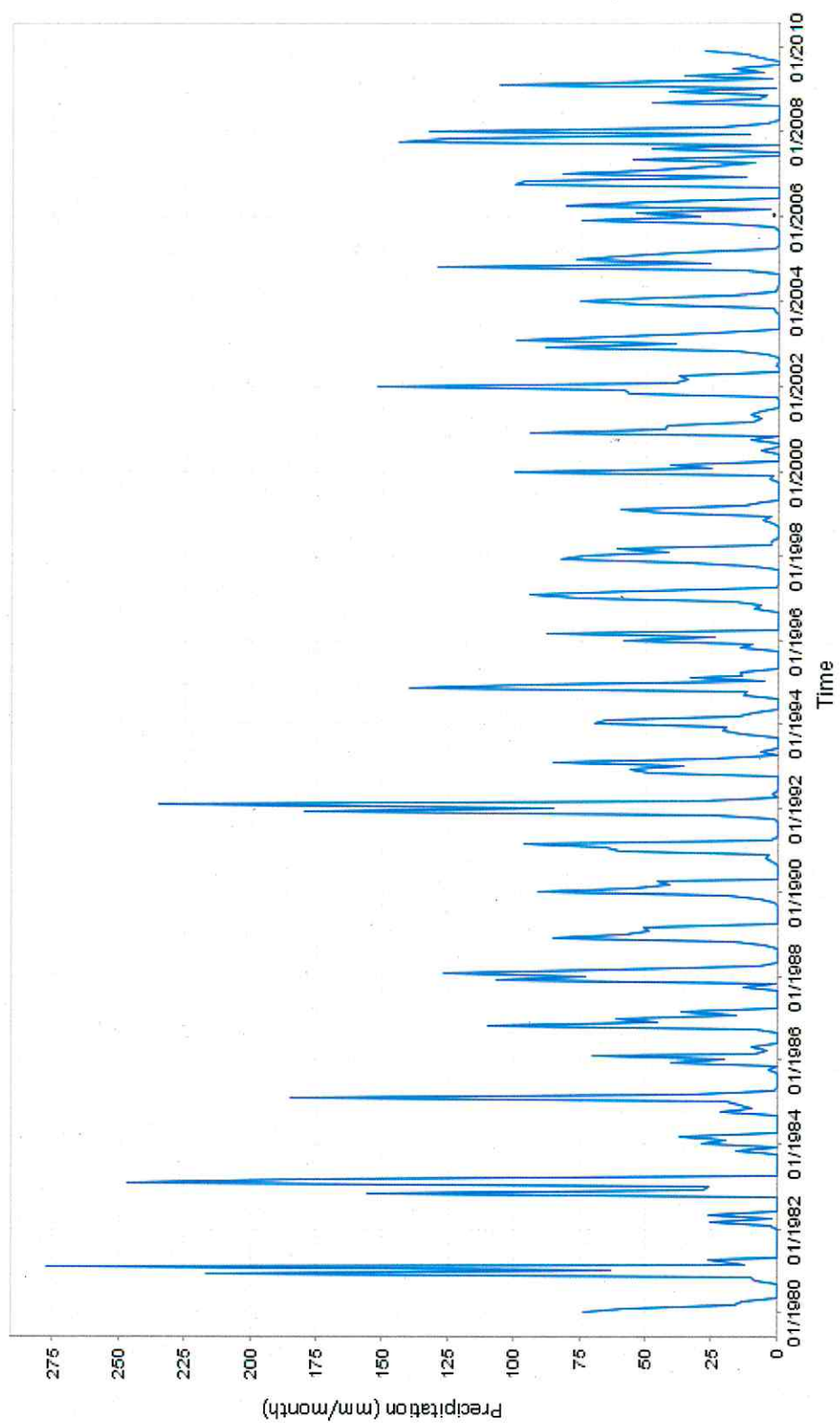
Fig. 3.18: Average monthly amount of rainfall over the super mesh.
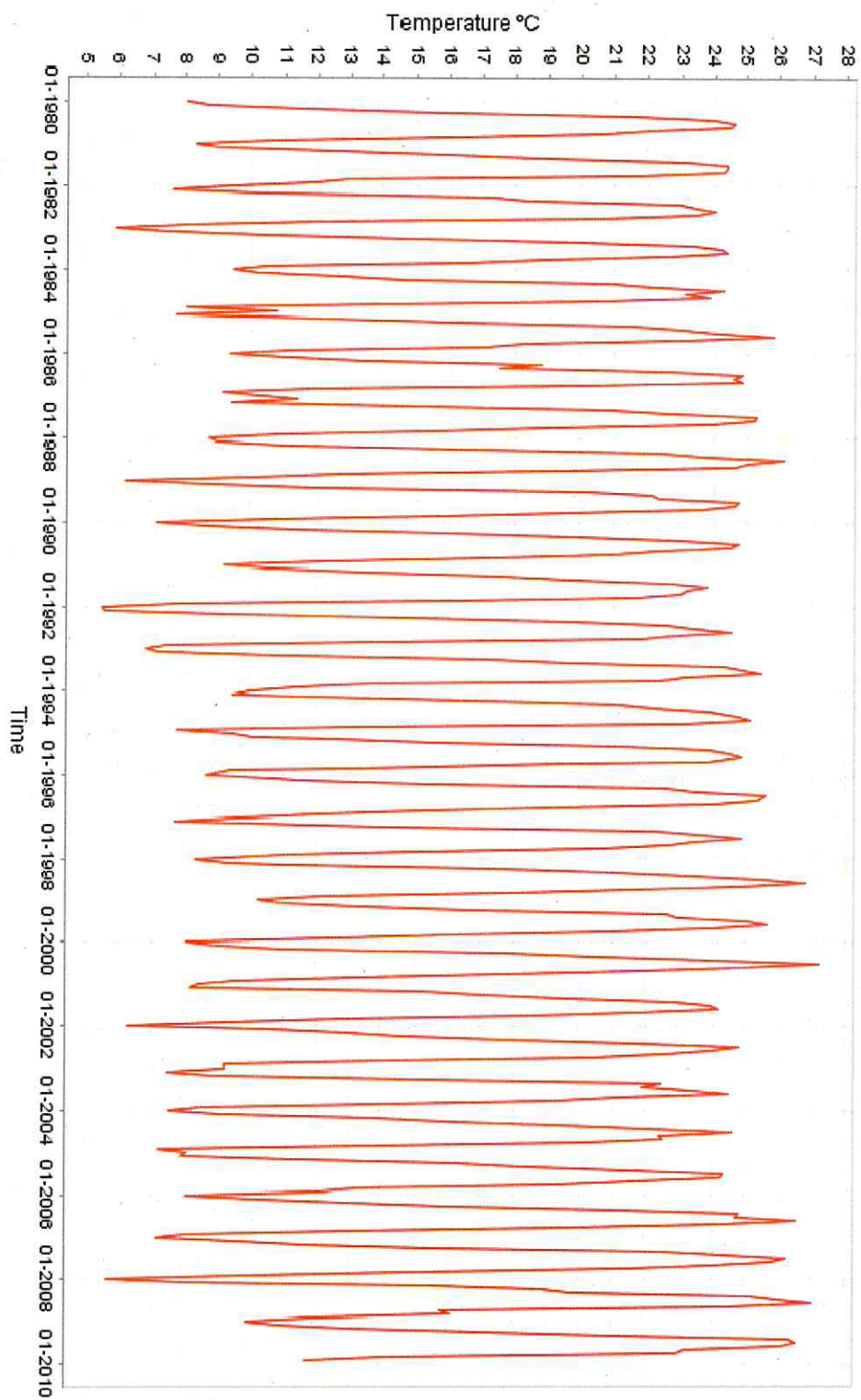
Fig. 3.19: Average monthly temperature over the super mesh.

96
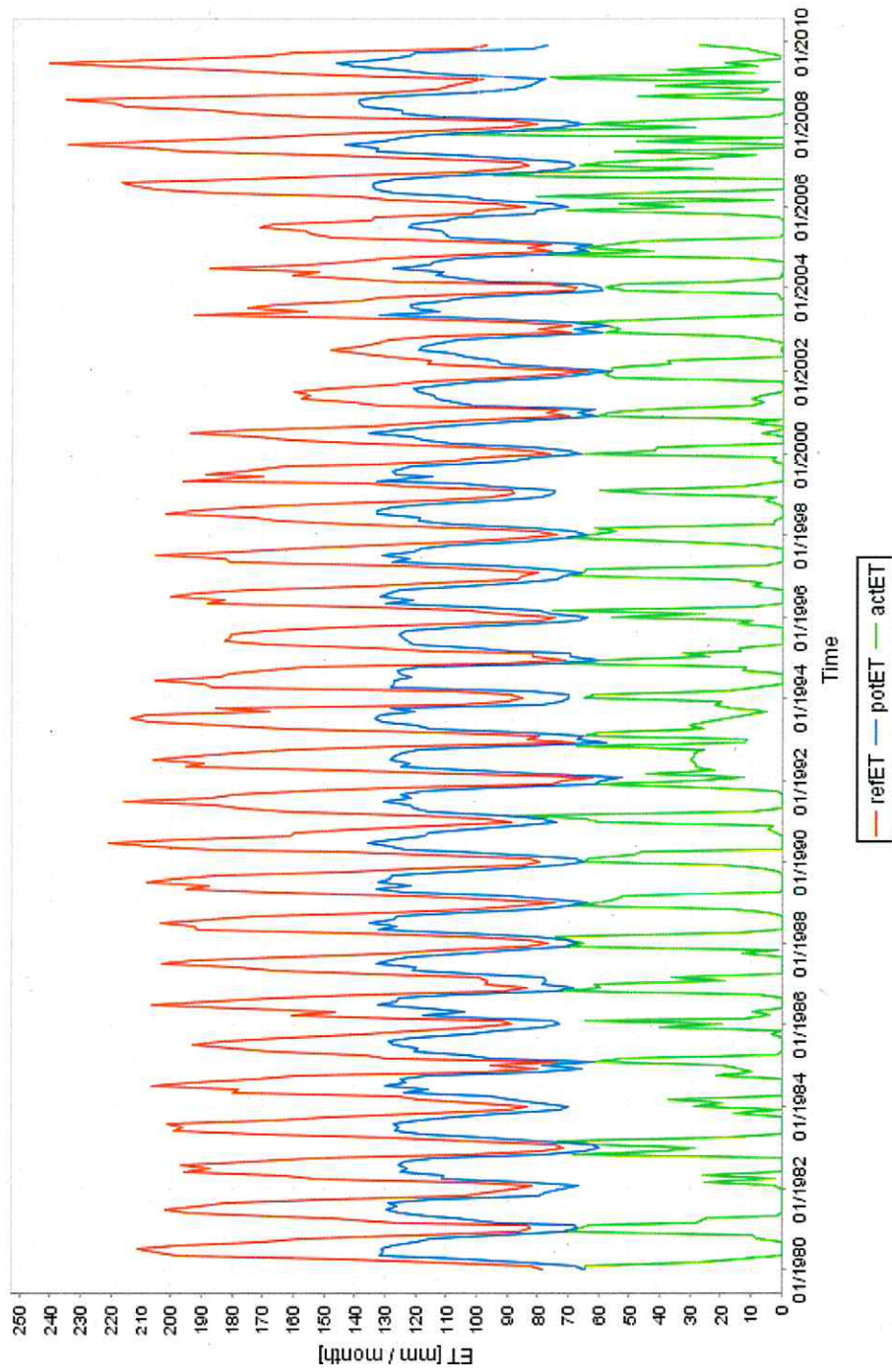
Fig. 3.20: Actual evapotranspiration (actET) from the soil horizon and the plant cover over the super mesh. The potential evapotranspiration (potET) exceeds the actual one while both of them are more than the average reference global evapotranspiration (refET).
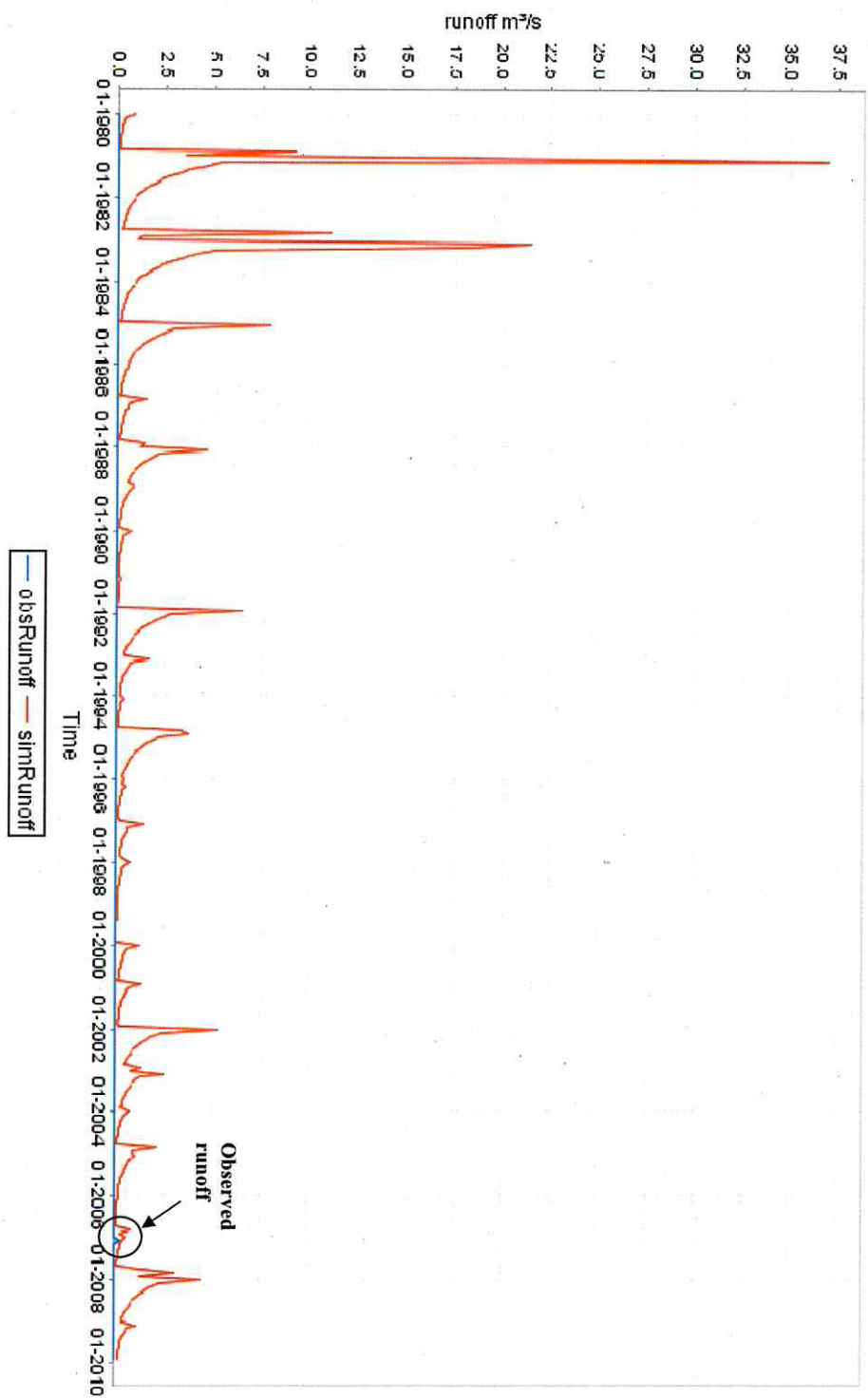
Fig. 3.21: Modelled hydrograph of Zerka Ma'in River. The river discharge consist of flash flood (SimRunoff) and the observed value (obsRunoff) represents a direct field measurement of site NO.1.

98

maximum value. This could be a result of the decrease in rainfall. Zerka Ma'in River discharge recorded data are unavailable. Therefore, field flow measurements were carried out for the Zerka Ma'in River during flash floods to roughly calibrate the modelled hydrograph, by modifying the soil physical parameters (Fig. 3.22).

In the upper part of the Wadi most of the springs are equal or below 6th magnitude (63 to 630 mL/s) therefore the river has no remarkable base flow and most of its discharge is flash flood. On the other hand, the groundwater level in the lower part of the catchment area is higher than the river level; hence the river is a losing stream in the upper part and is slightly improved to a gaining stream in the lower part.

Climatologically, the studied area is heterogeneous since there is a sharp difference in the rainfall distribution where it reaches up to 600 mm/year in the upper part of the catchment and 100 mm/year in the lower part. Potential evapotranspiration distribution exhibits similarity with a bigger difference, it reaches up to 2000 mm/year in the upper part and 4000 mm/year in the lower part (Al-Bakri et al. 2010).

From a geomorphologic prospective view, the catchment area is considered also heterogeneous. This is indicated by the two major trends of the drainage network, N-S and E-W, and by the high asymmetry and low similarity value which control the slope aspect and angle; and hence the runoff and the groundwater recharge (Beven 2001, Srinivasan & Engel 1991).

That geomorphological and climatic heterogeneity led to the spatial distribution of the groundwater recharge presented in Figure 3.23. It shows the highest amount of groundwater
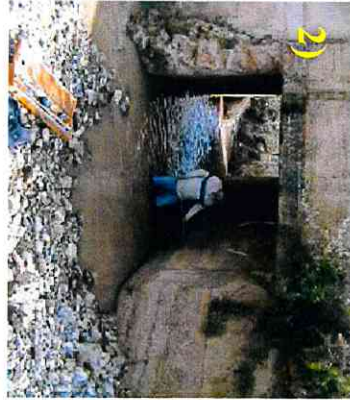
Discharge = 0.12 m³/s
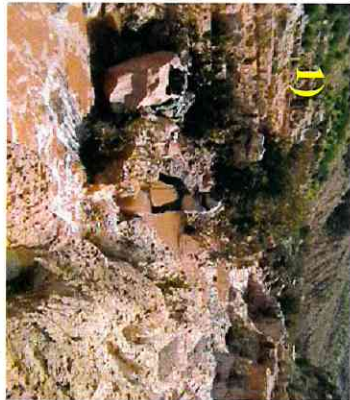
Discharge = 0.21 m³/s
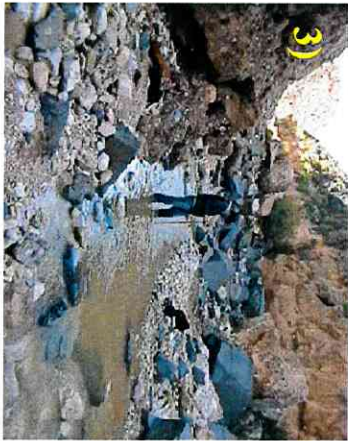
Discharge = 0.15 m³/s
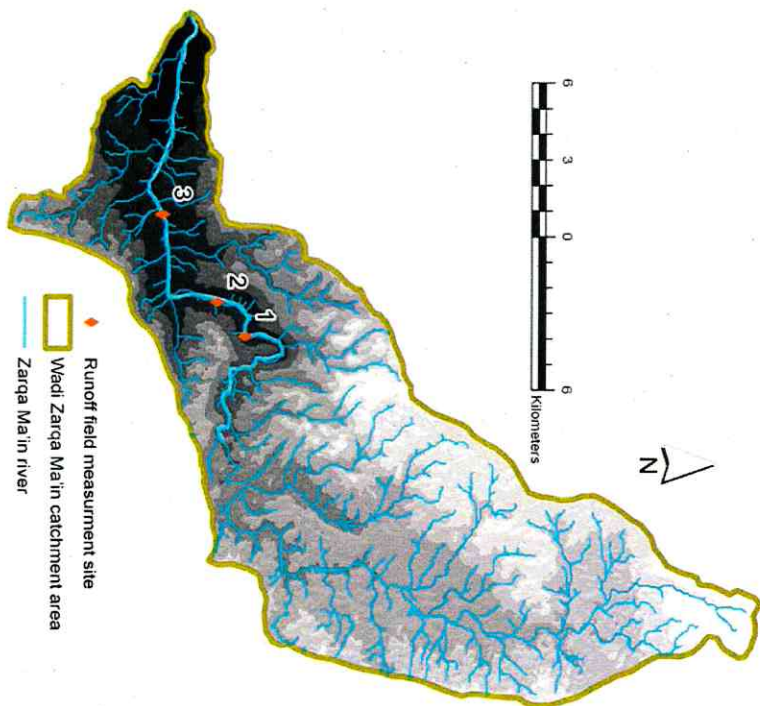
Fig. 3.22: Some sites of the field measurement of Zerka Ma'in River discharge. The upper part of the river and up to site 2 the river is a losing stream, the groundwater level is lower than the surface water level. After site 2 the River becomes gaining, the groundwater level is equal or slightly higher than the surface water level. The field measurement of site NO.1 was used for calibration.
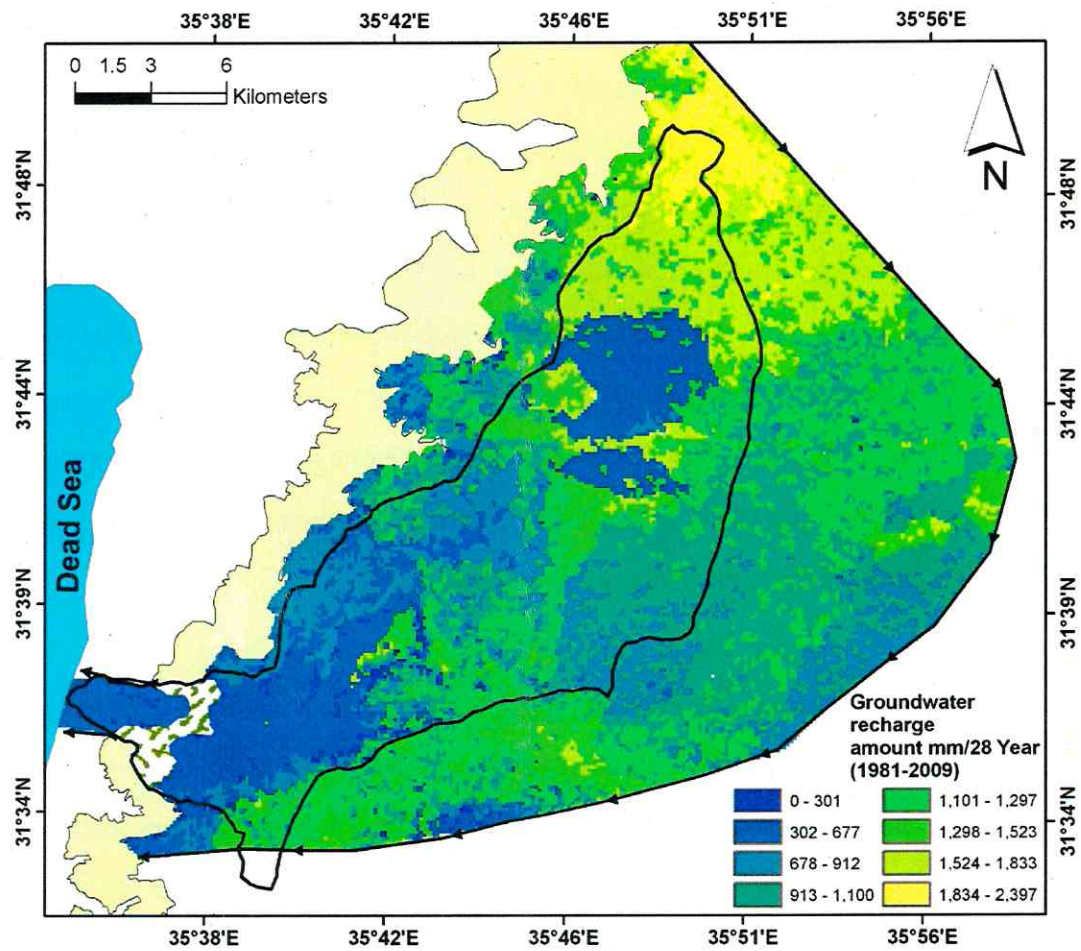
Fig. 3.23: Spatial distribution of groundwater recharge of the last 28 years (1981-2009). The low value of recharge in the lower part of the studied area is due to the low amount of precipitation while in the upper part is due to the urbanized area of Madaba city.

recharge in the upper part of the studied area where the rainfall amount is maximum (i.e. reaching up to 300 mm/year), while the lower part is the minimum (i.e. 100 mm/year). However, the low recharge zone in the upper part of the catchment area is due to the urbanized area of Madaba city where the amount of runoff is high (Butler & Davies 2000); and hence the amount of groundwater recharge is low. The asymmetry of the catchment area generates a rift zone in the northern middle part with high slope angles. That rift area has a zone of low recharge amount due to the large runoff converted water by the high slope angles (Cheng et al. 2008). The southern middle part of the catchment area has lower slope angles and therefore lower runoff and higher groundwater recharge incomparable to the northern middle part (Cheng et al. 2008, Butler & Davies 2000).

The climatic change affects surface water runoff directly through changes in the major long-term climate variables such as temperature and precipitation (Jones et al. 2005, Pruski and Nearing). Groundwater recharge is related to climate change through the direct interaction with surface runoff (Jones et al. 2005). Quantifying the impact of climate change on groundwater resources requires an accurate estimation of groundwater recharge (Holman 2006).

The HRUs consider the heterogeneity of the catchment area in the groundwater recharge modelling and therefore obtain an accurate estimation for the groundwater recharge (Flügel 1997). The average yearly recharge of the groundwater (Fig. 3.24) multiplied by the area of the super mesh (611.25 km²) gave the yearly quantities of groundwater. Figure 3.25 shows that the groundwater recharge quantities fluctuate almost regularly; while there is a peak of groundwater recharge every two years. However, the general trend of groundwater recharge is decreasing as a result of the decreased rainfall and the increased temperature and the consequent decrease in runoff and increased evapotranspiration, respectively. During the last
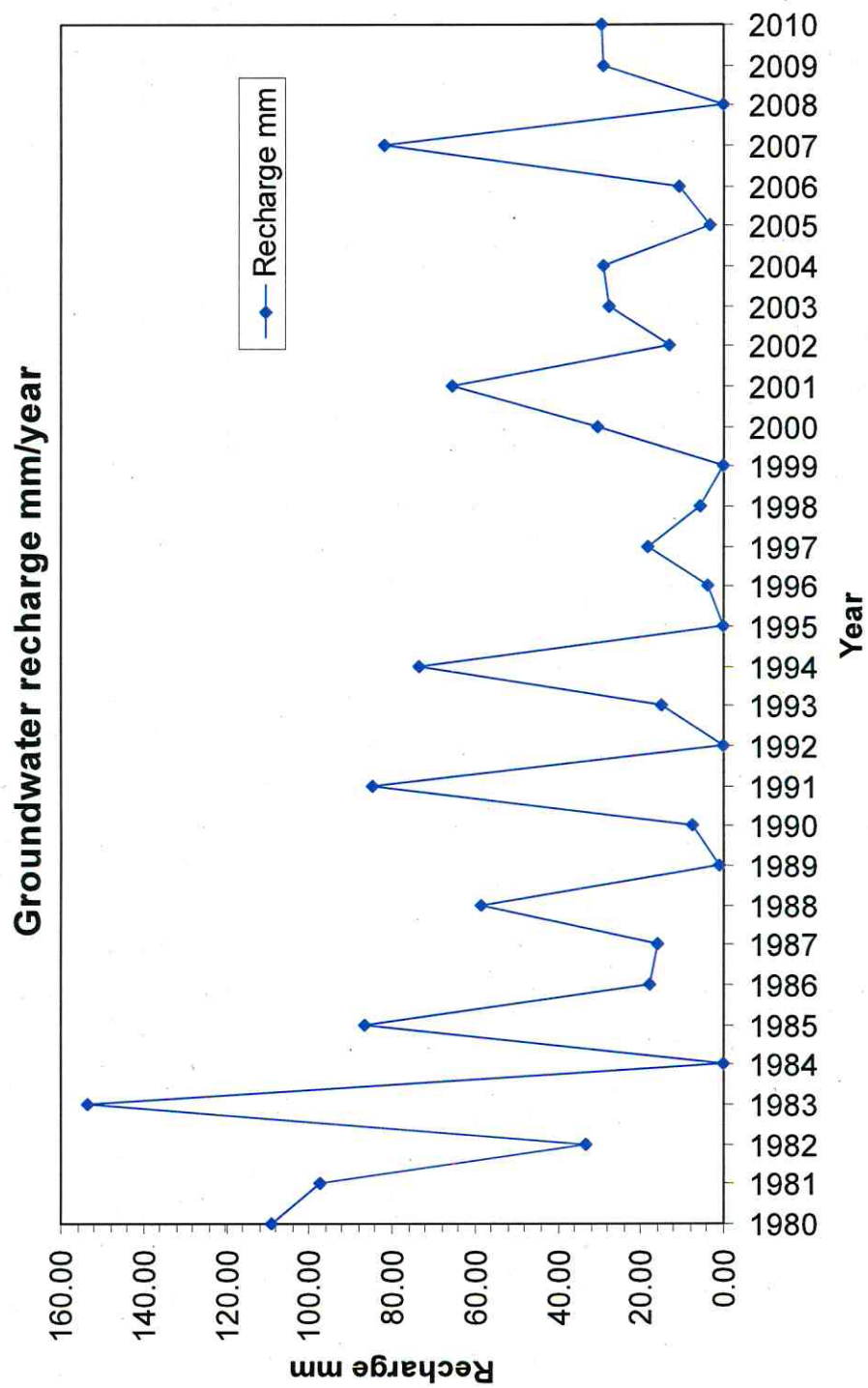
Fig. 3.24: Groundwater recharges mm/year as a result of the water budget for the years 1980 - 2010.
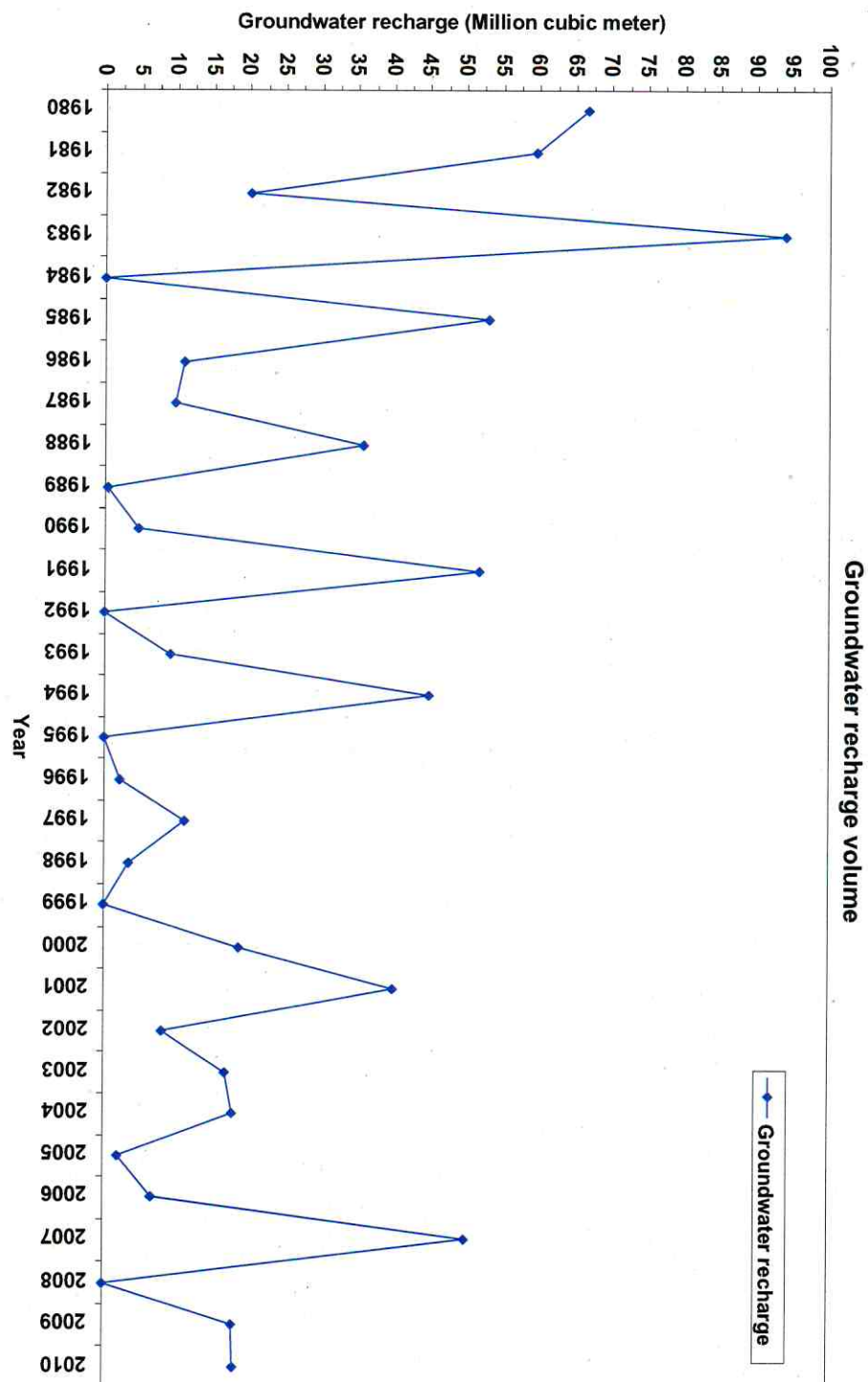
Fig. 3.25: Amount of groundwater recharge in the years 1981-2010. The general trend of groundwater recharge is decreasing as a result of decreasing rainfall due to climatic changes.

28 years, the maximum amount of groundwater recharge of about 95 million cubic meters occurred in 1983 while after 1992 the groundwater recharge quantity does not pass the 50 million cubic meter as a result of climatic change, rainfall decrease and temperature increase.

3.4 Groundwater flow modelling

Faults are often analysed due to sealing capacity of gas, oil, and groundwater in sedimentary basins. Fluid flow in hard rock is that fault zones are responsible for the largest amount of fluid transport in the bedrock. In order to understand the influence of faults and fracture zones on hard rock numerical modelling is needed (Domenico & Schwartz 1997). This modelling is used to investigate the groundwater flow directions and the hydrogeological prosperities as a result of the faulting (Ganerød et al. 2008, Allen & Michel 1999).

3.4.3 Steady-state groundwater flow model

Steady-state groundwater flow occurs when the magnitude and direction of the flow velocity are constant with time at any point in a flow field. Transient groundwater flow occurs when at any point in the flow field the magnitude or the direction of the flow velocity can change with time (Freeze and Cherry 1979). We consider the steady-state modelling for evaluating the effect of the structures on the groundwater flow.

The upper limestone aquifer of the study area has secondary porosity, while the lower sandstone aquifer has both primary and secondary porosity. Accordingly, the groundwater in the upper aquifer has a preferential flow through the structural features such as joints, faults planes, and cracks; while the groundwater of the sandstone aquifer has mainly a matrix flow through the sandstone pores (Domenico & Schwartz 1997 and Margane et al. 2002).

105

Heterogeneity of the aquifers refers to water-bearing materials that conform to no single system of groundwater flow. The structural features of the limestone lead to more water bearing materials and hence more heterogeneity than the lower sandstone aquifer (Allen and Michel 1999). Therefore, a steady groundwater flow for the upper limestone aquifer was assumed where we expect more effects through the faults on the groundwater flow. The lower aquifer is assumed to be homogeneous and connected with the upper aquifer through the embedded faults. However, the hydrological data scarcity concerning the lower aquifer hinders a comprehensive steady-state groundwater flow modelling.

Steady-state conditions indicate that the inputs and outputs of the groundwater are in equilibrium so that there is no net change in the groundwater system with time (Domenico & Schwartz 1997, Freeze and Cherry 1979). According to the simulation, a value of groundwater recharge for the year 2007 of 80 mm/year was used, where a groundwater level map was interpolated by the groundwater level measurement of the same time period, and an average hydraulic conductivity value of 1.5×10^{-5} m/s, that was estimated by a pumping test (Margane et al. 2002). To calibrate the result of the simulation, PEST programme (Doherty 2003) as an interface module was used. The benefit of PEST is doing the calibration automatically. It requested three files as follow:

1) Input file called template file that is supplied by the FeFlow software.

2) Result file (instruct file): it is determined by the position of the resulting values for the observation points in the FeFlow results file. Figure 3.26 shows the hydrogeological observation points that were used for the calibration.

3) Higher-ranking file (control file): It compares the template file to the original (*.fem file) and the instruct file to the original (*.dar file) and arranges all observation point data and the numerical settings.

Figure 3.27 shows the results of the steady-state groundwater modelling, where the groundwater flow of the upper aquifers runs directionally from the north to west. However, the groundwater head contours become closer to each other in the middle of the model within the faulted part of the study area where we observe a connection between the two aquifers. The major strike slip fault divides the modelled area into different zones of permeability where the highest permeability zones are located within the zone of the strike slip fault and it's embedded normal faults. However, those normal faults generate a permeable zone in the aquiclude unit and make connection, conduit, between the two aquifers.

Fig. 3.26: Boundary condition of the groundwater flow model. In addition to the field water level measurements of wells and springs, observations at hydrogeological points were generated in the groundwater flow map by GIS to increase the accuracy of the calibration.

Legend:
- • Groundwater level point for calibration
- ▢ The hydrological boundary of Wadi Zerka Ma'in catchment
- ▢ Super elements that were used for generating the supermesh
- (hatched) Connection zone by the normal faults

Fig. 3.27: Steady-state groundwater modelling result for the upper aquifer.

Chapter 4

Summary and conclusions

4.1 Summary of accomplishments

An interdisciplinary research of hydrogeology and structural geology was carried out in the catchment area of Wadi Zarqa Ma'in during the time period of 2006 until 2011. The major accomplishments are as follows:

1) The structural setting of Wadi Zerka Ma'in catchment area was evaluated by four geomorphological indices:

1.1) Drainage network directions were represented by rose diagrams with the result that orientations of the drainage network are parallel to the fault systems.

1.2) Catchment area asymmetry was estimated by using transverse topographic symmetry factors (T): The T value reach up to 80, indicating that the catchment area is highly asymmetric while the asymmetry arrows are parallel the oldest fault system.

1.3) Zerka Ma'in river topographic profile was extracted by using a high resolution DEM of 15 m. Two knickpoints along that profile were identified which are crossed by two major embedded normal faults of a regional transtensive fault.

1.4) Catchment area similarity was evaluated by a convex hypsometric curve. It could be shown that the catchment area is a convex landform as a result of the recent embedded normal faults.

2) The influence of the Wadi structural setting on the groundwater chemistry of the aquifers was evaluated according to geochemical analyses:

2.1) Plotting the data of the major ions in Durove diagram revealed some evidence for three groundwater types.

A) Alkaline – earth water predominantly bicarbonate (water group A) in the upper aquifer.

B) Alkaline – earth water predominantly sulphate (water group B) in the upper faulted aquifer.

C) Alkaline – earth water predominantly chloride (water group C) in the lower aquifer.

2.2) Chemical signatures of the trace and rare earth elements and saturation indices along groundwater flow path line that passes the two aquifers and the aquiclude layer were investigated. Each water group shows some evidence for a particular signature of trace and rare elements, and saturation indices.

2.3) An Estimation of groundwater mixing between water group A and water group C was performed with the result that water group B is composed of 96% from water group A and 4% from water group C.

3) The influence of the structural setting in the groundwater recharge was evaluated by recharge modelling and field measurements:

3.1) Groundwater recharge modelling according to hydrologic response units (HRUs) method: the model was fed with high resolution surface data which reach up to 15 meter. These data were extracted by remote sensing and GIS approach.

3.2) Field measurements for Zerka Ma'in river discharge was performed during flash floods at several crossed river profiles to calibrate the runoff model and specify where the river becomes a losing and where it becomes gaining.

4) The influence of structural setting on the groundwater flow was evaluated by steady-state groundwater modelling in five steps:

4.1) Building a 3D geological model by constructive interpolation of geological cross sections to generate the aquifer geometry was done with GMS 6.5.

4.2) Unifying the geological layers into three hydrogeological units.

4.3) Groundwater level map were plotted by interpolation of the groundwater level measurements using ArcGIS 9.3 software and IDW method. .

4.4) Groundwater flow model boundaries were defined at groundwater devides and the 3D geological model was clipped according to the subsurface catchment.

4.5) Running and calibrating the steady-state model revealed that the faulted zone represents a high permeability zone too and the groundwater flow runs directionally from the north to the west where the groundwater head contours become closer to each other within that zone.

4.2 Conclusions

The geomorphological features of the catchment areas develop simultaneously with growth of tectonic structures. Therefore, the structural geology of the Wadis can be evaluated by an investigation of their geomorphological characteristics. For the Wadi Zerka Ma'in catchment area, we have the following conclusions:

- The drainage network of the Wadi Zerka Ma'in catchment area follows the same directions as the local oldest fault systems.

- The regional strike-slip fault of Wadi Zerka Ma'in has embedded normal faults that cause two major topographic lowerings along the Zerka Ma'in River: 1) 34 km from the source with a lowering of 200 m; 2) 49 km from the source with a lowering of 250 m.

- The catchment area of Wadi Zerka Ma'in is asymmetrical due to the NW-SE fault system. The asymmetric arrows have the same trends as the fault systems.

- The hypsometry graph shows that the catchment area is convex. This is a result of the two topographic lowering that result from the embedded normal faults within the regional strike-slip fault. The catchment area of Wadi Zerka Ma'in is in an early stage of the geomorphic cycle.

In the active tectonic area, such as the Dead Sea rift valley, faults have a major influence in the groundwater chemistry development. Wadi Zerka Ma'in catchment area locates in the Middle Eastern side of that rift and has three hydrogeological units: (1) The upper unconfined limestone aquifer, (2) marly aquiclude aquifer and (3) the lower confined sandstone aquifer.

113

In this catchment area, the groundwater of the upper aquifer is contaminated naturally by the influence of the faults in the groundwater chemistry. However, the major hydrogeological findings are as follows:

- The major strike slip fault of the Wadi Zerka Ma'in catchment area passes perpendicularly to the hydrogeological units and its embedded normal faults form conduits between the upper aquifer and the lower one.

- The confined groundwater of the lower aquifer rises up through the conduits, the embedded normal fault, to the upper aquifer and creates a mixed groundwater.

- There are three groundwater groups in Wadi Zerka Ma'in aquifers: (1) Alkaline – earth water predominantly bicarbonate (water group A) in the upper aquifer. (2) Alkaline – earth water predominantly sulphate (water group B) a mixed groundwater in the upper aquifer. (3) Alkaline – earth water predominantly sulphate-chloride (water group C) in the lower aquifer.

- It was found that the chloride ion is an excellent indicator for groundwater mixing where for each water groups A, B and C has a distinguished chloride concentration interval.

- Some trace elements and saturation index signatures characterize the three water groups A, B and C.

- The three water groups (A, B and C) have three REE signatures. The REE signature of water group B is depleted with REE concentration as a result of the intensive sorption on clay minerals of the marl rocks during rising up in the conduits.

- The groundwater of the two aquifers is recharged by rainfall from different climatic origins. Therefore, the stable isotope components of $\delta18O$ and $\delta2H$ of the two aquifers is not consistent and does not show regular mixing.

- Water group B is modelled as the result of an uprising mixture of the upper aquifer water with the lower aquifer water. The result of the modelling is 94% of the groundwater of the upper aquifer is mixing with 6% of groundwater of the lower aquifer. This mixing leads to contaminate and increase the salinity hazard in the upper aquifer.

The structural setting of the catchment area has led to heterogeneous zones of groundwater recharge and flow. Therefore, a structural evaluation of the Wadi is essential for understanding its groundwater system. In Wadi Ma'in, the structural setting has impacted the groundwater system as follows:

- The study area receives a direct groundwater recharge within hydrogeological boundaries of 611.25 km².

- The study area is heterogeneous from a geomorphical and a climatic prospective, which leads to a spatially heterogeneous distribution of groundwater recharge.

115

- The major strike slip fault zone causes a high permeability zone in the upper aquifer with the highest permeability areas located within that zone.

The climatic changes influenced the groundwater recharge of Wadi Zerka Main as follow:

- The trend of groundwater recharge is decreasing as a result of rainfall decreasing and temperature increasing and subsequent increase of evapotranspiration and decreasing runoff.

- The groundwater recharge quantities fluctuate almost regularly where every two years a peak of groundwater recharge was observed.

- For the last 28 years the maximum value of groundwater recharge was found to be 95 million cubic meters in 1983 while after 1991 recharge was not exceeding 50 million cubic meters per year as a result of climatic change, decrease in rainfall, and increase in temperature.

Chapter 5

Outlook and Recommendations

Wadi Zerka Main catchment area is a complicated study area from geomorphologically, hydrochemically, hydrologically and hydrogeologically point of view. The conceptual system of that complicated system was clarified to a large extent by an advanced approach of remote sensing, GIS and, numerical modelling. However, the following issues still need to be studied and clarified:

1) Geomorphology: Wadi Zerka Main catchment area was recognized to be a recent basin. However, it has not been unambiguously proven whether the studied catchment was separated from Wadi Al Mujb catchment area, the largest catchment area at the eastern side of the Dead Sea, through a strike slip fault displacement. Introductory evidence is the drainage network offset between the two catchments. Therefore, chronological and sedimentlogical studies of the sediments of the two catchments are recommended to clarify the relationship between the two catchment areas.

2) Hydrogeochemistry: Some evidences were found for mixing between the groundwater of the two aquifers and the ratio of mixing was estimated to be 94% from the upper and 6% from the lower aquifer. Mixing between two different solutions may lead to a change of the saturations indices and follow up reactions. It has not been clarified how the geochemical reactions behave as a result of groundwater mixing of the two aquifers. Therefore, an aqueous geochemistry study for the groundwater mixing of the two aquifers is recommended.

117

3) Hydrologically: A groundwater recharge modelling for the catchment area was performed. However, the runoff model calibration was done only by monthly field measurements. To obtain more accuracy and reliability for the runoff calibration, establishing a automated monitoring station at a safe site is recommended. This will give high resolution river discharge data which can be used to calibrate the model with higher accuracy.

It was found during the field measurements of the runoff discharge of Zerka Ma'in River that there is a relationship between the hydraulic situation of the river (losing or gaining) and the river sinuosity: the introductory result shows that the river is behaving as losing stream in the high sinuosity area in the upper part of the river and vice versa in the lower part where the river has a low sinuosity. However, a detailed hydraulic study of the river discharge and the river sinuosity is needed to provide a clear proof of that relationship.

4) Hydrogeology: The groundwater mining from the upper aquifer is severe to supply Madaba city, the largest city at the eastern side of the Dead Sea by drinking water. It was found that the groundwater level is decreasing because the groundwater pumping exceeds the groundwater recharge. This might lead to an increase of contamination of the groundwater in the upper aquifer as a result of increasing groundwater mixing with the lower aquifer which has three times salinity of the upper one. However, the steady-state model developed within this study was suitable to forecast the drawdown of the groundwater level as a result of groundwater abstraction. Therefore, a transient groundwater modelling is recommended based on the steady-state groundwater model and groundwater recharge model that was generated in this study. As a result of this transient groundwater model the optimized amount of the groundwater utilization could be specified and sustainable groundwater management can be proposed.

References

Al Sawarieh, A. (2005): Heat sources of the groundwater in the Zara-Zarqa Ma'in-Jiza area, Central Jordan. *Published PhD thesis, University of Karlsruhe*, Germany.

Al-Bakri, J., Suleiman, A., Abdulla, F., and Ayad, J. (2010): Potential impact of climate change on rainfed agriculture of a semi-arid basin in Jordan. *Physics and Chemistry of the Earth*. In prees.

Allen, M. and Michel, A., (1999): Characterizing a faulted aquifer by field testing and numerical simulation. *Ground Water 37*, pp.718-728.

Allison, G., Barnes, C., Hughes, M. and Lenay, F. (1983): Effect of climate and vegetation on oxygen-18 and deuterium profiles in soils. *International atomic energy agency symposium 270*, Vienna.

Anderson, P., and Woessner, W. (2002): Applied groundwater modeling: Simulation of flow and advective transport, *Academic Press*, USA.

Andrews, J. (1991): Palaeozoic lithostratigraphy in the subsurface of Jordan. - *Geol. Bul 2, (Natural Resources Authority)*. Amman.

Appelo, J. and Postma, D. (2005): Geochemistry, Groundwater and Pollution. A.A. Balkema Publishers, Leiden.area, Jordan. *Geol, Jb. Reihe, B 53*, pp. 55-75.

Audi, R. (2003): Epistemology: a contemporary introduction to the theory of knowledge. *Routledge*, New York.

Aydin, A. and Johnson, A. (1978): Development of fault as zone of deformation bands and as slip surface in sandstone. *Pure and applied geophysics 116*, pp. 931 -942.

Aydin, A. and Reches, Z. (1982): Number and orientation of fault sets in the field and in experiments. *Geology 10*, pp.107 – 112.)

Bajjali, W. and Abu-Jaber, N. (2001): Climatological signals of the paleogroundwater in Jordan. *Journal of Hydrology 243*, pp.133 – 147.

Bayer, J. (1988): Wadi Araba und Jordantal, Ein tektonischer Graben und zugleich Blattverschiebung. *Natur und Museum 118*, pp.33-45.

Ben-Avraham, Z. (1991): Development of asymmetric basins along continental transform faults. *Tectonophysics 215*, pp.209-220.

Bender, F. (1974): Geology of Jordan. Contribution of the Regional Geology of the Earth, *Borntraeger*, Berlin.

Beven, K. (2001): Rainfall-runoff modelling: the primer. *John Wiley and Sons Inc*.USA.

BGR Bundesanstalt fuer Bodenforschung und Rohstoffe (1992): investigations of the regional basalt aquifer system in Jordan and Syria, *E/ESCWA/ENR/1*. Hannover.

119

Bier, G. (2007): Hydrological modeling: theory and practice. *Wageningen University*, USA.

Bishop, P. Hoey, B. Jansen, D. and Artza, L. (2005): Knickpoint recession rate and catchment area: the case of uplifted rivers in Eastern Scotland. *Earth Surface Processes and Landforms 30*, pp. 767-778.

Bormann, H. (2010): Towards a hydrologically motivated soil texture classification. *Geoderma 157*, pp. 142-153.

Burbank, D. and Anderson, R., (2001): Tectonic Geomorphology. *Blackwell Science*, Oxford.

Butler, D. and Davies, J. (2000): Urban Drainage. *Spon Press*, USA.

Chebaane, M., El-Naser, H., Fitch, J. Hijazi, A. and Jabbarin, A. (2004): Participatory groundwater management in Jordan: Development and analysis of options. *Hydrogeology Journal 12*, pp.14-32.

Cheng, Q. and Cai, Q. (2008): The relative importance of soil crust and slope angle in runoff and soil loss: a case study in the hilly areas of the Loess Plateau, North China. *GeoJournal 71*, pp.1572 - 9893.

Clark, D. and Fritz P. (1997): Environmental isotopes in hydrogeology, *Lewis Publishers*, New York.

Cook, G., Walker, R. and Jolly, D. (1989): Spatial Variability of Groundwater Recharge in a Semi-Arid Region. *Journal of Hydrology 111*. pp. 195-212.

Cordova, C., Foley, C., Nowell, A., and Bisson, M. (2004): Landforms, sediments, soil development, and prehistoric site settings on the Madaba-Dhiban Plateau, Jordan. *Geoarchaeology 20*, pp. 29-56.

Coroza, O., Evans, D., and Bishop, I. (1997): Enhancing runoff modeling with GIS, *Landscape Urban Plan 38*, pp.13–23.

Dayan, U. and Morin, E. (2006): Flash flood-producing rainstorms over the Dead Sea: a review, *Geological Society of* America *Special Paper 401*, pp. 53–62.

De Vries, J. and Simmers, I. (2002): Groundwater recharge: an overview of processes and challenges. *Hydrogeolgy Journal 10*. pp.5-17.

Department of Statistics 2009: *Report of population growth in Jordan 2009*. Amman.

Dinesh, S. (2008): Computation and Characterization of Basic Morphometric Measures of Catchments Extracted From Digital Elevation Models. *Journal of Applied Sciences Research 4*, pp.1488-1495.

Doherty, J. (2003): Groundwater model calibration using pilot points and regularisation. *Ground Water 41* pp. 170-177.

Domenico, P. and Schwartz, F. (1997): Physical and chemical hydrogeology. *John Wiley and sons, Inc*. New York.

Dregne, H. (1976): Soils of arid regions. *Elsevier*, Amsterdam.

Epstein, S. and Mayeda, T. (1953): Variation of O-18 content of water from natural sources. Geochim. Cosmochim. *Acta 4*, pp.213–224.

Eugster, P. and Jones, F. (1979): Behavior of major solutes during closed-basin brine evolution. *Am. J. Sci. 279*, pp. 609–631.

Fisher, P., Comber, J. and Wadsworth, A., (2005): Land use and Land cover: Contradiction or Complement. Re-Presenting GIS, *Wiley*, Chichester.

Fitts, C. (2002): Groundwater science, *Academic Press*, an imprint of Elsevier science, London.

Flexer, A. (1968): Stratigraphy and facies development of the Mount Scopus Group in Israel and adjacent countries. *Israel Journal of Earth Science17*, pp.85-114.

Flügel, W. (1997): Combining GIS with regional hydrological modelling using hydrological response units (HRUs): An application from Germany. *Mathematics and Computers in Simulation 43*. pp.297-304.

Franke, L., Reilly, E., and Bennett, D. (1987): Definition of boundary and initial conditions in the analysis of saturated ground-water flow systems – An introduction: *Techniques of Water-Resources Investigations of the United States Geological Survey, Book 3, Chapter B5*, USA.

Freeze, A. and Cherry, J. (1979): Groundwater, *Prentice-Hall, Inc.*, Englewood Cliff.

Gardner, W. (1983): Experimental study of knickpoint and longitudinal evolution in cohesive, homogeneous material. *Geological Society of America Bulletin 94*, pp. 664–672.

Garfunkel, Z. and Ben-Avraham, Z. (1996): The structure of the Dead Sea basin. *Tectonophysics 266*, pp.155 – 176.

Garrote, J., Cox, T., Swann, C., Ellis, M., (2006): Tectonic geomorphology of the Southeastern Mississippi Embayment in northern Mississippi, USA. *Geological Society of America Bulletin 118-9*, pp.1160–1170.

Gat, J. and Carmi, I., (1970): Evolution of the isotopic composition of atmospheric waters in Mediterranean Sea area. *J. Geophys. Res.75*, pp. 3039-3078.

Ganerød, V., Braathen, A. and Willemoes-Wissing, B. (2008): Predictive permeability model of extensional faults in crystalline. *Journal of Structural Geology 30*, pp.993-1004.

Gauckler, P. (1867): Theoretical and practical studies on the flow and the Movement of Water. *Proceedings of the Academy of Sciences*, Paris, France, Tome 64, pp. 818-822.

Gong, J. and Xie, J. (2009): Extraction of drainage networks from large terrain datasets using high through put computing, *Computers & Geosciences Vol.35*, pp. 337-346.

Guangcai, W., Zuochen, Z., Min, W., Cravotta III, C. and Chenglong, L. (2005): Implications of Ground Water Chemistry and Flow Patterns for Earthquake Studies. *GROUND WATER 43*, pp. 478–484.

Hack, T. (1973): Stream-profile analysis and stream-gradient index. *Journal of Research of the U.S. Geological Survey 1*, pp. 421–429.

Hatheway, W., and Kanaori, Y. (2002): Engineering Geology 65, 7th *Annual Report on the International Status of Engineering Geology*, pp. 47-79, Amsterdam.

Henderson, P. (1984): Rare Earth Element Geochemistry. *Elsevier*, Amsterdam.

Holman, P. (2006): Climate change impacts on groundwater recharge-uncertainty, shortcomings, and the way forward? *Hydrogeology Journal 14*, pp. 637-647.

Horowitz, A. (2001): The Jordan Rift Valley. *Ballkema*, Rotterdam. pp 1-730.

Hilley, G., Arrowsmith, J. and Coutand, I. (2003): Differential structural and geomorphic mountain-front evolution in an active continental collision zone: The northwest Pamir, southern Kyrgyzstan. *GSA Bulletin 115*, pp. 166–181

Hurtrez, E., Sol, C., and Lucazeau, F. (1999): Effect of drainage area on hypsometry from an analysis of small-scale drainage basins in the Siwalik Hills (central Nepal), *Earth Surface Processes and Landforms 24*, pp. 799-808.

Hwang, S.(2004): Effect of texture on the performance of soil particle-size distribution models. *Geoderma 123*, pp.363-371.

Ingebritse, S. (2006): Groundwater in Geologic Processes. *Cambridge University Press*, UK.

Iwahashi, J. and Pike, R. (2007): Automated classifications of topography from DEMs by an unsupervised nested-means algorithm and a three-part geometric signature. *Geomorphology Vol. 86*, pp. 409-440.

Johannesson H., Stetzenbach J. and Hodge. F. (1997): Rare earth elements as geochemical tracers of regional groundwater mixing. *Geochimica et Cosmochimica Acta 61*, pp. 3605-3618.

Johannesson, K. (2005): Rare Earth Elements in Groundwater Flow Systems. *Water Science and Technology Library volume 51*, USA.

Johnson, P. (1998): Tectonic map of Saudi Arabia and adjacent areas. *Technical report USGS-TR-98-3*.

Jones, R., Chiew, F., Boughton, W. and Zhang, L. (2005): Estimating the sensitivity of mean annual runoff to climate change using selected hydrological models. *Advances in Water Resources 29*, pp. 1419-1429.

Kam, T (1995): Integrating GIS and remote sensing techniques for urban land-cover and landuse analysis. *Geocarto International 10*, pp.39-49.

Keller, A., Pinter,N. (2002): Active Tectonics: Earthquakes,Uplift, and Landscape (2ndEd.). *Prentice Hall*, New Jersey.

Keller, E., Gurrola, L. and Tierney, T. (1999): Geomorphic criteria to determine direction of lateral propagation of reverse faulting and folding. *Geology 27*. pp. 515-518.

Khdeir K. (1997): An assessment of regional hydrogeological framework of the Mesozoic aquifer system of Jordan. PhD thesis, *University of Birmingham*, UK.

Khouri, H. Salameh, E. and Udluft, P. (1984): "On the Zerqa Main (Thermal Kallirhoes) Travertine/Dead Sea". *N. Jb. Geol. Paleontl. Mh., H. 8*, pp.472-484.

Klinger, Y., Avouac, P., Dorbath L., Abou Karaki, N., and Tisnerat, N. (2000): Seismic behavior of the Dead Sea fault along Araba valley (Jordan). *Geophys. J. Int. 142*, pp.769-782.

Knighton, D. (1998): Fluvial forms and processes: *Edward Arnold*, New York.

Köppen, W. (1931): Grundriss der Klimakunde. *Berlin: W. de Gruyter*.

Kralisch, S., Krause, P. and David, O. (2005): Using the Object Modeling System for hydrological model development and application. *Advances in Geosciences 4*. pp.75–81.

Krause, P. and Kralisch, S. (2005): The hydrological modelling system J2000 – knowledge core for JAMS", in 'MODSIM. *International Congress on Modelling and Simulation*.

Lerner, N., Issar, S. and Simmers, I. (1990): Groundwater recharge. A guide to understanding and estimating natural recharge. IAH Int Contrib Hydrogeol 8. Heinz Heise, Hannover, pp. 345.

McMaster, K. (2002): Effects of digital elevation model resolution on derived stream network positions, *Water Resources Research 38*, pp. 1–9.

Maidment, R. (1993): Handbook of Hydrology, *McGraw-Hill, Inc.*, New York.

Margane, A., Hobler, M., Almomani, M. and Subah, A. (2002): Contributions to the Hydrogeology of Northern and Central Jordan, E. *Schweizerbart Science Publishers*, Stuttgart.

Mata, J. (2008): Influence of climate change on droughts and water scarcity in dry regions. *Washington DC: The World Bank*, USA.

Meteorological Department (2010): Open files. *http://met.jometeo.gov.jo*.

Möller, P., Dulski, P., Salameh, E., and Geyer, S. (2006): Characterizsation of the sources of thermal spring- and well water in Jordan by rare earth element and yttrium distribution and stable isotopes of H2O. *Acta Hydrochim. Hydrobiol. 34*, pp.101–116.

Monteith, L. (1965): Evaporation and environment. *Academic Press, Inc.*, NY, pp. 205-234.

123

Naumov, B., Dorofeeva, A., Mironova, F. (2009): Principal physicochemical parameters of natural mineral-forming fluids. *Geochemistry International 47*, pp.777-802.

Niemi, T. and Ben-Avraham, Z. (1997): The Dead Sea: the lake and its setting. *Oxford Monographs on Geology and Geophysics Press 36*, Oxford University.

O'Callaghan, J. and Mark, D. (1984): The extraction of drainage networks from digital elevation data, Comput. *Vision Graph. 28*, pp.323–344.

Odeh, T., Salameh, E., Schirmer, M., and Strauch, G. (2009): Structural control of groundwater flow regimes and groundwater chemistry along the lower reaches of the Zerka River, West Jordan, using remote sensing, GIS, and field methods. *Environ Geol 58*, pp.1797–1810.

Ohmori, H. (1993): Changes in the hypsometric curve through mountain building. *Geomorphology 8*, pp.263 - 277.

Pellig-ba, K. (1996): Trace elements in groundwater from some crystline rocks in the upper regions of Ghana. *Water, Air, and Soil Pollution 103*, pp.71-89.

Phillips, J. and Lutz, D. (2008): Profile convexities in bedrock and alluvial streams. *Geomorphology 102*, pp. 554–566.

Pruski, F., and Nearing, A. (2002): Runoff and soil-loss responses to changes in precipitation: A computer simulation study. *J SoilWater Cons 57*. pp.7–16.

Pittman, D. (1981): Effect of fault-related granulation on porsity and permability of quartz sandstone, Simpson group (ordovican). *Oklahma Am. Assc. Petr. Geol. Bull. 64* pp. 2381-2387).

Quennel, M. (1958): The structure and the geomorphic evolution of the Dead Sea Rift, *Quarterly J. Geol. Soc. 114*, pp. 2-24.

Rodríguez-Iturbe, I. and Rinaldo, A. (1997): Fractal River Basins: Chance and Self-Organization. *Cambridge Universit Press*, New York.

Ribolini, A. and Spagnolo, M. (2008): Drainage network geometry versus tectonics in the Argentera Massif (French–Italian Alps). *Geomorphology 93*, pp. 253-26.

Rushton, R. and Ward, C. (1979): The estimation of groundwater recharge. *Journal of Hydrology 41* pp. 345-361.

Salameh, E. and Bannayan, H. (1993): Water Resources of Jordan- Present Status and Future Potentials. *Friedrich Ebert Stiftung*, Amman.

Salameh, E. (1996): Water Quality in Jordan (impacts on environments and future generations resources base). *Friedrich Ebert Stiftung, Royal Society for the conservation of nature*, Amman.

Salameh, E.and Al Farajat, M. (2007): The role of volcanic eruptions in blocking the drainage leading to the Dead Sea formation. *Environmental geology Journal 52*, pp 519-527.

Salbu, B. and Steinnes, E. (1995): Trace elements in natural waters, *CRC Press, Boca Raton, Ann Arbor*, London.

Santanello, J. , Peters-Liard, C., Garcia, M., Mocko, M. Tischler, Moran, S. and Thoma, D. (2007): Using remotely sensed estimates of soil moisture to infer soil texture and hydraulic properties across a semi -arid watershed. *Remote Sensing of Environment 110* pp. 79-97.

Saraf, K., Choudhury, R., Roy, B. , Sarma, B. , Vijay, S. and Choudhury, S. (2004): GIS based surface hydrological modelling in identification of groundwater recharge zones. *International Journal of Remote Sensing 25*, pp. 5759-5770.

Scheffer, F. and Schachtschabel, P. (2002): Lehrbuch der Bodenkunde. 15. *Aufl.,Spektrum Akademischer Verlag*, Heidelberg.

Schneider, W., Abed, A. and Salameh, E. (1984): Mineral content and diagenetic pattern – useful tools for lithostratigraphic subdivision and correlation of the Nubian Series: results of work in the Wadi Zerqa Ma'in area, Jordan. *Geologisches Jahrbuch, Reihe B, Hanover, Heft B53*, pp. 55–75.

Seiler, P. and Gat, R. (2007): Groundwater Recharge from Run-off, Infiltration and Percolation. *Water Science and Technology Library 55*, USA.

Semmens, J., Hernandez, M., Goodrich, C., and Kepner, G. (2006): Hydrologic model uncertainty associated with simulating future land-use/cover scenarios, *Proceedings of the Second International Conference on Research in the Watersheds*, Otto.

Şen, Z. (2008): Wadi Hydrology. *CRC Press*, New York.

Setti, M., Marinoni L. and Lopez-Galindo A (2004): Mineralogical and geochemical characteristics (major, minor, trace elements and REE) of detrital and authigenic clay minerals in a Cenozoic sequence from Ross Sea, Antarctica. *Clay mineral 39*, pp.405–421.

Shadfan, H. (1983): Clay minerals and potassium status in some soils of Jordan. *Geoderma 31*, pp. 41-56.

Shahzad, F., Mahmood, S. and Gloaguen, R., (2009): Drainage Network and Lineament Analysis: An Approach for Potwar Plateau (Northern Pakistan*). J. Mt. Sci 6*, pp. 14–24.

Shahzad, F. and Gloaguen, R. (2009): Understanding tectonics from digital elevation model, part 1: Drainage network preparation and stream profile analysis. *Computer and Geosciences 57*, pp. 250 - 260.

Shahzad, F. and Gloaguen, R. (2010): TecDEM: A MATLAB based toolbox for Tectonic Geomorphology, Part 2: Surface dynamics and basin analysis. *Computer and Geosciences 37*, pp.1-30.

Shawabekeh, K. (1998): The geology of Ma'in area map sheet NO.3153 (III), *the Jordanian Natural Resources authority publication Vol.40*.

125

Shtober-Zisu, N., Greenbaum, N., Inbar, M. and Flexer, A. (2008): Morphometric and geomorphic approaches for assessment of tectonic activity, DeadSea Rift (Israel). *Geomorphology 102*, pp. 93-104.

Smith, L., Forster, C. and Evans, J., (1990): Interaction of fault zones, fluid flow, and heat transfer at the basin scale. In: Neuman, S.P. and Neretnieks, I. Hydrogeology of Low Permeability Environments. *Verlag Heinz Heise*, Germany.

Sneh, A. (1996): The Dead Sea Rift: lateral displacement and down faulting phases, *Tectonophysics 263*, pp. 277-292.

Srinivasan, R. and Engel, A. (1991): Effect of slope prediction methods on slope and erosion estimates. *Applied Engineering in Agriculture 7*, 779 - 783.

Steinitz, G. and Bartov, Y. (1992): The Miocene-Pleistocene History of the Dead Sea Segment of the Rift in Light of K-Ar Ages of Basalts, *Israel J. Earth Sci. 40*, pp.199–208.

Thornthwaite, W. and Mather, W. (1955): The Water Balance. Publ. Climatol. Lab. *Climatol. Drexel Inst. Technol 8*, pp. 1-104.

Trefry, M and Muffels, C. (2007): FEFLOW: A Finite-Element Ground Water Flow and Transport Modeling Tool. *Groundwater 45*, pp. 525-528.

Troiani, F. and Della, M. (2008): The use of the Stream Length–Gradient index in morphotectonic analysis of small catchments: A case study from Central Italy. *Geomorphology 102*, pp. 159–168.

Trondalen, J. (2009): Climate Changes, Water Security and Possible Remedies for the Middle East. *United Nation Educational, Scientific and Cultural Organization pubilcation 75352*, France.

Trotter, M. (1991): Remotely sensed data as an information source for geographical information systems in natural resource management: a review. *International Journal of Geographic Information System, 5*. pp.225–239.

Tucker, E., and Slingerland, L. (1994): Erosional dynamics, flexural isostasy, and long-lived escarpments: a numerical modeling study. *Journal of Geophysical Research 99*, pp.229–12 243.

US Department of agriculture (USDA) (1993): Soil Survey Manual, Soil Survey Staff, Natural Resource Conservation Service, Handbook No. 18, U.S. *Government Printing Office*, Washington D.C..

Van der Beek, P., Champel, B., and Mugnier, L. (2002): Control of detachment dip on drainage development in regions of active fault- propagation folding. *Geology 30*, pp. 471–474.

Vivoni, R., Benedetto, F., Grimaldi, S., and Eltahir, E., (2008): Hypsometric control on surface and subsurface runoff. *Water Resour. Res. 44*, pp. 12502- 1251.

Wang, X.. and Yin, Z. (1998): A comparison of drainage networks derived from digital elevation models at two scales. *Journal of Hydrology 210*, pp.221–241.

Whipple, X. and Tucker, E. (1999): Dynamics of the stream-power river incision model: Implications for height limits of mountain ranges, landscape response timescales, and research needs. *Journal of Geophysical Research 104*, pp. 17,674-17,661.

Wilson, T. and Dominic, J. (1998): Fractal interrelationships between topography and structure. *Earth Surface Processes and Landforms 23*, pp. 509-525.

Zhang, J., Liu, Z. and Sun, W. (1997): Three dimensional mathematical models of geological bodies and their graphics display. *Proc 30th Int Geol Congr 25*, pp.103–14.

Appendix 1 Climatic data (Meteorological Department (2010))

A) Madaba station (Relative Humidity, Temp., Wind speed, Sun hours)

Date	Relative Humidity (%)	Temp.° C	Wind speed (mph)	Sun-hour
01.01.1980	74	8	4	10
01.02.1980	72	9	4	11
01.03.1980	66	12	4	12
01.04.1980	55	16	4	13
01.05.1980	37	21	3	14
01.06.1980	40	24	4	14
01.07.1980	54	25	6	14
01.08.1980	55	24	4	13
01.09.1980	55	22	4	12
01.10.1980	48	21	3	11
01.11.1980	51	16	2	11
01.12.1980	70	11	2	10
01.01.1981	71	8	4	10
01.02.1981	69	9	4	11
01.03.1981	58	13	4	12
01.04.1981	48	16	3	13
01.05.1981	40	19	3	14
01.06.1981	43	23	4	14
01.07.1981	50	24	4	14
01.08.1981	51	24	3	13
01.09.1981	45	24	3	12
01.10.1981	55	22	2	11
01.11.1981	62	13	3	11
01.12.1981	65	12	3	10
01.01.1982	68	9	3	10
01.02.1982	65	8	3	11
01.03.1982	64	10	2	12
01.04.1982	48	17	3	13
01.05.1982	51	18	4	14
01.06.1982	43	23	4	14
01.07.1982	55	23	4	14
01.08.1982	56	24	5	13
01.09.1982	53	23	3	12
01.10.1982	48	21	2	11
01.11.1982	60	12	3	11
01.12.1982	70	8	3	10
01.01.1983	73	6	4	10
01.02.1983	73	8	3	11
01.03.1983	69	11	3	12
01.04.1983	58	15	3	13
01.05.1983	46	20	3	14
01.06.1983	44	23	4	14
01.07.1983	58	24	5	14
01.08.1983	56	24	5	13
01.09.1983	61	23	4	12
01.10.1983	55	19	3	11
01.11.1983	59	17	2	11
01.12.1983	67	11	2	10

Date	Relative Humidity (%)	Temp.° C	Wind speed (mph)	Sun-hour
01.01.1984	73	9	3	10
01.02.1984	58	10	3	11
01.03.1984	65	13	4	12
01.04.1984	61	15	3	13
01.05.1984	43	21	3	14
01.06.1984	53	22	4	14
01.07.1984	51	24	5	14
01.08.1984	54	23	5	13
01.09.1984	47	24	3	12
01.10.1984	44	21	2	11
01.11.1984	69	14	2	11
01.12.1984	68	8	3	10
01.01.1985	64	11	3	10
01.02.1985	75	8	4	11
01.03.1985	46	12	3	12
01.04.1985	53	16	3	13
01.05.1985	51	22	3	14
01.06.1985	52	23	4	14
01.07.1985	51	24	4	14
01.08.1985	58	26	3	13
01.09.1985	53	23	2	12
01.10.1985	56	18	2	11
01.11.1985	54	17	2	11
01.12.1985	60	11	3	10
01.01.1986	68	9	3	10
01.02.1986	67	11	3	11
01.03.1986	61	14	3	12
01.04.1986	48	19	3	13
01.05.1986	57	18	3	14
01.06.1986	54	23	4	14
01.07.1986	46	25	4	14
01.08.1986	53	25	3	13
01.09.1986	52	25	2	12
01.10.1986	61	20	2	11
01.11.1986	68	12	2	11
01.12.1986	69	9	3	10
01.01.1987	62	10	3	10
01.02.1987	63	11	3	11
01.03.1987	67	9	3	12
01.04.1987	52	15	3	13
01.05.1987	37	21	2	14
01.06.1987	44	23	3	14
01.07.1987	47	25	4	14
01.08.1987	49	25	3	13
01.09.1987	51	24	2	12
01.10.1987	55	19	1	11
01.11.1987	47	16	2	11
01.12.1987	73	11	2	10
01.01.1988	79	9	2	10
01.02.1988	71	9	2	11
01.03.1988	69	11	3	12
01.04.1988	51	16	3	13

129

Date	Relative Humidity (%)	Temp.° C	Wind speed (mph)	Sun-hour
01.05.1988	35	22	3	14
01.06.1988	42	24	3	14
01.07.1988	47	26	3	14
01.08.1988	54	25	3	13
01.09.1988	45	25	2	12
01.10.1988	57	19	1	11
01.11.1988	55	13	2	11
01.12.1988	70	10	3	10
01.01.1989	70	6	2	10
01.02.1989	50	9	3	11
01.03.1989	59	12	3	12
01.04.1989	30	20	2	13
01.05.1989	35	22	3	14
01.06.1989	44	22	4	14
01.07.1989	48	25	4	14
01.08.1989	50	25	4	13
01.09.1989	49	24	3	12
01.10.1989	51	20	2	11
01.11.1989	58	16	3	11
01.12.1989	67	11	1	10
01.01.1995	75	9	2	10
01.02.1995	74	10	2	11
01.03.1995	65	13	3	12
01.04.1995	56	16	3	13
01.05.1995	46	21	3	14
01.06.1995	51	24	4	14
01.07.1995	58	24	4	14
01.08.1995	61	25	4	13
01.09.1995	57	24	3	12
01.10.1995	56	20	3	11
01.11.1995	54	13	2	11
01.12.1995	75	9	3	10
01.01.1996	80	9	3	10
01.02.1996	69	11	3	11
01.03.1996	72	11	4	12
01.04.1996	56	15	3	13
01.05.1996	45	23	3	14
01.06.1996	53	23	4	14
01.07.1996	56	26	4	14
01.08.1996	57	25	4	13
01.09.1996	55	24	3	12
01.10.1996	59	19	2	11
01.11.1996	60	15	3	11
01.12.1996	74	12	2	10
01.01.1997	72	10	2	10
01.02.1997	67	8	3	11
01.03.1997	69	10	3	12
01.04.1997	59	14	3	13
01.05.1997	42	22	3	14
01.06.1997	49	24	3	14
01.07.1997	53	25	5	14

Date	Relative Humidity (%)	Temp.º C	Wind speed (mph)	Sun-hour
01.08.1997	59	23	4	13
01.09.1997	56	23	3	12
01.10.1997	52	21	1	11
01.11.1997	62	15	2	11
01.12.1997	73	11	2	10
01.01.1998	80	8	3	10
01.02.1998	72	9	2	11
01.03.1998	67	11	3	12
01.04.1998	54	18	2	13
01.05.1998	49	21	3	14
01.06.1998	53	23	3	14
01.07.1998	51	26	4	14
01.08.1998	54	27	3	13
01.09.1998	50	25	3	12
01.10.1998	48	22	2	11
01.11.1998	55	18	1	11
01.12.1998	60	12	2	10
01.01.1999	68	10	2	10
01.02.1999	67	11	2	11
01.03.1999	59	13	3	12
01.04.1999	53	17	2	13
01.05.1999	41	23	3	14
01.06.1999	59	23	4	14
01.07.1999	59	25	4	14
01.08.1999	62	26	3	13
01.09.1999	60	24	3	12
01.10.1999	62	21	2	11
01.11.1999	51	16	1	11
01.12.1999	53	13	1	10
01.01.2000	76	8	2	10
01.02.2000	72	9	2	11
01.03.2000	71	11	2	12
01.04.2000	50	18	2	13
01.05.2000	44	20	2	14
01.06.2000	46	24	3	14
01.07.2000	47	27	3	14
01.08.2000	61	25	3	13
01.09.2000	66	22	1	12
01.10.2000	69	18	2	11
01.11.2000	64	13	2	11
01.12.2000	85	10	3	10
01.01.2001	77	8	2	10
01.02.2001	78	8	3	11
01.03.2001	58	15	3	12
01.04.2001	53	17	2	13
01.05.2001	50	20	3	14
01.06.2001	42	23	2	14
01.07.2001	55	24	2	14
01.08.2001	62	24	1	13

Date	Relative Humidity (%)	Temp.° C	Wind speed (mph)	Sun-hour
01.09.2001	70	22	1	12
01.10.2001	65	19	1	11
01.11.2001	71	13	2	11
01.12.2001	83	9	1	10
01.01.2002	85	6	3	10
01.02.2002	64	11	3	11
01.03.2002	62	13	2	12
01.04.2002	65	15	2	13
01.05.2002	57	18	1	14
01.06.2002	55	22	2	14
01.07.2002	49	25	1	14
01.08.2002	56	24	1	13
01.09.2002	54	23	1	12
01.10.2002	59	20	1	11
01.11.2002	62	14	4	11
01.12.2002	83	9	4	10
01.01.2003	76	9	3	10
01.02.2003	78	8	5	11
01.03.2003	77	9	4	12
01.04.2003	57	15	2	13
01.05.2003	37	22	3	14
01.06.2003	47	22	2	14
01.07.2003	47	23	3	14
01.08.2003	51	25	2	13
01.09.2003	61	21	2	12
01.10.2003	59	19	2	11
01.11.2003	62	14	2	11
01.12.2003	82	9	3	10
01.01.2004	84	8	3	10
01.02.2004	79	9	3	11
01.03.2004	59	14	3	12
01.04.2004	52	16	3	13
01.05.2004	50	19	3	14
01.06.2004	51	22	2	14
01.07.2004	47	25	3	14
01.08.2004	64	22	3	13
01.09.2004	59	23	2	12
01.10.2004	49	20	1	11
01.11.2004	64	14	2	11
01.12.2004	68	7	2	10
01.01.2005	69	8	3	10
01.02.2005	73	8	4	11
01.03.2005	62	11	2	12
01.04.2005	42	16	3	13
01.05.2005	44	18	2	14

Date	Relative Humidity (%)	Temp.° C	Wind speed (mph)	Sun-hour
01.06.2005	44	21	2	14
01.07.2005	42	24	2	14
01.08.2005	48	24	2	13
01.09.2005	50	22	1	12
01.10.2005	46	19	1	11
01.11.2005	54	13	2	11
01.12.2005	51	12	2	10
01.01.2006	65	8	2	10
01.02.2006	58	10	3	11
01.03.2006	50	13	3	12
01.04.2006	52	16	3	13
01.05.2006	34	21	3	14
01.06.2006	29	25	3	14
01.07.2006	38	25	4	14
01.08.2006	35	27	3	13
01.09.2006	40	24	2	12
01.10.2006	52	20	2	11
01.11.2006	48	13	2	11
01.12.2006	50	8	2	10
01.01.2007	63	7	2	10
01.02.2007	67	10	3	11
01.03.2007	57	12	3	12
01.04.2007	47	15	4	13
01.05.2007	37	22	3	14
01.06.2007	34	24	3	14
01.07.2007	34	26	4	14
01.08.2007	42	26	3	13
01.09.2007	50	24	3	12
01.10.2007	45	21	2	11
01.11.2007	49	15	2	11
01.12.2007	59	10	2	10
01.01.2008	61	6	3	10
01.02.2008	60	8	3	11
01.03.2008	40	15	3	12
01.04.2008	34	19	3	13
01.05.2008	34	20	3	14
01.06.2008	30	25	3	14
01.07.2008	34	26	3	14
01.08.2008	34	27	4	13
01.09.2008	44	24	3	12
01.10.2008	55	20	2	11
01.11.2008	50	15	2	11
01.12.2008	49	11	2	10
01.01.2009	50	9	2	10
01.02.2009	60	10	4	11

133

Date	Relative Humidity (%)	Temp.° C	Wind speed (mph)	Sun-hour
01.03.2009	57	11	4	12
01.04.2009	40	17	3	13
01.05.2009	38	21	3	14
01.06.2009	28	26	3	14
01.07.2009	37	27	4	14
01.08.2009	40	26	3	13
01.09.2009	49	23	3	12
01.10.2009	38	23	2	11
01.11.2009	60	14	2	11
01.12.2009	64	12	3	10

Appendix 1 Climatic data (Meteorological Department (2010))

B) All climatic stations (Rainfall mm/year), -9999 means not measured.

Date	Queen Alia Airport St.	Mushaqqar St.	Madaba St.	Main St.	Firestation St.	Airport St.	Ghor Safi St.
01.01.1980 00:00	-9999	-9999	70	69	-9999	-9999	-9999
01.02.1980 00:00	-9999	-9999	67	69	-9999	-9999	-9999
01.03.1980 00:00	-9999	-9999	47	65	-9999	-9999	-9999
01.04.1980 00:00	-9999	-9999	18	19	-9999	-9999	-9999
01.05.1980 00:00	-9999	-9999	0	0	-9999	-9999	-9999
01.06.1980 00:00	-9999	-9999	0	0	-9999	-9999	-9999
01.07.1980 00:00	-9999	-9999	0	0	-9999	-9999	-9999
01.08.1980 00:00	-9999	-9999	0	0	-9999	-9999	-9999
01.09.1980 00:00	-9999	-9999	0	0	-9999	-9999	-9999
01.10.1980 00:00	-9999	-9999	3	1	-9999	-9999	-9999
01.11.1980 00:00	-9999	-9999	2	0	-9999	-9999	-9999
01.12.1980 00:00	-9999	-9999	217	-9999	-9999	-9999	-9999
01.01.1981 00:00	-9999	-9999	63	-9999	-9999	-9999	-9999
01.02.1981 00:00	-9999	-9999	66	15	-9999	-9999	-9999
01.03.1981 00:00	-9999	-9999	33	80	-9999	-9999	-9999
01.04.1981 00:00	-9999	-9999	5	0	-9999	-9999	-9999
01.05.1981 00:00	-9999	-9999	0	-9999	-9999	-9999	-9999
01.06.1981 00:00	-9999	-9999	0	-9999	-9999	-9999	-9999
01.07.1981 00:00	-9999	-9999	0	-9999	-9999	-9999	-9999
01.08.1981 00:00	-9999	-9999	0	-9999	-9999	-9999	-9999
01.09.1981 00:00	-9999	-9999	0	-9999	-9999	-9999	-9999
01.10.1981 00:00	-9999	-9999	0	-9999	-9999	-9999	-9999
01.11.1981 00:00	-9999	-9999	0	-9999	-9999	-9999	-9999
01.12.1981 00:00	-9999	-9999	0	-9999	-9999	-9999	-9999
01.01.1982 00:00	-9999	-9999	0	-9999	-9999	-9999	-9999
01.02.1982 00:00	-9999	-9999	3	-9999	-9999	-9999	-9999
01.03.1982 00:00	-9999	-9999	25	-9999	-9999	-9999	-9999
01.04.1982 00:00	-9999	-9999	2	-9999	-9999	-9999	-9999
01.05.1982 00:00	-9999	-9999	26	-9999	-9999	-9999	-9999
01.06.1982 00:00	-9999	-9999	0	-9999	-9999	-9999	-9999
01.07.1982 00:00	-9999	-9999	0	-9999	-9999	-9999	-9999
01.08.1982 00:00	-9999	-9999	0	-9999	-9999	-9999	-9999
01.09.1982 00:00	-9999	-9999	0	-9999	-9999	-9999	-9999
01.10.1982 00:00	-9999	-9999	0	-9999	-9999	-9999	-9999
01.11.1982 00:00	-9999	-9999	48	23	-9999	-9999	-9999
01.12.1982 00:00	-9999	-9999	22	20	-9999	-9999	-9999
01.01.1983 00:00	-9999	-9999	56	68	-9999	-9999	-9999
01.02.1983 00:00	-9999	-9999	149	125	-9999	-9999	-9999
01.03.1983 00:00	-9999	-9999	56	27	-9999	-9999	-9999
01.04.1983 00:00	-9999	-9999	0	0	-9999	-9999	-9999
01.05.1983 00:00	-9999	-9999	0	0	-9999	-9999	-9999
01.06.1983 00:00	-9999	-9999	0	0	-9999	-9999	-9999
01.07.1983 00:00	-9999	-9999	0	0	-9999	-9999	0
01.08.1983 00:00	-9999	-9999	0	0	-9999	-9999	0
01.09.1983 00:00	-9999	-9999	0	0	-9999	-9999	0

01.10.1983 00:00	-9999	-9999	0	0	-9999	-9999	0
01.11.1983 00:00	-9999	-9999	17	18	-9999	-9999	0
01.12.1983 00:00	-9999	-9999	0	0	-9999	-9999	0
01.01.1984 00:00	-9999	-9999	35	29	-9999	-9999	2
01.02.1984 00:00	-9999	-9999	27	15	-9999	-9999	0
01.03.1984 00:00	-9999	-9999	33	48	-9999	-9999	16
01.04.1984 00:00	-9999	-9999	0	0	-9999	-9999	0
01.05.1984 00:00	-9999	-9999	0	0	-9999	-9999	0
01.06.1984 00:00	-9999	-9999	0	0	-9999	-9999	0
01.07.1984 00:00	-9999	-9999	0	0	-9999	-9999	0
01.08.1984 00:00	-9999	-9999	0	0	-9999	-9999	0
01.09.1984 00:00	-9999	-9999	0	0	-9999	-9999	0
01.10.1984 00:00	12	0	46	-9999	-9999	-9999	0
01.11.1984 00:00	4	0	21	-9999	-9999	-9999	0
01.12.1984 00:00	18	33	6	-9999	-9999	-9999	0
01.01.1985 00:00	0	27	32	-9999	-9999	-9999	0
01.02.1985 00:00	260	196	196	-9999	-9999	-9999	4
01.03.1985 00:00	0	45	50	-9999	-9999	-9999	4
01.04.1985 00:00	0	3	0	-9999	-9999	-9999	4
01.05.1985 00:00	0	0	0	-9999	-9999	-9999	0
01.06.1985 00:00	0	0	0	-9999	-9999	-9999	0
01.07.1985 00:00	0	0	0	-9999	-9999	-9999	0
01.08.1985 00:00	0	0	0	-9999	-9999	-9999	0
01.09.1985 00:00	0	0	0	-9999	-9999	-9999	0
01.10.1985 00:00	0	0	4	7	-9999	-9999	0
01.11.1985 00:00	0	0	0	0	-9999	-9999	0
01.12.1985 00:00	30	31	57	51	-9999	-9999	1
01.01.1986 00:00	50	44	1	15	-9999	-9999	5
01.02.1986 00:00	105	92	102	41	-9999	-9999	0
01.03.1986 00:00	7	14	8	9	-9999	-9999	0
01.04.1986 00:00	18	4	2	0	-9999	-9999	0
01.05.1986 00:00	10	31	10	0	-9999	-9999	0
01.06.1986 00:00	0	0	0	0	-9999	-9999	0
01.07.1986 00:00	0	0	0	0	-9999	-9999	0
01.08.1986 00:00	0	0	0	0	-9999	-9999	0
01.09.1986 00:00	0	0	0	0	-9999	-9999	0
01.10.1986 00:00	20	25	5	0	-9999	-9999	0
01.11.1986 00:00	125	133	136	110	-9999	-9999	0
01.12.1986 00:00	51	43	57	49	-9999	-9999	8
01.01.1987 00:00	36	83	85	64	-9999	-9999	0
01.02.1987 00:00	26	33	6	18	-9999	-9999	0
01.03.1987 00:00	40	55	44	31	-9999	-9999	0
01.04.1987 00:00	0	1	0	0	-9999	-9999	0
01.05.1987 00:00	0	0	0	0	-9999	-9999	1
01.06.1987 00:00	0	0	0	0	-9999	-9999	0
01.07.1987 00:00	0	0	0	0	-9999	-9999	0
01.08.1987 00:00	0	0	0	0	-9999	-9999	0
01.09.1987 00:00	0	0	0	0	-9999	-9999	0
01.10.1987 00:00	25	14	14	11	-9999	-9999	0
01.11.1987 00:00	4	1	0	0	-9999	-9999	0

01.12.1987 00:00	166	94	116	123	-9999	-9999	0
01.01.1988 00:00	79	88	71	93	-9999	-9999	2
01.02.1988 00:00	165	152	153	122	-9999	-9999	6
01.03.1988 00:00	64	74	82	65	-9999	-9999	7
01.04.1988 00:00	-9999	12	6	6	-9999	-9999	1
01.05.1988 00:00	-9999	0	0	0	-9999	-9999	0
01.06.1988 00:00	-9999	0	0	0	-9999	-9999	0
01.07.1988 00:00	-9999	0	0	0	-9999	-9999	0
01.08.1988 00:00	-9999	0	0	0	-9999	-9999	0
01.09.1988 00:00	-9999	0	0	0	-9999	-9999	0
01.10.1988 00:00	-9999	0	11	5	-9999	-9999	1
01.11.1988 00:00	-9999	23	16	20	-9999	-9999	0
01.12.1988 00:00	-9999	131	78	86	-9999	-9999	19
01.01.1989 00:00	-9999	74	50	75	-9999	-9999	5
01.02.1989 00:00	-9999	49	45	70	-9999	-9999	3
01.03.1989 00:00	-9999	66	53	56	-9999	-9999	0
01.04.1989 00:00	-9999	0	0	0	-9999	-9999	0
01.05.1989 00:00	-9999	0	0	0	-9999	-9999	0
01.06.1989 00:00	-9999	0	0	0	-9999	-9999	0
01.07.1989 00:00	-9999	0	0	0	-9999	-9999	0
01.08.1989 00:00	-9999	0	0	0	-9999	-9999	0
01.09.1989 00:00	-9999	0	0	0	-9999	-9999	0
01.10.1989 00:00	-9999	4	0	0	-9999	-9999	0
01.11.1989 00:00	-9999	7	12	4	-9999	-9999	0
01.12.1989 00:00	-9999	31	20	18	-9999	-9999	2
01.01.1990 00:00	-9999	87	100	94	-9999	-9999	67
01.02.1990 00:00	-9999	77	57	53	-9999	-9999	10
01.03.1990 00:00	-9999	51	26	38	-9999	-9999	66
01.04.1990 00:00	-9999	44	45	51	-9999	-9999	36
01.05.1990 00:00	-9999	0	0	0	-9999	-9999	0
01.06.1990 00:00	-9999	0	0	0	-9999	-9999	0
01.07.1990 00:00	-9999	0	0	0	-9999	-9999	0
01.08.1990 00:00	-9999	0	0	0	-9999	-9999	0
01.09.1990 00:00	-9999	0	0	0	-9999	-9999	0
01.10.1990 00:00	-9999	4	3	0	-9999	-9999	0
01.11.1990 00:00	-9999	6	5	5	-9999	-9999	1
01.12.1990 00:00	-9999	2	4	4	-9999	-9999	0
01.01.1991 00:00	-9999	74	58	76	-9999	-9999	0
01.02.1991 00:00	-9999	76	75	72	-9999	-9999	0
01.03.1991 00:00	-9999	107	85	131	-9999	-9999	15
01.04.1991 00:00	-9999	4	5	0	-9999	-9999	0
01.05.1991 00:00	-9999	0	0	0	-9999	-9999	0
01.06.1991 00:00	-9999	0	0	0	-9999	-9999	0
01.07.1991 00:00	-9999	0	0	0	-9999	-9999	0
01.08.1991 00:00	-9999	0	0	0	-9999	-9999	0
01.09.1991 00:00	-9999	0	0	0	-9999	-9999	0
01.10.1991 00:00	-9999	4	1	0	-9999	-9999	1
01.11.1991 00:00	-9999	24	44	16	-9999	-9999	0
01.12.1991 00:00	-9999	211	301	104	-9999	-9999	7
01.01.1992 00:00	-9999	112	81	103	-9999	-9999	2

01.02.1992 00:00	-9999	289	297	224	-9999	-9999	8
01.03.1992 00:00	-9999	39	32	31	-9999	-9999	0
01.04.1992 00:00	-9999	0	0	0	-9999	-9999	0
01.05.1992 00:00	-9999	7	0	0	-9999	-9999	0
01.06.1992 00:00	-9999	0	0	0	-9999	-9999	0
01.07.1992 00:00	-9999	0	0	0	-9999	-9999	0
01.08.1992 00:00	-9999	0	0	0	-9999	-9999	0
01.09.1992 00:00	-9999	0	0	0	-9999	-9999	0
01.10.1992 00:00	-9999	0	0	0	-9999	-9999	0
01.11.1992 00:00	-9999	53	58	56	-9999	-9999	0
01.12.1992 00:00	-9999	84	37	37	-9999	-9999	97
01.01.1993 00:00	-9999	48	39	38	-9999	-9999	0
01.02.1993 00:00	-9999	117	87	88	-9999	-9999	15
01.03.1993 00:00	-9999	30	27	28	-9999	-9999	1
01.04.1993 00:00	-9999	0	0	0	-9999	-9999	0
01.05.1993 00:00	-9999	8	8	7	-9999	-9999	0
01.06.1993 00:00	-9999	0	0	0	-9999	-9999	0
01.07.1993 00:00	-9999	0	0	0	-9999	-9999	0
01.08.1993 00:00	-9999	0	0	0	-9999	-9999	0
01.09.1993 00:00	-9999	0	0	0	-9999	-9999	0
01.10.1993 00:00	-9999	35	12	5	-9999	-9999	0
01.11.1993 00:00	-9999	36	19	20	-9999	-9999	0
01.12.1993 00:00	-9999	29	23	16	-9999	-9999	0
01.01.1994 00:00	-9999	94	73	73	-9999	-9999	5
01.02.1994 00:00	-9999	98	71	60	-9999	-9999	0
01.03.1994 00:00	-9999	24	16	12	-9999	-9999	2
01.04.1994 00:00	-9999	7	8	15	-9999	-9999	0
01.05.1994 00:00	-9999	0	0	0	-9999	-9999	0
01.06.1994 00:00	-9999	0	0	0	-9999	-9999	0
01.07.1994 00:00	-9999	0	0	0	-9999	-9999	0
01.08.1994 00:00	-9999	0	0	0	-9999	-9999	0
01.09.1994 00:00	-9999	0	0	0	-9999	-9999	99
01.10.1994 00:00	-9999	15	6	19	-9999	-9999	1
01.11.1994 00:00	-9999	195	152	140	-9999	-9999	6
01.12.1994 00:00	-9999	130	109	89	-9999	-9999	8
01.01.1995 00:00	-9999	6	5	8	-9999	-9999	0
01.02.1995 00:00	-9999	34	41	31	-9999	-9999	15
01.03.1995 00:00	-9999	21	14	13	-9999	-9999	1
01.04.1995 00:00	-9999	17	16	15	-9999	-9999	1
01.05.1995 00:00	-9999	0	0	0	-9999	-9999	0
01.06.1995 00:00	-9999	0	0	0	-9999	-9999	0
01.07.1995 00:00	-9999	0	0	0	-9999	-9999	0
01.08.1995 00:00	-9999	0	0	0	-9999	-9999	0
01.09.1995 00:00	-9999	0	0	0	-9999	-9999	0
01.10.1995 00:00	-9999	0	0	0	-9999	-9999	0
01.11.1995 00:00	-9999	16	17	16	-9999	-9999	0
01.12.1995 00:00	-9999	15	12	6	-9999	-9999	0
01.01.1996 00:00	-9999	87	52	51	-9999	-9999	40
01.02.1996 00:00	-9999	50	23	11	-9999	-9999	9
01.03.1996 00:00	-9999	110	108	86	-9999	-9999	3

01.04.1996 00:00	-9999	0	0	0	-9999	-9999	0
01.05.1996 00:00	-9999	0	0	0	-9999	-9999	0
01.06.1996 00:00	-9999	0	0	0	-9999	-9999	0
01.07.1996 00:00	-9999	0	0	0	-9999	-9999	0
01.08.1996 00:00	-9999	0	0	0	-9999	-9999	0
01.09.1996 00:00	-9999	0	0	0	-9999	-9999	0
01.10.1996 00:00	-9999	15	15	3	-9999	-9999	0
01.11.1996 00:00	-9999	9	7	8	-9999	-9999	0
01.12.1996 00:00	-9999	24	12	21	-9999	-9999	5
01.01.1997 00:00	-9999	94	84	80	-9999	-9999	8
01.02.1997 00:00	-9999	105	119	96	-9999	-9999	5
01.03.1997 00:00	-9999	68	72	37	-9999	-9999	13
01.04.1997 00:00	-9999	1	1	1	-9999	-9999	0
01.05.1997 00:00	-9999	0	0	0	-9999	-9999	0
01.06.1997 00:00	-9999	0	0	0	-9999	-9999	0
01.07.1997 00:00	-9999	0	0	0	-9999	-9999	0
01.08.1997 00:00	-9999	0	0	0	-9999	-9999	0
01.09.1997 00:00	-9999	0	0	0	-9999	-9999	0
01.10.1997 00:00	-9999	11	9	11	-9999	-9999	4
01.11.1997 00:00	-9999	3	2	103	-9999	-9999	0
01.12.1997 00:00	-9999	98	93	80	-9999	-9999	36
01.01.1998 00:00	-9999	91	76	84	-9999	-9999	9
01.02.1998 00:00	-9999	44	43	50	-9999	-9999	14
01.03.1998 00:00	-9999	79	61	66	-9999	-9999	12
01.04.1998 00:00	-9999	4	2	3	-9999	-9999	0
01.05.1998 00:00	-9999	5	2	2	-9999	-9999	2
01.06.1998 00:00	-9999	0	0	0	-9999	-9999	0
01.07.1998 00:00	-9999	0	0	0	-9999	-9999	0
01.08.1998 00:00	-9999	0	0	0	-9999	-9999	0
01.09.1998 00:00	-9999	0	0	0	-9999	-9999	0
01.10.1998 00:00	-9999	0	0	5	-9999	-9999	0
01.11.1998 00:00	-9999	0	3	15	-9999	-9999	0
01.12.1998 00:00	-9999	4	3	2	-9999	-9999	0
01.01.1999 00:00	-9999	44	54	47	-9999	-9999	0
01.02.1999 00:00	-9999	71	82	53	-9999	-9999	0
01.03.1999 00:00	-9999	26	12	10	-9999	-9999	0
01.04.1999 00:00	-9999	5	14	0	-9999	-9999	0
01.05.1999 00:00	-9999	0	0	0	-9999	-9999	0
01.06.1999 00:00	-9999	0	0	0	-9999	-9999	0
01.07.1999 00:00	-9999	0	0	0	-9999	-9999	0
01.08.1999 00:00	-9999	0	0	0	-9999	-9999	0
01.09.1999 00:00	-9999	0	0	0	-9999	-9999	0
01.10.1999 00:00	-9999	0	0	0	-9999	-9999	0
01.11.1999 00:00	-9999	6	4	2	-9999	-9999	1
01.12.1999 00:00	-9999	2	3	2	-9999	-9999	1
01.01.2000 00:00	-9999	139	101	105	-9999	-9999	13
01.02.2000 00:00	-9999	31	26	31	-9999	-9999	1
01.03.2000 00:00	-9999	17	68	47	-9999	-9999	0
01.04.2000 00:00	-9999	0	0	0	-9999	-9999	0
01.05.2000 00:00	-9999	0	0	0	-9999	-9999	0

01.06.2000 00:00	-9999	0	0	0	-9999	-9999	0
01.07.2000 00:00	-9999	0	0	0	-9999	-9999	50
01.08.2000 00:00	-9999	0	0	0	-9999	-9999	0
01.09.2000 00:00	-9999	0	0	0	-9999	-9999	0
01.10.2000 00:00	-9999	21	7	5	-9999	-9999	10
01.11.2000 00:00	-9999	0	0	0	-9999	-9999	1
01.12.2000 00:00	-9999	128	87	109	-9999	-9999	15
01.01.2001 00:00	-9999	53	52	39	-9999	-9999	10
01.02.2001 00:00	-9999	38	48	52	-9999	-9999	9
01.03.2001 00:00	-9999	6	7	18	-9999	-9999	3
01.04.2001 00:00	-9999	4	6	8	-9999	-9999	8
01.05.2001 00:00	-9999	10	14	9	-9999	-9999	5
01.06.2001 00:00	-9999	0	0	0	-9999	-9999	50
01.07.2001 00:00	-9999	0	0	0	-9999	-9999	0
01.08.2001 00:00	-9999	0	0	0	-9999	-9999	0
01.09.2001 00:00	-9999	0	0	0	-9999	-9999	0
01.10.2001 00:00	-9999	0	1	0	-9999	-9999	0
01.11.2001 00:00	-9999	62	43	49	-9999	-9999	99
01.12.2001 00:00	-9999	76	62	61	-9999	-9999	13
01.01.2002 00:00	-9999	180	180	159	-9999	-9999	15
01.02.2002 00:00	-9999	47	38	45	-9999	-9999	10
01.03.2002 00:00	-9999	44	40	37	-9999	-9999	0
01.04.2002 00:00	-9999	53	46	33	-9999	-9999	1
01.05.2002 00:00	-9999	0	0	0	-9999	-9999	0
01.06.2002 00:00	-9999	0	0	0	-9999	-9999	0
01.07.2002 00:00	-9999	0	0	0	-9999	-9999	4
01.08.2002 00:00	-9999	0	0	0	-9999	-9999	0
01.09.2002 00:00	-9999	0	0	0	-9999	-9999	0
01.10.2002 00:00	-9999	6	5	5	-9999	-9999	0
01.11.2002 00:00	-9999	26	14	11	-9999	-9999	13
01.12.2002 00:00	-9999	114	115	73	-9999	-9999	14
01.01.2003 00:00	-9999	56	38	41	-9999	-9999	5
01.02.2003 00:00	-9999	119	110	90	-9999	-9999	62
01.03.2003 00:00	-9999	76	63	72	-9999	-9999	8
01.04.2003 00:00	-9999	24	18	40	-9999	-9999	4
01.05.2003 00:00	-9999	0	0	0	-9999	-9999	0
01.06.2003 00:00	-9999	0	0	0	-9999	-9999	0
01.07.2003 00:00	-9999	0	0	0	-9999	-9999	0
01.08.2003 00:00	-9999	0	0	0	-9999	-9999	0
01.09.2003 00:00	-9999	0	0	0	-9999	-9999	0
01.10.2003 00:00	-9999	4	0	0	-9999	-9999	0
01.11.2003 00:00	-9999	7	0	0	-9999	-9999	0
01.12.2003 00:00	-9999	53	60	58	-9999	-9999	11
01.01.2004 00:00	-9999	112	78	69	-9999	-9999	19
01.02.2004 00:00	-9999	73	51	31	-9999	-9999	5
01.03.2004 00:00	-9999	29	18	13	-9999	-9999	9
01.04.2004 00:00	-9999	2	1	0	-9999	-9999	0
01.05.2004 00:00	-9999	2	0	0	-9999	-9999	0
01.06.2004 00:00	-9999	0	0	0	-9999	-9999	0
01.07.2004 00:00	-9999	0	0	0	-9999	-9999	0

01.08.2004 00:00	-9999	0	0	0	-9999	-9999	0
01.09.2004 00:00	-9999	0	0	0	-9999	-9999	0
01.10.2004 00:00	-9999	2	1	2	-9999	-9999	92
01.11.2004 00:00	-9999	164	167	115	-9999	-9999	5
01.12.2004 00:00	-9999	32	29	22	-9999	-9999	16
01.01.2005 00:00	-9999	95	100	64	-9999	-9999	15
01.02.2005 00:00	-9999	87	72	49	-9999	-9999	3
01.03.2005 00:00	-9999	50	37	36	-9999	-9999	17
01.04.2005 00:00	-9999	0	0	3	-9999	-9999	0
01.05.2005 00:00	-9999	0	0	0	-9999	-9999	0
01.06.2005 00:00	-9999	0	0	0	-9999	-9999	0
01.07.2005 00:00	-9999	0	0	0	-9999	-9999	0
01.08.2005 00:00	-9999	0	0	0	-9999	-9999	0
01.09.2005 00:00	-9999	0	0	0	-9999	-9999	0
01.10.2005 00:00	-9999	4	1	1	-9999	-9999	0
01.11.2005 00:00	-9999	33	24	18	-9999	-9999	2
01.12.2005 00:00	-9999	99	87	74	-9999	-9999	1
01.01.2006 00:00	-9999	52	29	26	-9999	-9999	0
01.02.2006 00:00	-9999	73	68	39	-9999	-9999	21
01.03.2006 00:00	-9999	7	4	2	-9999	-9999	0
01.04.2006 00:00	-9999	83	103	83	-9999	-9999	15
01.05.2006 00:00	-9999	-9999	-9999	-9999	-9999	50	0
01.06.2006 00:00	-9999	-9999	-9999	-9999	-9999	0	0
01.07.2006 00:00	-9999	-9999	-9999	-9999	-9999	0	0
01.08.2006 00:00	-9999	-9999	-9999	-9999	-9999	0	0
01.09.2006 00:00	-9999	-9999	-9999	-9999	-9999	0	0
01.10.2006 00:00	-9999	-9999	-9999	-9999	-9999	105	2
01.11.2006 00:00	-9999	-9999	-9999	-9999	-9999	101	5
01.12.2006 00:00	-9999	-9999	-9999	-9999	-9999	12	16
01.01.2007 00:00	-9999	-9999	-9999	-9999	-9999	86	7
01.02.2007 00:00	-9999	-9999	-9999	-9999	-9999	50	21
01.03.2007 00:00	-9999	-9999	-9999	-9999	-9999	26	5
01.04.2007 00:00	-9999	-9999	-9999	-9999	-9999	9	3
01.05.2007 00:00	-9999	-9999	-9999	-9999	-9999	58	1
01.06.2007 00:00	-9999	-9999	-9999	-9999	-9999	0	0
01.07.2007 00:00	-9999	-9999	-9999	-9999	-9999	0	0
01.08.2007 00:00	-9999	-9999	-9999	-9999	-9999	50	0
01.09.2007 00:00	-9999	-9999	-9999	-9999	-9999	0	0
01.10.2007 00:00	-9999	-9999	-9999	-9999	-9999	151	0
01.11.2007 00:00	-9999	-9999	-9999	-9999	-9999	131	0
01.12.2007 00:00	-9999	-9999	-9999	-9999	-9999	11	3
01.01.2008 00:00	-9999	-9999	-9999	-9999	-9999	139	7
01.02.2008 00:00	-9999	-9999	-9999	-9999	-9999	24	3
01.03.2008 00:00	-9999	-9999	-9999	-9999	-9999	2	51
01.04.2008 00:00	-9999	-9999	-9999	-9999	-9999	0	0
01.05.2008 00:00	-9999	-9999	-9999	-9999	-9999	0	0
01.06.2008 00:00	-9999	-9999	-9999	-9999	-9999	0	0
01.07.2008 00:00	-9999	-9999	-9999	-9999	-9999	0	0
01.08.2008 00:00	-9999	-9999	-9999	-9999	-9999	0	0
01.09.2008 00:00	-9999	-9999	-9999	-9999	-9999	50	0

01.10.2008 00:00	-9999	-9999	-9999	-9999	0	21	3
01.11.2008 00:00	-9999	-9999	-9999	-9999	9	1	0
01.12.2008 00:00	-9999	-9999	-9999	-9999	27	63	0
01.01.2009 00:00	-9999	-9999	-9999	-9999	2	0	0
01.02.2009 00:00	-9999	-9999	-9999	-9999	93	129	6
01.03.2009 00:00	-9999	-9999	-9999	-9999	86	47	3
01.04.2009 00:00	-9999	-9999	-9999	-9999	4	1	0
01.05.2009 00:00	-9999	-9999	-9999	-9999	26	51	0
01.06.2009 00:00	-9999	-9999	-9999	-9999	12	0	0
01.07.2009 00:00	-9999	-9999	-9999	-9999	36	0	0
01.08.2009 00:00	-9999	-9999	-9999	-9999	0	0	0
01.09.2009 00:00	-9999	-9999	-9999	-9999	-9999	0	0
01.10.2009 00:00	-9999	-9999	-9999	-9999	-9999	7	2
01.11.2009 00:00	-9999	-9999	-9999	-9999	-9999	13	4
01.12.2009 00:00	-9999	-9999	-9999	-9999	-9999	29	3

Appendix 2 Uncertainty in Chemical Analysis

A) Major, trace and rare earth elements.

Measurement	Method / Technique	Limits of detection [mg / l]
Ca $^{2+}$	ICP-AES^{+}	0,03
Mg $^{2+}$	ICP-AES	0,04
K $^{+}$	ICP-AES	0,3
Na $^{+}$	ICP-AES	0,4
Cl $^{-}$	IC^{+}	0,07
SO4 $^{2-}$	IC	0,12
NO3 $^{-}$	IC	0,12
HCO3 $^{-}$	Titration	
Br $^{-}$	IC	0,18
Ba $^{2+}$	ICP-AES	0,01
Sr $^{2+}$	ICP-AES	0,01

Measurement	Method / Technique	Limits of detection [µg / l]
U	ICP-MS	0,6
La	ICP-MS	1
Ce	ICP-MS	1
Pr	ICP-MS	0,7
Gd	ICP-MS	1
Tb	ICP-MS	0,5
Dy	ICP-MS	0,8
Ho	ICP-MS	0,5
Lu	ICP-MS	0,5

ICP-AES^{+}: Inductively-Coupled-Atomic Emission spectrometry (uncertainty 5%).
IC^{+} Ion chromatography (uncertainty 8.5%).
ICP-MS^{+} Inductively coupled plasma mass spectrometry (uncertainty 5%).

B) Physicochemical Parameters

Measurment	Method / Technique	Uncertainty	Limits of detection
EC (µS/cm)	Tetragon probe	+/-0.5%	Range Dependent
pH (pH value)	pH-electrode	+/-0.004	0.001
Eh (mV)	Standard-hydogen electrode for redox	+/-1	1
Temp. °C	integrated pt1000 temperature detector	+/- 0,1	0,5

EC: Electrical conductivity.
pH: potential of Hydrogen, a scale measures how acidic or basic a substance is and ranges from 0 to 14.
Temp. °C: Temperature degree Celsius.

Appendix 3 Curriculum Vitae

TALEB ODEH

Born in Jordan 1979

REMOTE SENSING AND GIS FOR STRCTURAL GEOLOGY & HYDROGEOLOGY (MODELLING APPROACH)

EDUCATION

2006 – Present *Doctoral research*

Hydrogeology Department, Helmholtz Centre for Environmental Research – UFZ, Halle, Germany

Remote Sensing Group, Technische Universität Bergakademie, Freiberg, Germany

2002 – 2005 *Postgraduate study*

Master of applied and environmental geology (grade 3.1/4, very good)

Major: Hydrogeology and structural geology

University of Jordan, Jordan

1998 –2002 *Undergraduate Study*

University of Jordan , Amman, Jordan

Faculty of science

Bachelor of Science (*Geology)*

WORK EXPERIENCE

2006 – Present (Hydrogeology department/ Helmholtz Centre for Environmental Research – UFZ and Remote Sensing Group, TU Freiberg)

1) PhD student for hydrogeology: groundwater chemistry, recharge and flow modelling.
2) PhD student for structural geology: Surface deformation, stream profile analysis and tectonic geomorphology.

2005 – 2006 (Geology department/university of Jordan and High Council for Science and Technology, Amman- Jordan)

1) Teacher assistance for the graduate student.

2) Researcher as hydrogeologist for local projects.

INTERNATIONAL PROJECTS EXPERIENCE

GLOWA Jordan River (GLOWA JR): an interdisciplinary and international research project providing scientific support for sustainable water management in the Jordan River region: My task was conceptual hydrological modelling for the lower reaches of Zerka River.

SUMAR Dead Sea (Sustainable Management of Water Resources (Quantity and Quality) in the Dead Sea Area): My task is groundwater assessment for Wadi Zerka Ma'in aquifers and hydrological modelling.

SCHOOLARSHIP AND GRANTS

DAAD Scholarship, German Academic Exchange Service, PhD Student (2006 – 2010).

Martin Luther University, Research assistance (2010 - 2011).

METIER - METhods of Interdisciplinary Environmental Research (Marie Curie Series of Events) full grant for oral presentation of METIER final conference in Brussels (2009).

METIER - METhods of Interdisciplinary Environmental Research (Marie Curie Series of Events) full grant for remote sensing coarse attending in Helsinki (2008).

PRESENTATIONS IN INTERNATIONAL CONFERANCES

Oral presentation

Odeh, T., Gloaguen, R., Schirmer, M., Geyer, S., Rödiger, T. and Siebert C (2009): Exploration of Wadi Zerka Ma'in rotational fault and its drainage pattern, Eastern of Dead

Sea, by means of remote sensing, GIS and 3D geological modeling, *proceeding of SPIE Europe's International Symposium on Remote Sensing (ERS09)*, Vol.7478, Berlin.

Odeh, T., Gloaguen, R., Schirmer, M., Geyer, S., Rödiger, T. and Siebert C. (2010): Investigation of Catchment Areas Migrations Through a Sinstral and Dextral Strike Slip Faults: The Case Study of Zerka Ma'in and Al Hasa Catchment Areas, East of the Dead Sea in Jordan. *Proceedings of the 4 ASME/WSEAS International conference on geology and Seismology (GES'10)*.Cambridge.

Odeh, T., Gloaguen, R., Schirmer, M., Geyer, S., Rödiger, T. and Siebert C. (2009): Groundwater flow within the fault system of Wadi Zerka Ma'in catchment area using remote sensing and GIS methods. *METIER final conference,* Brussels.

Poster

Odeh, T., Geyer, S., Rödiger, T., Siebert, C., Gloaguen, R., and Schirmer, M., (2010): Development of groundwater salinity in the wadi zerka ma'in catchment area, dead sea, jordan. *In 7th International Groundwater Quality Conference*, Zürch.

Taleb Odeh, Stefan Geyer, Tino Rödiger, Christian Siebert, Richard Gloaguen, Mario Schirmer (2010): Groundwater recharge modelling of strike slip faulted catchemnt area: the case of the Zerka Ma'in (Dead Sea, Jordan). *IWRM - Integrated Water Resources Management* , Karlsruhe.

PUBLICATIONS

INTERNATIONAL JOURNAL (PUBLISCHED)

Odeh T., Salameh E., Schirmer M. and Gerhard S. (2009): Structural control of groundwater flow regimes and groundwater chemistry along the lower reaches of the Zerka River, West Jordan, using remote sensing, GIS, and field methods. *Environmental geology journal 58*, pp.1797–1810.

INTERNATIONAL JOURNAL (SUBMITTED)

Odeh, T., Geyer, S., Gloaguen, R., Rödiger, T., Siebert, C. and Schirmer, M. (2010): groundwater chemistry within strike slip faulted aquifers: the case study of Wadi Zerka Ma'in aquifers, North East of the Dead Sea. *Environmental geology journal,* under review.

Odeh, T., Gloaguen, R., Schirmer, M., Rödiger, T., and Geyer, S. (2010): Structural control of drainage network and catchment area morphology – an evaluation using remote sensing and geographic information systems: the case study of Wadi Zerka Ma'in catchment area. *Journal of Structural Geology*, submitted.

Odeh, T., Rödiger, T., Geyer, S., Schirmer, M. and Gloaguen, R. (2010): Hydrol ogical modelling of a heterogeneous catchment area using an integrated approach of remote sensing and GIS: the case study of Wadi Zerka Ma'in. *Hydrological Processes*, submitted.

CONFERENCES PROCEEDINGS

Odeh, T., Gloaguen, R., Schirmer, M., Geyer, S., Rödiger, T. and Siebert C (2009): Exploration of Wadi Zerka Ma'in rotational fault and its drainage pattern, Eastern of Dead Sea, by means of remote sensing, GIS and 3D geological modeling, *proceeding of SPIE Europe's International Symposium on Remote Sensing (ERS09)*, Vol.7478, Berlin.

Odeh, T., Gloaguen, R., Schirmer, M., Geyer, S., Rödiger, T. and Siebert C. (2010): Investigation of Catchment Areas Migrations Through a Sinstral and Dextral Strike Slip Faults: The Case Study of Zerka Ma'in and Al Hasa Catchment Areas, East of the Dead Sea in Jordan. *Proceedings of the 4 ASME/WSEAS International conference on geology and Seismology (GES'10)*,Cambridge.

Odeh, T., Geyer, S., Rödiger, T., Siebert, C., Gloaguen, R., and Schirmer, M., (2010): Development of groundwater salinity in the wadi zerka ma'in catchment area, dead sea, jordan. *In 7th International Groundwater Quality Conference*, Zürch.

e-mail address: taleb_odeh@yahoo.com or taleb.odeh@ufz.de